

**Structural and contractile alterations in skeletal muscles
from the genetically obese (*ob/ob*) mouse:
impairment or adaptation?**

Justin Guy Kemp B.Ed., M.Sc., Ph.D.

Doctor of Philosophy

Victoria University
2008

**Structural and contractile alterations in skeletal muscles
from the genetically obese (*ob/ob*) mouse:
impairment or adaptation?**

TABLE OF CONTENTS

Summary	ix
Declaration	xiv
Acknowledgments	xv
List of abbreviations	xvi
List of figures	xxii
List of tables	xxvi
Chapter 1 General Introduction	1
1.1 Obesity	2
1.1.1 Pathogenic aspects of excess adiposity	4
1.2 Animal models of obesity	6
1.2.1 Rodent models of genetic obesity	8
1.2.2 The genetically obese (<i>ob/ob</i>) mouse	9
1.3 Skeletal muscle	12
1.3.1 Structure and morphology of skeletal muscle	12
1.3.2 Myosin and myofibrillar adenosine triphosphatase (ATPase) activity	14
1.3.3 Myosin heavy chain (MHC) polymorphism	16
1.3.4 Muscle fibre types	18

1.3.5	Diversity and plasticity of skeletal muscle	20
1.3.6	Excitation-contraction-relaxation (E-C-R) cycle in mammalian skeletal muscle	23
1.3.7	Sliding filament theory	27
1.3.8	Parameters describing the isometric contraction of an isolated skeletal muscle	29
	1.3.8.1 Isometric twitch response	31
	1.3.8.2 Isometric tetanus response	31
1.3.9	Muscle fatigue	36
	1.3.9.1 Recovery from fatigue	38
	1.3.9.2 Fatigue and muscle metabolism	40
	1.3.9.3 Lactate dehydrogenase (LDH) as a marker of metabolic capacity/phenotype	41
1.4	Obesity and skeletal muscle	43
	1.4.1 Structural alterations in skeletal muscle as a contributor to the pathogenesis of/pathologies associated with obesity	43
	1.4.2 Structural alterations in skeletal muscle as a consequence of obesity	45
	1.4.3 Obesity and skeletal muscle contractility	48
1.5	The aims of this study	48
Chapter 2	General Methods	50
2.1	Animals	51

2.2	Muscle dissection, handling and storage	51
2.3	Determination of muscle width	55
2.4	Dissection of single muscle fibres and mechanical removal of the surface membrane (skinning)	55
2.5	Determination of single fibre diameter, cross-sectional area (CSA) and volume	58
2.6	Single fibre preparation for analysis of MHC isoform (MHC _i) composition by SDS-PAGE	58
2.7	SDS-PAGE analyses of MHC _i composition in whole muscle homogenate and single fibre samples	60
2.8	Protein visualisation on SDS-polyacrylamide gels	64
2.9	Laser densitometry for quantitation of protein bands on SDS-polyacrylamide gels	66

Chapter 3 Morphological and biochemical characteristics of EDL, SM and SOL muscles from *ob/ob* mouse

3.1	Introduction	68
3.2	Methods	70
3.2.1	Animals and muscle preparations	70
3.2.2	Measurement of body size and whole muscle morphology characteristics	70
3.2.3	Measurement of single fibre size	71
3.2.3.1	Estimation of fibre number	71

3.2.4	Muscle homogenisation for biochemical analyses	72
3.2.5	Protein determination in muscle homogenates	73
3.2.6	Preparation of whole muscle homogenates for electrophoretic analysis of MHC content and MHC _i composition	73
3.2.7	Electrophoretic determination of MHC content in whole muscle homogenates	73
3.2.8	Determination of MHC _i composition in whole muscle homogenate and single fibre samples	76
3.2.9	Statistical analysis	77
3.3	Results	78
3.3.1	Body size and whole muscle morphology	78
3.3.2	Single fibre size	80
3.3.3	Muscle total protein content	86
3.3.4	MHC content	88
3.3.5	MHC _i composition	88
3.3.6	Fibre type composition	92
3.4	Discussion	99

**Chapter 4 Contractile characteristics of EDL, SM and SOL muscles
from *ob/ob* mouse**

4.1	Introduction	111
4.2	Methods	113
4.2.1	Animals and muscles	113

4.2.2	Determination of muscle mass	113
4.2.3	Set-up for whole muscle contractility experiments	113
4.2.3.1	Solution used for whole muscle contractility experiments	113
4.2.3.2	Mounting of the whole muscle in the system for isometric contractile testing	114
4.2.3.3	Calibration of the force transducer	117
4.2.4	Measurements of the isometric contractile characteristics of whole muscles	118
4.2.4.1	Twitch characteristics	119
4.2.4.2	Force-frequency relationship	120
4.2.4.3	Tetanic characteristics	121
4.2.5	Data analysis	121
4.2.6	Statistical analysis	123
4.3	Results	124
4.3.1	Parameters describing the force-generating capacity of EDL, SM and SOL muscles of <i>ob/ob</i> and lean mice	124
4.3.1.1	Twitch force	124
4.3.1.2	Tetanic force	127
4.3.1.3	Aspects of muscle architecture relevant to force generation by EDL, SM and SOL muscles from <i>ob/ob</i> and lean mice	128
4.3.2	Parameters describing the contractile kinetics of EDL, SM and SOL muscles of <i>ob/ob</i> and lean mice	131
4.3.2.1	Kinetics of the twitch response	131

4.3.2.2	Kinetics of the tetanus response	134
4.3.3	Force-frequency relationship	136
4.4	Discussion	140
Chapter 5	A single fibre investigation of the altered relaxation kinetics of EDL muscles from <i>ob/ob</i> mice	
5.1	Introduction	146
5.2	Methods	148
5.2.1	Animals and muscles	148
5.2.2	Skinned fibre preparation for contractile apparatus and sarcoplasmic reticulum experiments	148
5.2.3	Mounting of the single fibre on the set-up for contractile experiments	148
5.2.3.1	Calibration of the force transducer	149
5.2.3.2	Determination of sarcomere length	151
5.2.4	Contractile apparatus experiments	151
5.2.4.1	Solutions for contractile apparatus experiments	152
5.2.4.2	Determination of Ca ²⁺ sensitivity of the contractile apparatus	153
5.2.5	Sarcoplasmic reticulum (SR) Ca ²⁺ loading and leak experiments	155
5.2.5.1	Solutions for SR Ca ²⁺ loading and leak experiments	155
5.2.5.2	Generation of caffeine-induced force responses	157
5.2.5.3	Determination of endogenous SR Ca ²⁺ content	163

5.2.5.4	Determination of SR Ca ²⁺ loading capacity	164
5.2.5.5	Determination of passive SR Ca ²⁺ leak	166
5.2.6	Statistical analysis	167
5.3	Results	168
5.3.1	Ca ²⁺ sensitivity of the contractile apparatus	168
5.3.2	Properties of SR related to relaxation	171
5.3.2.1	Endogenous Ca ²⁺ content of the SR	172
5.3.2.2	SR Ca ²⁺ leak	174
5.3.2.3	The capacity of the SR to load Ca ²⁺	175
5.4	Discussion	181

**Chapter 6 Fatigue characteristics of EDL, SM and SOL muscles
 from *ob/ob* mouse**

6.1	Introduction	187
6.2	Methods	189
6.2.1	Animals and muscles	189
6.2.2	Protocol used to determine parameters describing the fatigue resistance and recovery from fatigue of whole muscles	189
6.2.3	Strategy used to confirm that the fatiguing protocol induces LFF in whole muscles	191
6.2.4	Data analysis	192
6.2.5	Determination of myofibrillar ATPase activity of mechanically skinned mouse single fibres	192

6.2.5.1	Reagent solutions	193
6.2.5.2	Protocol for measuring MgATPase activity in single fibre segments	193
6.2.5.3	Spectrophotometric determination of [P _i] in small volumes of reagent	197
6.2.6	Sample preparation for LDH isoenzyme analysis	199
6.2.6.1	Preparation of tissue extracts for PAGE	199
6.2.6.2	PAGE separation of LDH isoenzymes	199
6.2.7	Statistical analysis	202
6.3	Results	203
6.3.1	Evidence of low frequency fatigue in EDL, SM and SOL muscles from <i>ob/ob</i> and lean mice	203
6.3.2	Fatigue resistance of EDL, SM and SOL muscles from <i>ob/ob</i> and lean mice	208
6.3.3	Recovery from fatigue	210
6.3.4	Myofibrillar ATPase activity	214
6.3.5	LDH isoenzyme composition	216
6.4	Discussion	220
Chapter 7 General Discussion		227
Concluding Remarks		237
References		241

Obesity studies using humans are confounded by variables that are difficult to control and are restricted by ethical considerations. Given that they display many of the common attributes of obese humans, animal models of obesity have become invaluable tools for studying the etiology and related pathologies of the obese condition. Obese animals have been often reported to exhibit marked reductions in skeletal muscle size, but currently available data on the contractile function of skeletal muscles in rodent models of obesity are scarce and often conflicting. Therefore, the overall aim of this study was to further knowledge and understanding of the functional status of skeletal muscle in *ob/ob* mouse, a commonly used model of obesity, by employing a combination of biochemical and physiological methods and whole muscle and single fibre approaches. The animals were used at an age where there is no evidence of hyperglycemia or hypertension, thereby allowing the study of obesity without the often concurrent syndromes of diabetes and hypertension. The muscles examined included two hind limb muscles [extensor digitorum longus (EDL) – predominately locomotor; soleus (SOL) – predominately postural) and one trunk muscle [sternomastoid (SM) – involved in head/neck motion and respiratory assistance]. The data generated in the series of studies comprising this work is summarised as follows:

1. The EDL, SM and SOL muscles of *ob/ob* mice and controls were examined with respect to size [mass, muscle mass-to-body mass ratio, cross-sectional area (CSA)],

fibre CSA, protein content, myosin heavy chain (MHC) content, MHC isoform composition and fibre type composition. Compared with the controls, all three muscles from *ob/ob* mice were smaller in size, with EDL and SM being the most affected. The CSA values for fibres from the predominant fibre types in EDL and SM muscles (IIB and IIB+IID) were smaller than those for fibres from control muscles, and the fibre size differences were consistent with the differences in muscle size. No differences between EDL, SM and SOL muscles from *ob/ob* and lean mice were found with respect to total protein content and MHC content (both normalised to muscle mass). Electrophoretic analyses of MHC isoform composition in whole muscle homogenates and single muscle fibres showed a shift towards slower MHC isoforms and a greater proportion of hybrid fibres in all three muscles of *ob/ob* mice, which suggest that skeletal muscles of *ob/ob* mice may follow a different pattern of development or undergo an obesity-related structural remodeling which does not involve changes in protein content (*Chapter 3*).

2. Isometric contractile characteristics [twitch and tetanic force-generating capacity and kinetics; force-frequency relationship] of EDL, SM and SOL muscles from *ob/ob* and lean mice were explored using an isolated whole muscle preparation. The following statistically significant differences were observed for muscles from *ob/ob* mice when compared to muscles from lean mice: (i) lower force-generating capacity (P_0 /body mass) for EDL, SM and SOL muscles; (ii) slower kinetics of the twitch response (W_{50} value) for EDL and SOL muscles; (iii) lower rate of force development of the tetanic response for EDL muscle; (iv) slower relaxation kinetics of the tetanic response for

EDL and SOL muscles; (v) a leftward shift in the force-frequency relationship for EDL and SOL muscles. (*Chapter 4*).

3. The possibility that skeletal muscles of *ob/ob* mice displayed slower relaxation kinetics because of functional alterations in the contractile apparatus and/or SR function was explored using a single fibre approach. In these experiments, the following parameters were probed in mechanically skinned type IIB fibres (the predominant fibre type in both muscle groups) from EDL muscles of *ob/ob* and lean mice: (i) Ca^{2+} sensitivity (pCa_{50} ; pCa_{10} ; Hill coefficient: where $\text{pCa} = -\log_{10}[\text{Ca}^{2+}]$); (ii) endogenous SR Ca^{2+} content; (iii) SR Ca^{2+} leak rate; (iv) maximal SR Ca^{2+} loading capacity at two different $[\text{Ca}^{2+}]$ (an indicator of slow/fast SR properties); and, (v) maximal SR Ca^{2+} loading at $\text{pCa } 7.3$, normalised to maximum Ca^{2+} -activated force (an indicator of the density of SR Ca^{2+} pumps in the fibre). The data showed similarities in all the parameters except (v), suggesting that EDL type IIB fibres from *ob/ob* mice possess a lower density of the SR Ca^{2+} pumps per fibre volume. A lower density of SR Ca^{2+} pumps would reduce the ability of the SR to sequester Ca^{2+} and return $[\text{Ca}^{2+}]_i$ back to resting levels following a contractile response, thereby slowing relaxation. (*Chapter 5*).

4. The fatigability characteristics [fatigue resistance; recovery of peak tetanic force at 5 min and 60 min after cessation of fatiguing exercise; loss in the ability to generate force at stimulation frequencies of 5 to 90 (or 110) Hz, at 60 min after cessation of fatiguing exercise] of EDL, SM and SOL muscles from *ob/ob* and lean mice were explored using isolated whole muscle preparations and a fatiguing protocol that elicited a state of low-

frequency fatigue in all three muscles. As fatigability of the muscle is determined, in part, by the rate of energy supply relative to the rate of energy consumption, *ob/ob* and lean mice were also compared with respect to myofibrillar ATPase activity (determined in EDL type IIB fibres – the predominant fibre type) and lactate dehydrogenase (LDH) isoenzyme profile (determined in EDL, SM and SOL muscle homogenates). Muscle-specific decreases in fatigability were observed in muscles from *ob/ob* mice, with: (i) EDL displaying greater fatigue resistance; (ii) EDL exhibiting greater recovery of peak tetanic force at 5 min post-fatiguing exercise; (iii) EDL and SOL displaying greater recovery of force at 60 min post-fatiguing exercise; and (iv) EDL and SOL exhibiting a lower loss in the ability to generate force at low stimulation frequencies (≤ 30 Hz). The decreased fatigability of EDL muscles from *ob/ob* mice could not be related to lower myofibrillar ATPase activity in type IIB fibres. No simple relationship could be established between the fatigability characteristics of EDL, SM and SOL muscles of *ob/ob* mice and their LDH isoenzyme profile. This is because the LDH isoenzyme data showed a shift towards a more aerobic-oxidative phenotype for all three muscles of *ob/ob* mice, including SM which showed no changes in fatigability characteristics. (*Chapter 6*).

The data collected on EDL, SM and SOL muscles from lean mice revealed a number of notable inter-muscle differences in these animals: (i) SOL contains a larger proportion of hybrid fibres than EDL and SM (*Chapter 3*); (ii) SM has a lower force-generating capacity, as indicated by (peak tetanic force)/(estimated physiological cross-sectional area), than EDL and SOL (*Chapter 4*); (iii) SM displays faster contractile kinetics than EDL and

produces a different force-frequency curve (*Chapter 4*); and (iv) compared with SOL muscle, EDL and SM display a markedly greater loss of ability to develop force when stimulated at higher stimulation frequencies (≥ 50 Hz) at 60 min recovery from fatiguing exercise (*Chapter 6*). As EDL and SM muscles contain similar fibre type composition, their differences in contractile characteristics must be related to other factors, such as (but not limited to) differences in anatomical location and physiological function.

Declaration

I, Justin Guy Kemp, declare that the PhD thesis entitled “Structural and contractile alterations in skeletal muscles from the genetically obese (*ob/ob*) mouse: impairment or adaptation?” is no more than 100,000 words in length including quotes and exclusive of tables, figures, appendices, bibliography, references and footnotes. This thesis contains no material that has been submitted previously, in whole or in part, for the award of any other academic degree or diploma. Except where otherwise indicated, this thesis is my own work.

Acknowledgments

Firstly, and importantly, I thank Professor Gabriela Stephenson and Dr Ronnie Blazev for the time, energy and expertise that they offered over the years, in order to provide me with the skills and knowledge required for the production of this work; it is immensely appreciated.

I also thank past and present members of the Muscle Cell Biochemistry Laboratory for their support, guidance and sense of humour – Dr Susie Bortolotto-Smith, Dr Craig Goodman, Dr Long Nguyen, Dr Michael Patterson, Ian Sullivan, Joanne Babb and, especially, Dr Brett O’Connell.

I would like to thank my employer, Australian Catholic University, for its support of this work; in particular, the School of Exercise Science and Associate Professor Wayne Maschette.

Special thanks to Professor George Stephenson and Dr Niels Ørtenblad for their knowledge and wisdom, and Nick Athanasiou for being a great ‘science’ friend.

Finally, thanks to my family, friends, music brothers, and especially Jessica, for your patience, support and perspective.

List of abbreviations

1/2RT	twitch half-relaxation time
1/2RT _{tet}	tetanus half-relaxation time
A/D	analogue-to-digital
ADP	adenosine diphosphate
AMPK	adenosine monophosphate-activated protein kinase
ANOVA	analysis of variance
ATP	adenosine triphosphate
ATPase	adenosine triphosphatase
B6.V- <i>Lep</i> ^{ob}	genetically obese mouse strain (also referred to as C57BL/6J- <i>ob/ob</i>)
BM	body mass
BMI	body mass index
BSA	bovine serum albumin
C57BL/6J	mouse strain
C57BL/6J- <i>ob/ob</i>	genetically obese mouse strain (also referred to as B6.V- <i>Lep</i> ^{ob})
C57BL/KsJ	mouse strain
C	[<i>N,N'</i> -methylene-bis-acrylamide]/[acrylamide + <i>N,N'</i> -methylene-bis-acrylamide], expressed as %
Ca ²⁺	calcium ion
[Ca ²⁺] _i	intracellular calcium concentration
CBB	Coomassie Brilliant Blue
CLFS	chronic low-frequency stimulation

CrP	creatine phosphate
CSA	cross-sectional area
CSA _m	whole muscle cross-sectional area
CSA _{sf}	single fibre cross-sectional area
CV	coefficient of variation
+dP/dt	peak rate of force development
+dP/dt.P _o ⁻¹	peak rate of force development, normalised to peak tetanic force
-dP/dt	peak rate of relaxation (force decline)
-dP/dt.P _o ⁻¹	peak rate of relaxation, normalised to peak tetanic force
DHPR	dihydropyridine receptor
DHPRs	dihydropyridine receptors
<i>E</i> _{caff-area}	area under an endogenous caffeine-induced response normalised to F _{max}
<i>E</i> _{caff-peak}	peak force of an endogenous caffeine-induced response normalised to F _{max}
<i>E</i> _{caff-rate}	maximum upward slope of an endogenous caffeine-induced response normalised to the peak force of the endogenous caffeine-induced response
E-C	excitation-contraction
E-C-R	excitation-contraction-relaxation
EDL	extensor digitorum longus
EGTA	ethyleneglycol-bis(β aminoethylether)-N,N,N',N'-tetraacetic acid
FB	flexor brevis
FDB	flexor digitorum brevis
F _{max}	maximum Ca ²⁺ -activated force

H	lactate dehydrogenase subunit – represents <i>heart</i> , in recognition of the tissue in which it predominates
H ⁺	hydrogen ion
HDTA	1,6-diaminohexane-N,N,N',N'-tetraacetic acid
HEPES	N-2-hydroxyethyl-piper-azine-N'-2-ethanesulfonic acid
HFF	high-frequency fatigue
HMM	heavy meromyosin
IGF-1	insulin-like growth factor 1
IL-1 β	interleukin-1 β
IL-6	interleukin-6
K ⁺	potassium ion
kDa	kiloDalton
L _o	optimal length – defined as the muscle length providing peak twitch force
LDH	lactate dehydrogenase
LFF	low-frequency fatigue
LMM	light meromyosin
LT	longitudinal tubule (of the SR)
M	lactate dehydrogenase subunit – represents <i>muscle</i> , in recognition of the tissue in which it predominates
Mg ²⁺	magnesium ion
[Mg ²⁺] _{free}	free magnesium concentration
MHC	myosin heavy chain
MHC _i	myosin heavy chain isoform
MW	molecular weight

n	sample size
Na ⁺	sodium ion
NAD ⁺	nicotinamide adenine dinucleotide
NADH	reduced form of nicotinamide adenine dinucleotide
N _f	number of fibres
n _H	Hill coefficient
<i>ob</i>	mouse obese gene
<i>ob/ob</i>	genetically obese
OD	optical density
PAGE	polyacrylamide gel electrophoresis
pCa	$-\log_{10}[\text{Ca}^{2+}]$
pCa ₁₀	pCa generating 10% F _{max}
pCa ₅₀	pCa generating 50% F _{max}
PCSA	physiological cross-sectional area
PGC-1α	peroxisome proliferator-activated receptor-γ coactivator-1α
PGC-1β	peroxisome proliferator-activated receptor-γ coactivator-1β
P _i	inorganic phosphate
P _o	peak (tetanic) force
PPARδ	peroxisome proliferative-activated receptor δ
psP _o	peak tetanic force, normalised to the estimated muscle PCSA
psP _t	peak twitch force, normalised to the estimated muscle PCSA
P _t	peak (twitch) force

$R_{6.2/7.3}$	area under a caffeine-induced force curve following a 60-s incubation in load solution at pCa 6.2 divided by the area under a caffeine-induced force curve following a 240-s incubation in load solution at pCa 7.3
RyR	ryanodine receptor (i.e. calcium release channel)
RT	room temperature (22 to 26 °C)
S1	subfragment 1
SDH	succinate dehydrogenase
SDS	sodium dodecyl sulfate
SDS-PAGE	sodium dodecyl sulfate - polyacrylamide gel electrophoresis
S.E.	standard error of the mean
SERCA	sarco/endoplasmic reticulum Ca^{2+} ATPase (i.e. Ca^{2+} pump)
SM	sternomastoid
SOL	soleus
sP_o	peak tetanic force, normalised to muscle CSA
sP_t	peak twitch force, normalised to muscle CSA
$s-P_o$	peak tetanic force, normalised to body mass
SR	sarcoplasmic reticulum
T	[acrylamide + <i>N,N'</i> -methylene-bis-acrylamide], expressed as %w/v
TC	terminal cisternae (of the SR)
TEMED	<i>N,N,N',N'</i> -tetramethylethylenediamine
TNF- α	tumor necrosis factor- α
TPT	time to peak twitch force
Tris	Tris(hydroxymethyl)methylamine
T-tubule	transverse tubule

v/v	volume per volume
W_{50}	duration of the twitch response measured at half amplitude
w/v	weight per volume

List of figures

Figure 1.1 Annual number of obesity-related publications (from 1947-2006).	3
Figure 1.2 Schematic representation of the structure of mammalian skeletal muscle.	13
Figure 1.3 Schematic diagrams of the myosin molecule.	15
Figure 1.4 Schematic representation of the excitation-contraction-relaxation (E-C-R) cycle events in mammalian twitch muscle fibres.	24
Figure 1.5 Sarcoplasmic reticulum (SR) and transverse tubule (T-tubule) system.	26
Figure 1.6 Schematic representation of the cross-bridge cycle.	28
Figure 1.7 Parameters used to describe the isometric twitch response of skeletal muscle.	32
Figure 1.8 Parameters used to describe the isometric tetanus response of skeletal muscle.	34
Figure 2.1 Sternomastoid muscle dissected from mouse.	53
Figure 2.2 Mechanical skinning of a single muscle fibre.	57
Figure 2.3 Measurement of single muscle fibre diameter.	59
Figure 2.4 Apparatus employed for SDS-PAGE experiments.	61
Figure 2.5 Bio-Rad silver staining procedure.	65
Figure 3.1 Representative electrophoretogram and standard curve used to determine the MHC content of skeletal muscles from adult <i>ob/ob</i> and lean mice.	74
Figure 3.2 Frequency distribution of diameters of single muscle fibres randomly dissected from EDL, SM and SOL muscles of <i>ob/ob</i> and lean mice.	81
Figure 3.3 Mean fibre CSA (μm^2) for the single fibre populations of muscle fibres randomly dissected from EDL, SM, and SOL muscles of <i>ob/ob</i> and lean mice.	83

Figure 3.4 Representative electrophoretograms of MHC isoform profiles of EDL, SM and SOL muscles from adult <i>ob/ob</i> and lean mice.	90
Figure 3.5 MHC isoform composition of whole muscles from adult <i>ob/ob</i> and lean mice.	91
Figure 3.6 Representative electrophoretograms of the 13 MHC isoform-based fibres types found in a population of single fibres randomly dissected from EDL, SM and SOL muscles of adult <i>ob/ob</i> and lean mice.	93
Figure 3.7 Proportion of pure and hybrid fibres in populations of single fibres randomly dissected from muscles of adult <i>ob/ob</i> and lean mice.	94
Figure 3.8 Fibre type proportions in populations of single fibres randomly dissected from muscles of adult <i>ob/ob</i> and lean mice.	95
Figure 4.1 Apparatus for <i>in vitro</i> whole muscle contractility experiments.	115
Figure 4.2 <i>In vitro</i> chamber for whole muscle contractility experiments.	116
Figure 4.3 Calibration curve of force transducer employed in isolated whole muscle contractility experiments.	117
Figure 4.4 Representative data traces of twitch and peak tetanus responses for EDL, SM and SOL muscles from adult <i>ob/ob</i> and lean mice.	125
Figure 4.5 Force-frequency relationships for EDL, SM and SOL muscles from lean mice.	137
Figure 4.6 Force-frequency relationships for whole muscles from <i>ob/ob</i> and lean mice.	139
Figure 5.1 Force measurement device for single muscle fibre experiments.	150
Figure 5.2 Protocol followed in preliminary control experiments used to ascertain the loading time required for near maximal SR Ca ²⁺ loading at two different pCa.	158
Figure 5.3 Caffeine-induced force responses following SR Ca ²⁺ loading of varying durations for a type IIB EDL fibre from <i>ob/ob</i> mouse.	160
Figure 5.4 Caffeine-induced force responses following SR Ca ²⁺ loading of varying durations for a type IIB EDL fibre from lean mouse.	161

Figure 5.5 Protocol used for assessing the Ca ²⁺ loading ability of the SR and the passive leak of Ca ²⁺ from the SR in the mechanically skinned single fibre preparation.	165
Figure 5.6 Representative data of Ca ²⁺ sensitivity experiments for a single type IIB muscle fibre from EDL of <i>ob/ob</i> mouse.	169
Figure 5.7 Representative data of Ca ²⁺ sensitivity experiments for a single type IIB muscle fibre from EDL of lean mouse.	170
Figure 5.8 Caffeine-induced force responses obtained in SR Ca ²⁺ leak experiments.	176
Figure 5.9 Caffeine-induced force responses following maximal SR Ca ²⁺ loading at pCa 7.3 and pCa 6.2.	178
Figure 5.10 Maximal SR Ca ²⁺ content at pCa 7.3 in type IIB fibres from EDL muscles of <i>ob/ob</i> and lean mice, normalised to maximum Ca ²⁺ -activated force.	180
Figure 6.1 Measurement of sarcomere length in mechanically skinned EDL type IIB fibres used in experiments to determine myofibrillar ATPase activity.	196
Figure 6.2 Representative phosphate (P _i) standard calibration curve used to determine myofibrillar ATPase activity of mechanically skinned type IIB fibres from EDL muscles of adult <i>ob/ob</i> and lean mice.	198
Figure 6.3 Apparatus employed for PAGE experiments.	200
Figure 6.4 Protocol used for assessing low-frequency fatigue in EDL, SM and SOL muscles from <i>ob/ob</i> mice, including representative data traces.	204
Figure 6.5 Protocol used for assessing low-frequency fatigue in EDL, SM and SOL muscles from lean mice, including representative data traces.	205
Figure 6.6 Loss in tetanic force at different stimulation frequencies following 50-70 min recovery from fatiguing stimulation for whole muscles from adult <i>ob/ob</i> and lean mice.	206
Figure 6.7 Time to fatigue for EDL, SM and SOL muscles from <i>ob/ob</i> and lean mice during a protocol of repeated tetani.	209
Figure 6.8 Force recovery following fatiguing stimulation of whole muscles from <i>ob/ob</i> and lean mice.	211

Figure 6.9 Myofibrillar ATPase activity in single fibres from muscles of *ob/ob* and lean mice. 215

Figure 6.10 Representative electrophoretograms of LDH isoenzyme profiles of EDL, SM and SOL muscles from adult *ob/ob* and lean mice. 217

List of tables

Table 1.1 Ontogeny of pathological features of <i>ob/ob</i> mouse.	11
Table 1.2 Isometric contractile response.	30
Table 3.1: Muscle morphology data for EDL, SM and SOL from adult <i>ob/ob</i> and lean mice.	79
Table 3.2 Cross-sectional area (CSA) of electrophoretically-defined singles fibres randomly dissected from EDL, SM and SOL muscles of <i>ob/ob</i> and lean mice.	85
Table 3.3 Protein and MHC content in EDL, SM and SOL muscles from adult <i>ob/ob</i> and lean mice.	87
Table 3.4: Obesity-related changes in the proportion of each fibre type detected in populations of single fibres dissected from EDL and SM muscles of adult <i>ob/ob</i> and lean mice.	96
Table 3.5: The proportion of each fibre type in the SOL muscle of adult <i>ob/ob</i> and lean mice, expressed as per cent of total number of fibres in the SOL muscle of lean mice (N_f^{le}), and the obesity-related changes in the proportion of each fibre type in the SOL muscle of <i>ob/ob</i> mouse.	97
Table 4.1 Parameters describing the force-generating capacity of EDL, SM and SOL muscles of <i>ob/ob</i> and lean mice.	126
Table 4.2 Parameters describing the contractile kinetics of EDL, SM and SOL muscles of <i>ob/ob</i> and lean mice.	132
Table 5.1 Composition of solutions used in single fibre contractile apparatus experiments.	153
Table 5.2 Composition of solutions used in single fibre SR leak and loading experiments.	156
Table 5.3 Ca^{2+} -sensitivity parameters for type IIB fibres from EDL muscles of <i>ob/ob</i> and lean mice.	171
Table 5.4 Parameters describing SR Ca^{2+} handling properties of single type IIB fibres from EDL muscles of <i>ob/ob</i> and lean mice.	173

Table 6.1 Protocol employed to induce fatigue in isolated whole muscles.	190
Table 6.2 Tetanic forces developed by EDL, SM and SOL muscles from <i>ob/ob</i> and lean mice at different time points in recovery from the fatiguing exercise.	213
Table 6.3 LDH isoenzyme proportions in EDL, SM and SOL muscles from adult <i>ob/ob</i> and lean mice.	218
Table 7.1 Summary of alterations detected in skeletal muscles of adult <i>ob/ob</i> mouse as described in Chapters 3-6.	230
Table 7.2 Tetanic force-generating capacity of EDL and SOL muscles of <i>ob/ob</i> mice, relative to their control counterparts, at different frequencies of stimulation.	234

Chapter 1

General Introduction

1.1 Obesity

Current estimates suggest that approximately two billion adults worldwide are overweight [defined by a body mass index (BMI) = 25 to < 30 kg.m⁻²] or obese [BMI ≥ 30 kg.m⁻²] (World Health Organization, 2006). In Australia, data approximate that 60% of the adult population is overweight or obese (Cameron *et al.*, 2003), with prevalence rates in the U.S. being even greater (Flegal *et al.*, 2002). According to these estimates, approximately 20% of adult Australians and 30% of adult Americans are obese. Despite global recognition of obesity as a chronic disease, and an exponential rise in the annual number of publications produced by obesity-related research (see Figure 1.1), prevalence rates continue to increase at alarming rates worldwide (World Health Organization, 1998, 2006; Stein & Colditz, 2004).

Obesity is defined as an excess accumulation of body fat that may impair health (World Health Organization, 2006). Fundamentally, obesity results from a cumulative positive energy balance, where energy intake (calories consumed) exceeds energy expenditure (calories expended). This excess energy is stored in fat cells (adipocytes) that enlarge and, in some cases, increase in number (Bray, 2006), resulting in weight gain and excess whole-body adiposity. Some of the clinical problems of obesity, such as osteoarthritis (Roubenoff, 2000; Ells *et al.*, 2006), sleep apnea (Subramanian & Strohl, 2004) and social stigma (Gortmaker *et al.*, 1993), arise from the weight gain/increased fat mass itself. However, the persistent gains in adiposity can also lead to metabolic dysfunction in a variety of organs and tissues (Muoio & Newgard, 2006),

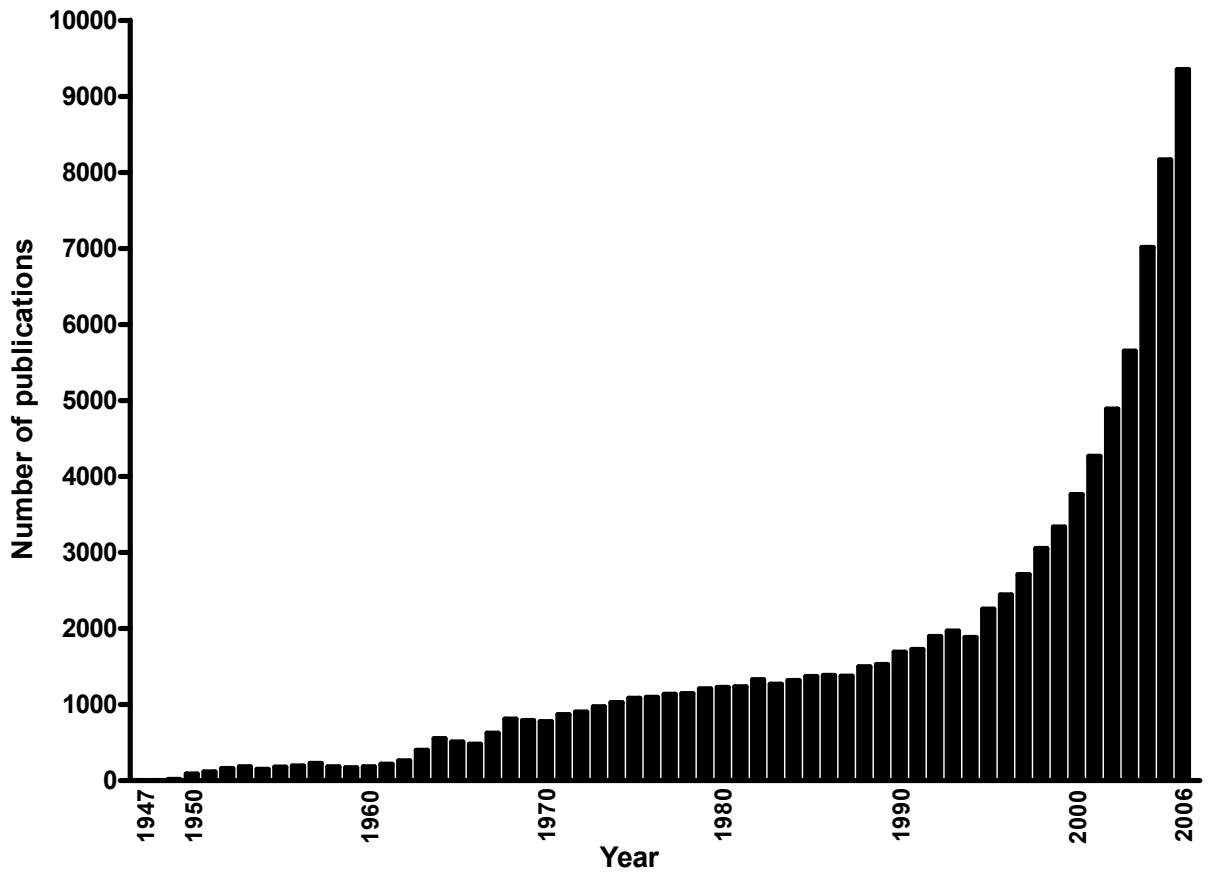


Figure 1.1 Annual number of obesity-related publications (from 1947-2006).

Publications were retrieved using the *PubMed* search engine (U.S. National Library of Medicine and the National Institutes of Health, <http://www.pubmed.gov>), with “obesity” as the sole keyword. Note: (a) there was one publication in 1947 and none in 1948 that matched the keyword; (b) prior to 1947, there were ten publications that matched the keyword; (c) the earliest work to match the keyword was published in 1880.

as well as increasing the risk of developing co-morbidities such as insulin resistance, diabetes mellitus, hypertension, hypercholesterolemia, coronary heart and vascular disease, metabolic syndrome, gallbladder disease, non-alcoholic fatty liver disease, and some forms of cancer (Bray, 2004; Haslam & James, 2005).

1.1.1 Pathogenic aspects of excess adiposity

The role played by excess adipose tissue in lipid-induced tissue dysfunction extends from its recognition as an endocrine organ (Kershaw & Flier, 2004; Berggren *et al.*, 2005; Hotamisligil, 2006). Adipocytes are now viewed not merely as storage sites of excess energy but as endocrine cells capable of communicating with the brain and peripheral tissues in matters of whole-body energy status. Adipocytes help modulate feeding behaviour, energy balance, and metabolic homeostasis through the production/secretion of a variety of hormones (e.g. leptin, adiponectin, resistin). For example, leptin, which is synthesised and secreted by adipocytes in proportion to fat mass, acts on central and peripheral receptors to effect changes in peptide production/release that affect food intake and energy expenditure (Zhang *et al.*, 1994; Maffei *et al.*, 1995; Pelleymounter *et al.*, 1995, 1998; Friedman, 1997; Cummings & Schwartz, 2003). Leptin, along with adiponectin, also mediates changes in fuel metabolism by decreasing triglyceride synthesis, enhancing fatty acid breakdown and improving insulin action in liver and skeletal muscle (Pelleymounter *et al.*, 1998; Ryo *et al.*, 2004; Muoio & Newgard, 2006). However, these regulatory roles are not fulfilled appropriately under conditions of excess adipose tissue due to the aberrant release by adipocytes of pro-inflammatory mediators [e.g. tumor necrosis factor- α (TNF- α), interleukin-1 β (IL-1 β) and interleukin-6 (IL-6)] collectively known as *adipokines* (Kershaw & Flier, 2004; Berggren *et al.*, 2005; Hotamisligil, 2006). In

particular, this over-expression of pro-inflammatory adipokines and their increased levels in tissue and blood are thought to contribute to impaired leptin action (mediated by peripheral leptin resistance) and reduced adiponectin levels (Ryo *et al.*, 2004; Haslam & James, 2005; Kojima *et al.*, 2005), thereby contributing to dysfunctional lipid and glucose homeostasis.

Many of the co-morbidities of obesity are also linked to the increased production/secretion of adipokines and the increased release of free fatty acids by hypertrophic adipocytes. Insulin resistance is linked to the release of TNF- α , IL-1 β and IL-6 (Hotamisligil *et al.*, 1993; Uysal *et al.*, 1997; Haslam & James, 2005; Hotamisligil, 2006; Muoio & Newgard, 2006; Sell *et al.*, 2006) and to increased intracellular fat deposits (Stannard & Johnson, 2004). Associated increases in insulin secretion result in hyperinsulinemia which, in turn, increases the synthesis and secretion of very low-density lipoprotein triglyceride and plasminogen activator inhibitor-1 (Bray, 2004). Plasminogen activator inhibitor-1, along with profibrinogen, increases blood viscosity and, together with adipocyte release of angiotensinogen (a precursor of angiotensin), may contribute to the onset of hypertension (Bray, 2004; Kershaw & Flier, 2004; Haslam & James, 2005). The elevated production/secretion of adipokines also establishes obesity as a metabolically triggered state of chronic low-grade inflammation (Berggren *et al.*, 2005; Hotamisligil, 2006), with inflammatory mechanisms implicated in arterial damage (Corti *et al.*, 2004; Kojima *et al.*, 2005). The chronic lipid excess also results in a failure of adipose tissue to adequately sequester and store the excess substrate. Consequently, excess lipid is stored at other sites, including the liver, kidney, heart and *skeletal muscle*, altering their adipokine milieu accordingly. Moreover, this redistribution of lipid to other organs and tissues

can also result in chronic elevations in circulating triglycerides and free fatty acids (a condition known as *hyperlipidemia*). Several of these maladaptations are also features of metabolic syndrome, a disease state characterised by a clustering of major health risk factors (Frisbee & Delp, 2006). Together, these consequences of obesity lead to systemic perturbations in lipid and glucose homeostasis, lipid-induced dysfunction in other tissues involved in energy balance (such as the liver, pancreatic islets and *skeletal muscle*) and, ultimately, whole-body functional impairments.

1.2 *Animal models of obesity*

The pathogenesis of obesity is the outcome of complex relationships between hereditary and environmental factors. These relationships involve multiple susceptibility genes, with 244 genes that, when mutated or expressed as transgenes, result in phenotypes that affect body weight and adiposity (Rankinen *et al.*, 2006). Human obesity studies are confounded by genetic diversity, gender, age and large individual variation in dietary, physical activity and lifestyle patterns. Furthermore, obesity research in humans is encumbered by obvious ethical issues, none more so than the prohibited induction of the disease in man. Fortunately, animal models of obesity resemble human obesity in many ways (Bray, 2004, Haslam & James, 2005), including traits of excess adiposity, hyperphagia, hyperlipidemia, hypercholesterolemia, hyperinsulinemia and insulin resistance (see Table 1.1 in Section 1.2.2; page 11). As briefly discussed below, animal models have become invaluable tools for studying obesity and its related pathologies.

Animal models of obesity have greatly advanced our understanding of the phenomena that underlie obesity, providing insight into the influence of genetic, physiological,

neuroendocrine, epigenetic (*in utero*) and environmental factors on the developmental progression, temporal sequence and severity of obesity and its associated disorders (Bray & York, 1971; Herberg & Coleman, 1977; Coleman, 1978; Bray & York, 1979; Bray *et al.*, 1989; Bray, 1997; York & Hansen, 1998; Martins & Redgrave, 2004; Speakman *et al.*, 2007). Moreover, these models have provided a means of determining the effectiveness of pharmacotherapeutic agents on disease pathogenesis (Powell, 2006). A variety of species, including non-human primates (York & Hansen, 1998; Speakman *et al.*, 2007), pigs (Andersson *et al.*, 1994), bats (Widmaier *et al.*, 1996), seals (Ortiz *et al.*, 2001) and dragonflies (Schilder & Marden, 2006), have been used as models of obesity, but the majority of work has been carried out with rodent species, which are susceptible to many of the same diseases as humans, including obesity and its related disorders. The use of rodent models has greatly facilitated the elucidation of the effect of the interplay between hereditary and environmental factors on the pathogenesis of obesity.

A variety of rodent models is currently available to address the disturbances that may lead to obesity and related disorders. Traditionally, these models have been grouped into three categories, according to the origin of the disorder (York, 2004):

- a. *genetic* models of obesity that involve: (i) single gene defects; (ii) the mutation or expression of transgenes; and, (iii) the combined action of many genes (i.e. polygenic models) (Bultman *et al.*, 1992; Zhang *et al.*, 1994; Naggert *et al.*, 1995; Bray, 1997; York and Hansen, 1998; Brockmann & Bevova, 2002; Martins & Redgrave, 2004; York, 2004; Rankinen *et al.*, 2006; Speakman *et al.*, 2007).

- b. *dietary* models of obesity that primarily involve the manipulation of food quantity and nutrient content (Kanarek & Orthen-Gambil, 1982; Sclafani, 1987; Surwit *et al.*, 1988; Ramirez, 1991; Speakman *et al.*, 2007).
- c. *neuroendocrine* models of obesity that have employed hypothalamic damage and endocrine manipulation (Bray & York, 1979; Bray *et al.*, 1989; York & Hansen, 1998) to probe the development and progression of the disease.

1.2.1 Rodent models of genetic obesity

Spontaneous obesity (and its accompanying disorders) that is inherited as a single gene defect in rodent models can be due to a dominant gene, as in the yellow-obese mouse, or a single recessive gene, as in the obese (*ob/ob*) mouse, diabetes (*db/db*) mouse, fat (*fat/fat*) mouse, tubby (*tub/tub*) mouse and the Zucker fatty (*fa/fa*) rat (Bray, 1977; Brockmann & Bevova, 2002; York, 2004). Spontaneous obesity can also be of polygenic origin, as it is the case for the Japanese KK and the New Zealand obese (NZO) mouse (Herberg & Coleman, 1977; Bray & York, 1979; Bray *et al.*, 1989; Bray, 1997; Martins & Redgrave, 2004; Speakman *et al.*, 2007), with these rodents often exhibiting more moderate forms of obesity, with weight gain progressing slowly and, in some cases, dietary manipulation being required for its development (Bray & York, 1979).

Of the obesities inherited as a single gene defect, each animal model has its own phenotypic peculiarities. For example, the dominant gene defect in the yellow-obese mouse results in moderate obesity of slow progression (Carpenter & Mayer, 1958), while the single recessive gene models of *ob/ob* and *db/db* mice display severe obesity of rapid development (Herberg & Coleman, 1977). The *db/db* mouse also suffers from

severe diabetes (Bray & York, 1971; Herberg & Coleman, 1977; Coleman, 1978; Srinivasan & Ramarao, 2007) while the *ob/ob* mouse experiences a transient hyperglycemia that normalises to control levels by maturity (Coleman & Hummel, 1973; Leiter, 1992; Dong *et al.*, 2006) (see Table 1.1 in Section 1.2.2; page 11). However, the severity of the metabolic irregularities is determined not only by the mutation itself but also by the genomic characteristics of the animal. Thus, when the *ob* mutation was expressed on the C57BL/6J background (also referred to as B6.V-*Lep^{ob}*), marked obesity, hyperinsulemia, and transient hyperglycemia resulted, whereas expression of the mutation in the C57BL/KsJ inbred strain resulted in severe diabetes with less pronounced obesity (Coleman & Hummel, 1973).

Among the rodent models of genetic obesity, the *ob/ob* mouse, with its rapid weight gain attributed to excess adiposity and its euglycemia when the *ob* mutation is expressed on the C57BL/6J background, is a suitable model for the researcher wishing to study obesity and its related pathologies without the co-existence of severe diabetes.

1.2.2 *The genetically obese (ob/ob) mouse*

The *ob/ob* mouse, first described by Ingalls *et al.* (1950), inherits its obesity as an autosomal recessive mutation on chromosome 6 (Coleman, 1978). The genetic basis of the mutation arises from a single base pair deletion that results in a premature stop codon in the leptin gene (Zhang *et al.*, 1994). The absence of leptin, and its action as a satiety factor at the level of the hypothalamus (Campfield *et al.*, 1995), alters feeding behaviour, metabolism and endocrine function, resulting in hyperphagia, decreased

energy expenditure and severe obesity (Zhang *et al.*, 1994; Pelleymounter *et al.*, 1995, 1998; Friedman, 1997; Cummings & Schwartz, 2003).

In *ob/ob* mice, obesity and its related pathological changes follow a general pattern of development. Table 1.1 describes the time course and severity of many of these changes. Briefly, accelerated weight gain is recognized at 3-4 weeks of age (Ingalls *et al.*, 1950; Dubuc, 1976a; Thurlby & Trayhurn, 1978; Grundleger *et al.*, 1980), at which time hyperphagia is also observed. Elevated circulating levels of the glucocorticoid corticosterone, a key hormone in the development of obesity (Saito & Bray, 1984; Smith & Romsos, 1985; Tokuyama & Himms-Hagen, 1987; Bray *et al.*, 1989; York & Hansen, 1998), are also present by about 3 weeks (Dubuc, 1976b). Rapid weight gain ensues over the next 2-3 months (Ingalls *et al.*, 1950; Dubuc, 1976a; Trostler *et al.*, 1979; Campion *et al.*, 1984), and this weight gain is largely attributed to an increased fat content, involving both hypertrophy and hyperplasia of adipocytes (Bates *et al.*, 1955; Bray & York, 1971, 1979). This increased fat content resides in large subcutaneous and central deposits, and as increases in intramuscular and circulating triglycerides (Bates *et al.*, 1955; Bray & York, 1971; Bergen *et al.*, 1975; Dubuc, 1976a; Thurlby & Trayhurn, 1979; Trostler *et al.*, 1979, 1982; Almond & Enser, 1984; York & Hansen, 1998; Dong *et al.*, 2006). An increased rate of lipogenesis in liver and adipose tissue is consistent with the accelerated accumulation of fat and, in line with the increased adiposity, these mice also display abnormal production of pro-inflammatory adipokines, including TNF- α (Hotamisligil *et al.*, 1993; Nakao *et al.*, 2000; Hotamisligil, 2006). As seen in Table 1.1, the hyperglycemia that is present at 4-12 weeks of age undergoes remission, so that by 18 weeks, *ob/ob* mouse is euglycemic (Coleman & Hummel, 1973; Leiter, 1992;

Table 1.1 Ontogeny of pathological features of *ob/ob* mouse.

Feature	Age (weeks)				References
	4	6	12	18	
Increased body mass	+	+++	+++	+++	Ingalls <i>et al.</i> , 1950; Bates <i>et al.</i> , 1955; Dubuc, 1976a; Thurlby & Trayhurn, 1978; Trostler <i>et al.</i> , 1979; Grundleger <i>et al.</i> , 1980; Campion <i>et al.</i> , 1984.
Excess adipose tissue	+	+++	+++	+++	Bates <i>et al.</i> , 1955; Bray & York, 1971, 1979; Dubuc, 1976a; Coleman, 1978.
Hyperphagia	-/+	+	++	++	Dubuc, 1976c; Bray & York, 1979.
Hyperglycemia	-*	++	+	-	Westman, 1968; Coleman & Hummel, 1973; Dubuc, 1976a, 1976b, 1976c; Grundleger <i>et al.</i> , 1980; Leiter, 1992; Uysal <i>et al.</i> , 1997; Haluzik <i>et al.</i> , 2004; Dong <i>et al.</i> , 2006; Kim <i>et al.</i> , 2007.
Hyperinsulinemia	+	++	+++	+++	Coleman & Hummel, 1973; Dubuc, 1976a; Grundleger <i>et al.</i> , 1980; Uysal <i>et al.</i> , 1997.
Insulin resistance	-	+	++	+++	Westman, 1968; Bray & York, 1979; Grundleger <i>et al.</i> , 1980.
Hypothermia	+	++	++	++	Trayhurn <i>et al.</i> , 1977; Bray & York, 1979.
Hypoactivity	-/+	+	+	+	Yen & Acton, 1972; Joosten & van der Kroon, 1974.
Elevated circulating corticosterone	+	++	++	+	Dubuc, 1976b; Smith & Romsos, 1985; Tokuyama & Himms-Hagen, 1987; Bray <i>et al.</i> , 1989; York & Hansen, 1998.
Hyperlipidemia/ hypercholesterolemia	?	+	+	+	Mayer & Jones, 1953; Haluzik <i>et al.</i> , 2004; Dong <i>et al.</i> , 2006; Kim <i>et al.</i> , 2007.
Hypertension	?	?	-	?	Dong <i>et al.</i> , 2006.
Decreased circulating leptin	?	+++	+++	?	Murphy <i>et al.</i> , 1997; Minhas <i>et al.</i> , 2005; Dong <i>et al.</i> , 2006.
Decreased adiponectin levels	?	?	+++	?	Delporte <i>et al.</i> , 2004; Haluzik <i>et al.</i> , 2004; Kim <i>et al.</i> , 2007.
Elevated pro-inflammatory adipokines	?	-/+	++	?	Hotamisligil <i>et al.</i> , 1993; Nakao <i>et al.</i> , 2000; Hotamisligil, 2006.

Each feature is judged against control values for lean mice. Key: - absent (i.e. not different to lean mice); +/- variable (i.e. similarity and difference to lean mice have been reported); + mild; ++ moderate; +++ severe; ? data not found. *a brief period of hypoglycemia has also been reported. Note: A qualitative assessment of the severity of each feature is not always indicated in the literature.

Dong *et al.*, *al.*, 2006). In addition, the mature mouse is normotensive (Dong *et al.*, 2006). Therefore, the data available show the adult *ob/ob* mouse to be a useful model of obesity without the often concurrent syndromes of diabetes and hypertension.

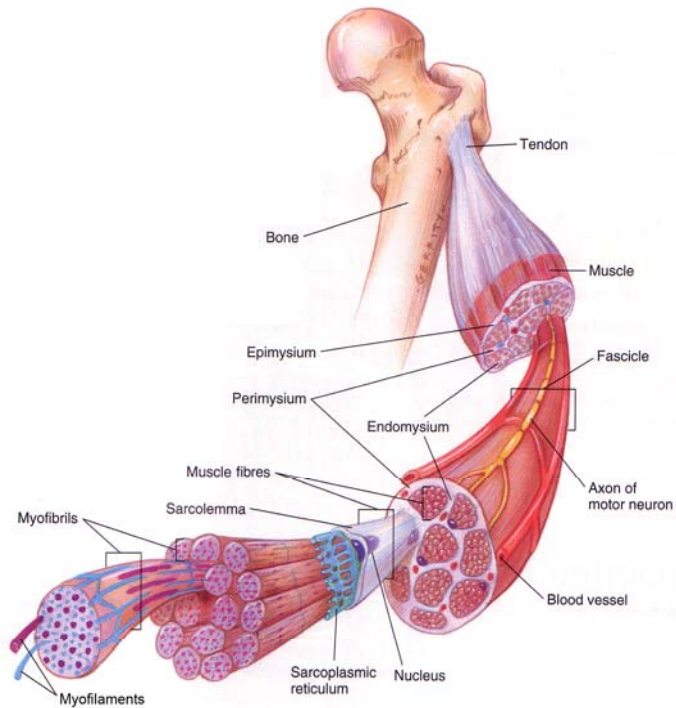
1.3 Skeletal muscle

As briefly mentioned in Section 1.1.1, skeletal muscle is a contributor to whole-body fuel homeostasis, being a major site of energy transduction and storage. However, the predominant function of skeletal muscle is to generate force and produce movement. This unique ability makes this tissue responsible for several basic features of life: (i) purposeful movement of an organism (e.g. locomotion); (ii) postural maintenance; (iii) stabilisation of joints; (iv) respiration (i.e. ventilation of the lungs); and, (v) heat production in times of cold stress. Therefore, ‘normal’ skeletal muscle function is critical to the survival and health of the organism.

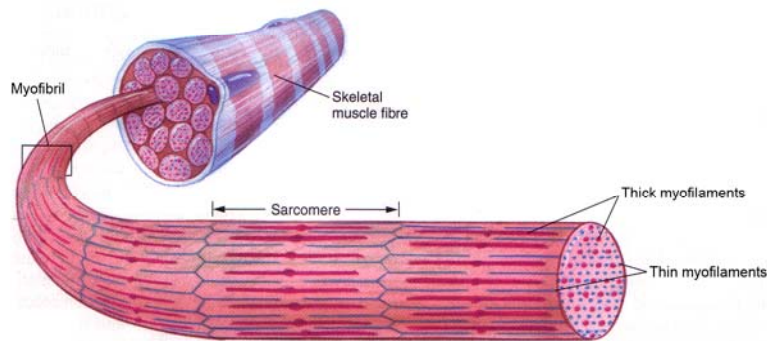
1.3.1 Structure and morphology of skeletal muscle

Skeletal muscle comprises, in addition to muscle fibres (or muscle cells), nerve cells, blood vessels and different forms of connective tissue (e.g. epimysium, perimysium, endomysium) (see Figure 1.2). The structure of a muscle can be considered in a hierarchical manner, with the *whole muscle* being made up of *muscle fascicles*, which, in turn, are made up of *muscle fibres* (the elementary unit of muscle). Each muscle fibre is a single multi-nucleated cell. Contained within the muscle fibre, running longitudinally and in parallel and spanning the length of the fibre, are *myofibrils*; these structures have the ability to shorten, thereby causing a contraction of the muscle fibre. A myofibril contains a regular arrangement of repeating units called *sarcomeres* (often referred to as the basic contractile units of a muscle fibre), which in

A



B



C

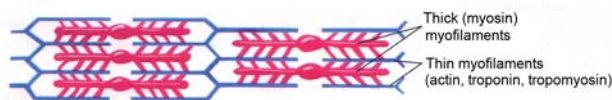


Figure 1.2 Schematic representation of the structure of mammalian skeletal muscle.

A. Overall structure of skeletal muscle, including connective tissue. B. The microstructure of a muscle, showing the striated pattern produced by the inter-digitating thick and thin myofilaments. C. Arrangement of thick and thin myofilaments in the sarcomere. (Modified from Powers & Howley, 2001).

turn contain inter-digitating thick and thin myofilaments that produce a transverse banding ('striated') pattern distinguishable in light microscopy. The thick myofilament is comprised predominately of the key contractile protein, myosin (the molecular motor in muscle contraction), and the thin myofilament is made up of another key contractile protein, actin, and the Ca^{2+} regulatory proteins, troponin and tropomyosin (Schiaffino & Reggiani, 1996; Gordon *et al.*, 2000).

Great variability exists in the dimensions of single muscle fibres. Muscle fibres range from only a few sarcomeres in length in some muscles of small animals to several hundred thousand sarcomeres in fibres from limb muscles of large mammals, while muscle fibre width can range from several to $\sim 150 \mu\text{m}$ (Stephenson, 1996). Moreover, the length of one sarcomere is not a constant entity among muscles and species (Stephenson, 1996). These differences directly influence force production and shortening velocity and, thus, have particular physiological relevance to skeletal muscle function at the whole-organism level.

1.3.2 *Myosin and myofibrillar adenosine triphosphatase (ATPase) activity*

Muscle contraction results from the cyclic interaction between the myofibrillar proteins myosin and actin (see Section 1.3.7). Structurally, myosin is a large molecule [molecular weight (MW) $\sim 520 \text{ kDa}$] consisting of six polypeptide chains – two heavy chains (MW $\sim 220 \text{ kDa}$) and four light chains (MW $\sim 20 \text{ kDa}$) (Ohtsuki *et al.*, 1986; Moss *et al.*, 1995). The two myosin heavy chain (MHC) molecules comprise a parallel coiled-coil tail region ($\sim 150 \text{ nm}$), called the myosin rod, which connects, via a flexible linkage (*hinge* region), to the myosin heads [referred to as *subfragment 1* (S1) – see Figure 1.3] (Cooke, 1997; Sweeney & Houdusse, 2004). A myosin head consists

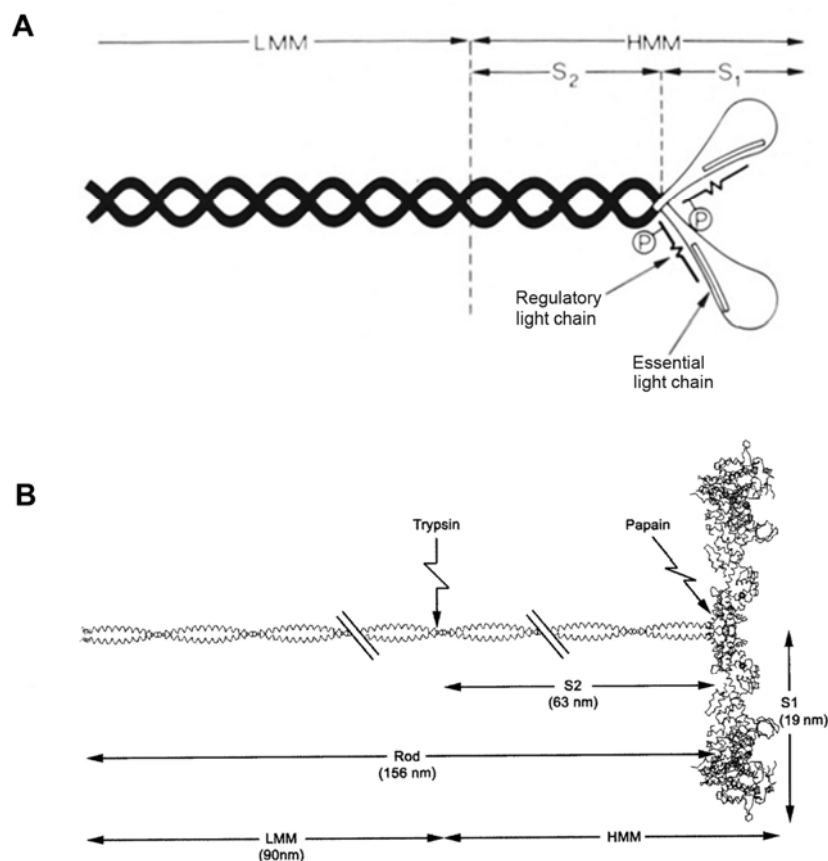


Figure 1.3 Schematic diagrams of the myosin molecule. Myosin consists of six polypeptide chains: two heavy chains and four light chains. The two myosin heavy chain (MHC) molecules comprise the α -helical parallel coiled-coil tail region (i.e. *rod*), and each MHC forms a myosin head (i.e. *S1*). *S1* consists of a globular region (that contains an actin binding site and an ATP binding site) and a neck region (comprising MHC and a *regulatory* and an *essential* myosin light chain). The principal sites of enzymatic attack (by trypsin and papain) to form stable myosin fragments are shown (HMM - heavy meromyosin fragment; LMM - light meromyosin fragment). Hinge regions are at the *S1-S2* junction and at the *S2-LMM* junction. A. Reproduced from Gergely & Seidel (1983) with modifications. B. Reproduced from Craig & Padrón (2004).

of:

- (i) a large globular catalytic region that contains an actin binding site and a binding site for the high energy nucleotide, adenosine triphosphate (ATP), and is composed entirely of MHC; these two binding sites were confirmed by single crystal x-ray diffraction (Rayment *et al.*, 1993).
- (ii) a neck region, composed of MHC and stabilised by two light chains (see *regulatory light chain* and *essential light chain* in Figure 1.3), that extends from the catalytic domain to the junction with the myosin rod.

Myosin is a mechanochemical enzyme that converts chemical energy into mechanical energy via ATPase activity (Stevens *et al.*, 2006). Thus, the binding of ATP to myosin is essential for the hydrolysis of ATP that provides the energy required for the conformational changes in myofibrillar proteins that result in force generation. These conformational changes form the basis of the *swinging-lever-arm hypothesis* (Sweeney & Houdusse, 2004), according to which the structural change occurring in the catalytic domain of the MHC during ATP hydrolysis is amplified by movement of the myosin neck region, as it acts like a lever arm (see Figure 1.6 in Section 1.3.7; page 28). The light chain domain of this region is thought to be involved in force transmission when the myosin head is in the force-generating state (Cooke, 1997), and may also influence maximal shortening velocity (Larsson & Moss, 1993) and the kinetics of the cross-bridge cycle (Andruchov *et al.*, 2006).

1.3.3 Myosin heavy chain (MHC) polymorphism

The proteins responsible for muscle contraction can be separated electrophoretically, using sodium dodecyl sulfate (SDS – an anionic detergent), into their subunit

components. The MHC exists in several molecular forms (isoforms). It is clear from a survey of the literature that research groups have differed in nomenclature used to report MHC isoforms. For the purposes of this work, the nomenclature employed is that of Pette & Staron (2000), where MHC isoforms are identified by a roman numeral and a lower case letter (i.e. MHC I, MHC IIa, MHC IIb, MHC IIc or I, IIa, IIb, IIc), while fibre type is identified by a roman numeral and the corresponding capital letter (i.e. type I, IIA, IIB, IID). Fibres expressing only one MHC isoform (such as type I, IIA, IIB, IID fibres) are referred to as *pure* fibres. In the case where a muscle fibre expresses more than one MHC isoform (referred to as a *hybrid* fibre – see Section 1.3.5), nomenclature will follow as per this example: a fibre co-expressing the MHC IIb and MHC IIc isoforms will be identified as a type IIB+IID fibre. Note that the term *hybrid* fibre may also be applied to fibres displaying the heterogeneous expression of other polymorphic proteins, such as myosin light chain, troponin and tropomyosin; however, in the present study, the term will only be used to describe fibres co-expressing multiple MHC isoforms.

To date, at least ten MHC isoforms have been identified in mammalian muscle fibres (Pette & Staron, 2000; Stephenson, 2006) based on electrophoretic mobility, antibody staining, and mRNA detection. These include:

- (i) two slow-twitch MHC isoforms: MHC I/ β , and MHC α
- (ii) five fast-twitch MHC isoforms: MHC IIa, MHC IIb, MHC IIc(x), MHC eo/III, and MHC IIm – the latter two isoforms are found in extraocular and laryngeal muscles, and masticatory muscles, respectively.
- (iii) two developmental MHC isoforms: MHC-emb(ryonic) and MHC-neo(natal) – found in developing or regenerating muscles.

- (iv) one slow-tonic MHC isoform: MHC_{ton} – found in specialised adult muscles (e.g. laryngeal muscles; mylohyoid muscle).

Four of these MHC isoforms (MHC I, MHC IIa, MHC IIb, MHC IIc) predominate in skeletal muscles across species, with muscles of small mammals containing all four isoforms (Schiaffino *et al.*, 1989; LaFramboise *et al.*, 1990; Pette & Staron, 1990; Schiaffino & Reggiani, 1994; Bortolotto *et al.*, 1999; Weiss *et al.*, 1999). The MHC isoform (MHC_i) expression of a muscle fibre has been found to be closely related to a number of contractile characteristics, such as maximum velocity of shortening, peak mechanical power, stretch activation kinetics (Bottinelli *et al.*, 1991, 1996; Galler *et al.*, 1994; Sieck & Prakash, 1997; Andruchov *et al.*, 2004), ATP consumption rate during isometric contraction and tension cost (Bottinelli *et al.*, 1994; Stienen *et al.*, 1996; Sieck & Prakash, 1997). Therefore, determination of MHC_i composition (cellular marker of contractile phenotype) provides an insight into the functional characteristics of a fibre and, as such, has been used for fibre type identification (see below).

1.3.4 Muscle fibre types

Muscle fibres within and across skeletal muscles exhibit marked heterogeneity with respect to their physiological, biochemical, and morphological characteristics, but they can be classified into various groups/types based on a number of criteria:

a. Histochemical approach:

- (i) Staining patterns for myofibrillar actomyosin ATPase after alkaline and acid pre-incubation (Brooke & Kaiser, 1970; Staron & Pette, 1986).

(ii) Determination of metabolic phenotype as indicated by aerobic (e.g. succinate dehydrogenase – SDH) and anaerobic (e.g. lactate dehydrogenase – LDH) enzyme activities (Bottinelli & Reggiani, 2000).

One should note that these methods cannot accurately identify all fibre types, in particular hybrid fibres.

b. Twitch characteristics of a contracting fibre (Close, 1972) following:

(i) Maximal Ca^{2+} activation.

(ii) Electrical stimulation.

c. Calcium/strontium activation characteristics (Fink *et al.*, 1986)

d. Stretch activation kinetics (Galler *et al.*, 1994; Andruchov *et al.*, 2004)

e. MHC_i expression:

(i) Identified immunohistochemically using antibodies specific to MHC isoforms (Ecob-Prince *et al.*, 1989a, 1989b; Hoh & Hughes, 1989; Franchi *et al.*, 1990; Gorza, 1990; Lucas *et al.*, 2000).

(ii) Identified electrophoretically based on differences in electrophoretic mobility on SDS-polyacrylamide gels (SDS-PAGE) (Schiaffino *et al.*, 1989; LaFramboise *et al.*, 1990; Pette & Staron, 1997; Bortolotto *et al.*, 1999).

It is now generally accepted that the most suitable methods for the delineation and classification of the full spectrum of fibre types (i.e. pure and hybrid fibres) are those based on MHC_i expression (Pette *et al.*, 1999; Pette & Staron, 2000; Stephenson, 2001). However, there are limitations associated with the MHC_i -based immunohistochemistry and SDS-PAGE techniques (Schiaffino & Salviati, 1998; Pette *et al.*, 1999; Stephenson, 2006). For example, MHC_i -based immunohistochemistry is limited: (i) by the specificity of anti- MHC_i antibodies; (ii) in the detection of hybrid

fibre (in some cases); and, (iii) by an inability to quantify MHC_i proportions in individual hybrid fibres. By comparison, MHC_i migration during SDS-PAGE, combined with densitometric analysis, provides a means for the quantification of MHC_i proportions but does not allow assessment of the intramuscular distribution of fibre types. In the present study, fibre types were established based on MHC_i composition using single fibre SDS-PAGE.

1.3.5 Diversity and plasticity of skeletal muscle

There are many factors (e.g. architectural design, fibre size, fibre type composition, metabolic profile) that make each skeletal muscle unique in structure and function. Diversity in muscle phenotype is even observed in homologous muscles from different species or strains, and this diversity widens as new physiological, biochemical and genetic techniques are introduced. Moreover, skeletal muscles and their muscle fibres are not static elements but are adaptive and dynamic structures that have the capacity to alter their size and phenotypic properties under the influence of altered physiological or pathological conditions, a property referred to as *muscle plasticity*. This adaptive capability extends the potential diversity in the attributes of skeletal muscles, making each muscle a functionally customised and regulatable entity.

A variety of conditions can lead to changes in the size/mass and/or in the fibre type/MHC_i composition of a given muscle, a process referred to as *muscle transformation*. These include: (i) developmental maturation (Whalen, 1985; Pette & Staron, 1997; Staron, 1997; Rennie *et al.*, 2004); (ii) altered neuromuscular activity, as in models of chronic low-frequency stimulation (CLFS) (Simoneau & Pette, 1988;

Termin *et al.*, 1989; Leeuw & Pette, 1993; Jaschinski *et al.*, 1998; Peuker *et al.*, 1999), exercise training (Andersen & Henriksson, 1977; Jansson & Kaijser, 1977; Green *et al.*, 1984; Baumann *et al.*, 1987; Rennie, 1996) and spontaneous hyperactivity (Asmussen *et al.*, 2003); (iii) mechanical loading/unloading, by techniques such as synergist tenotomy/removal/ablation (Goldberg, 1967; Ianuzzo *et al.*, 1976; Baldwin *et al.*, 1982; Frischknecht & Vrbova, 1991; Frischknecht *et al.*, 1995; Roy *et al.*, 1982; Timson *et al.*, 1985; Yamaguchi *et al.*, 1996), load addition (Awede *et al.*, 1999), hypergravity (Picquet *et al.*, 2002; Bozzo *et al.*, 2004), microgravity (Fitts *et al.*, 2001) and hindlimb suspension (Fitts *et al.*, 1986; Rennie, 1996; Stevens *et al.*, 1999); and, (iv) alterations in the hormonal milieu (Lyons *et al.*, 1986; Falduto *et al.*, 1990; Biolo & Wolfe, 1993; Polla *et al.*, 1994; Staron *et al.*, 2000; Seene *et al.*, 2003; Rennie *et al.*, 2004; Harridge, 2006, 2007). Under these conditions, changes in the MHC_i expression of a muscle and its fibres may emerge as a sequential transition in fibre type/MHC_i composition in a fast-to-slow direction, in the order MHC IIb → MHC IId → MHC IIa, with the transition from MHC IIa → MHC I being often incomplete, or, conversely, in a slow-to-fast direction, in the order MHC I → MHC IIa → MHC IId → MHC IIb (Pette, 2006). *Transforming muscle* typically displays an increase in the number and complexity of hybrid fibres, which appear to bridge the gap between the disappearance of one *pure* fibre type/MHC isoform and the appearance of the next in these transition sequences. Based on the MHC_i combinations commonly observed in hybrid fibres of transforming muscle (I+IIa, IIa+IId, IIb+IId, I+IIa+IId, IIa+IIb+IId, I+IIa+IIb+IId), it has been suggested that the transition process follows a defined pattern [known as the ‘nearest neighbour’ rule of MHC_i expression (Pette & Staron, 1997)].

Regarding the concept of hybrid fibres, it is worth noting that:

- there are also reports of ‘atypical’ MHC expression in single fibres (e.g. MHC I + IIb; MHC I + IIc) that do not follow the ‘nearest neighbour’ rule (Caiozzo *et al.*, 1998, 2003; Talmadge *et al.*, 1999; Bortolotto *et al.*, 2000; Stephenson, 2001, 2006; Picquet *et al.*, 2002; O’Connell *et al.*, 2004).
- large proportions of hybrid fibres have been reported (Galler *et al.*, 1994; Bortolotto *et al.*, 2000; Caiozzo *et al.*, 2003) in ‘normal’ muscles (e.g. from adult animals, free from disease, displaying normal activity patterns), particularly in muscles of specialised function (Dammeijer *et al.*, 2000; Wu *et al.*, 2000; Korfage *et al.*, 2005; Ren & Mu, 2005). These findings suggest that the expression of hybrid fibres in ‘normal’ muscle may represent an avenue through which a muscle can expand its repertoire of activities.

Importantly, hybrid fibre expression appears to play a vital role in the remarkable ability of mammalian skeletal muscle to alter its fibre type composition in response to changing functional demands, thereby contributing to the diversity observed in skeletal muscle structure and function.

Recently, several signaling pathways have been proposed to mediate the plasticity of skeletal muscle with respect to fibre type-specific gene expression, as well as oxidative enzyme expression and mitochondrial biogenesis. These include: (a) intracellular Ca^{2+} signaling pathways which involve calcineurin and calcium/calmodulin-dependent protein kinases (referred to as *excitation-transcription coupling*) (Chin, 2005; Schiaffino *et al.*, 2006); (b) activation of an endogenous transcription factor, peroxisome proliferative-activated receptor δ (i.e. PPAR δ) (Wang *et al.*, 2004); (c) expression of the transcription co-factors peroxisome proliferator-

activated receptor- γ coactivator-1 α and -1 β (i.e. PGC-1 α and PGC-1 β) (Reznick & Shulman, 2006; Schiaffino *et al.*, 2006); and (d) activation of adenosine monophosphate-activated protein kinase (i.e. AMPK) (Reznick & Shulman, 2006).

1.3.6 Excitation-contraction-relaxation (E-C-R) cycle in mammalian skeletal muscle

The E-C-R cycle (see Figure 1.4) is a phrase used to describe the sequence of cellular events that take place in a skeletal muscle fibre (regardless of its MHC_i composition), and involve: (1) the initiation of an action potential (by neural stimulation or direct activation) and its propagation along the sarcolemma and transverse (T)-tubule system; (2) depolarization-induced activation of the dihydropyridine receptors (DHPRs) in the T-tubule and transmission of the signal from DHPRs to the sarcoplasmic reticulum (SR) where Ca²⁺ is stored; (3) activation of the ryanodine receptor (RyR)/Ca²⁺ release channel and the release of Ca²⁺ from the SR into the myoplasm; (4) a transient rise in [Ca²⁺]_i; (5) activation of the contractile apparatus by Ca²⁺, and generation of force; and, (6) a return of [Ca²⁺]_i to resting levels via Ca²⁺ re-uptake by the SR, resulting in muscle relaxation (Stephenson *et al.*, 1998; Berchtold *et al.*, 2000; Dulhunty, 2006; Payne & Delbono, 2006; Rizzuto & Pozzan, 2006).

For the production of force, Ca²⁺ ions released from the SR into the myoplasm bind to troponin-C, thereby activating the cross-bridge cycle (see Section 1.3.7). Cessation of the stimulus leads to a fall in [Ca²⁺]_i and a subsequent discontinuation of cross-bridge cycling (i.e. muscle relaxation) as Ca²⁺ returns to resting myoplasmic levels. The magnitude and time course of the transient rise in [Ca²⁺]_i is determined by the balance between the different Ca²⁺ fluxes associated with the SR and the reversible binding of Ca²⁺ to a variety of myoplasmic sites (Gillis, 1985; Stephenson *et al.*, 1998). The rate

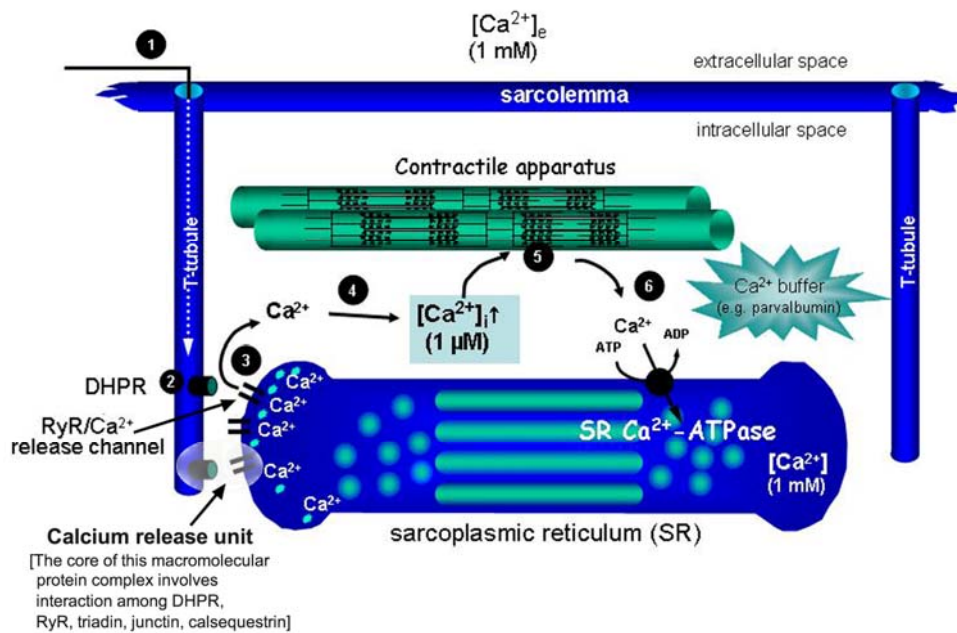


Figure 1.4 Schematic representation of the excitation-contraction-relaxation (E-C-R) cycle events in mammalian twitch muscle fibres. These events include: (1) action potential propagation along the sarcolemma and transverse (T)-tubule system; (2) depolarisation-induced activation of the dihydropyridine receptor (DHPR) in the T-tubule and transmission of the signal to the sarcoplasmic reticulum (SR) where Ca^{2+} is stored; (3) activation of the ryanodine receptor (RyR)/ Ca^{2+} release channel and the release of Ca^{2+} from the SR into the myoplasm; (4) transient rise in $[Ca^{2+}]_i$; (5) activation of the contractile apparatus by Ca^{2+} , with a subsequent generation of force; (6) a return of $[Ca^{2+}]_i$ to resting levels via Ca^{2+} re-uptake by the SR, resulting in muscle relaxation. The *calcium release unit* provides continuity from the lumen of the T-tubule to the lumen of the SR, and is modulated by interactions with a range of other cytoplasmic components (Dulhunty, 2006). Diagram courtesy of Dr Niels Ørtenblad, with modifications.

of SR Ca^{2+} release is dependent on several factors, including (i) the number of Ca^{2+} release channels, (ii) the average open time of Ca^{2+} release channels, and, (iii) the electrochemical gradient of Ca^{2+} across the SR membrane, while a return to resting $[\text{Ca}^{2+}]_i$ requires all released Ca^{2+} to be re-sequestered by the SR via ATP-dependent Ca^{2+} pumps [also known as the sarco/endoplasmic reticulum Ca^{2+} -ATPase (SERCA)].

Given its role in controlling $[\text{Ca}^{2+}]_i$, the SR is a pivotal organelle in the force generation of a muscle or fibre, determining in part the kinetics of contraction/relaxation, and, in repetitive stimulation, the susceptibility of the muscle or fibre to fatigue (Berchtold *et al.*, 2000). The SR is a membranous network surrounding each myofibril and is composed of two major regions relevant to the E-C-R cycle: (i) the terminal cisternae (TC); and, (ii) the longitudinal tubules (LT) (see Figure 1.5). At specific locations in the sarcomere, specialised junctions (called ‘triads’) are formed between the T-tubule and two neighbouring TC (Franzini-Armstrong, 2004; Dulhunty, 2006). These structures are involved in the transmission of the excitatory signal from the surface membrane to the SR via a macromolecular protein complex (known as the ‘calcium release unit’) that extends from the lumen of the T-tubule to the lumen of the SR, and includes DHPRs/voltage sensors and the RyR/ Ca^{2+} release channel (Dulhunty, 2006) (see Figure 1.4). The DHPR undergoes a conformational change upon depolarization of the T-tubule membrane and the activated DHPR is proposed to interact mechanically with the RyR to release Ca^{2+} from the TC (Payne & Delbono, 2006). In contrast, the longitudinal tubules, which run parallel to the myofibrils, contain a high density of SR Ca^{2+} pumps (Franzini-Armstrong, 2004; Rizzuto & Pozzan, 2006), which act against a large electrochemical gradient of Ca^{2+} and are responsible for SR Ca^{2+} re-uptake following stimulation.

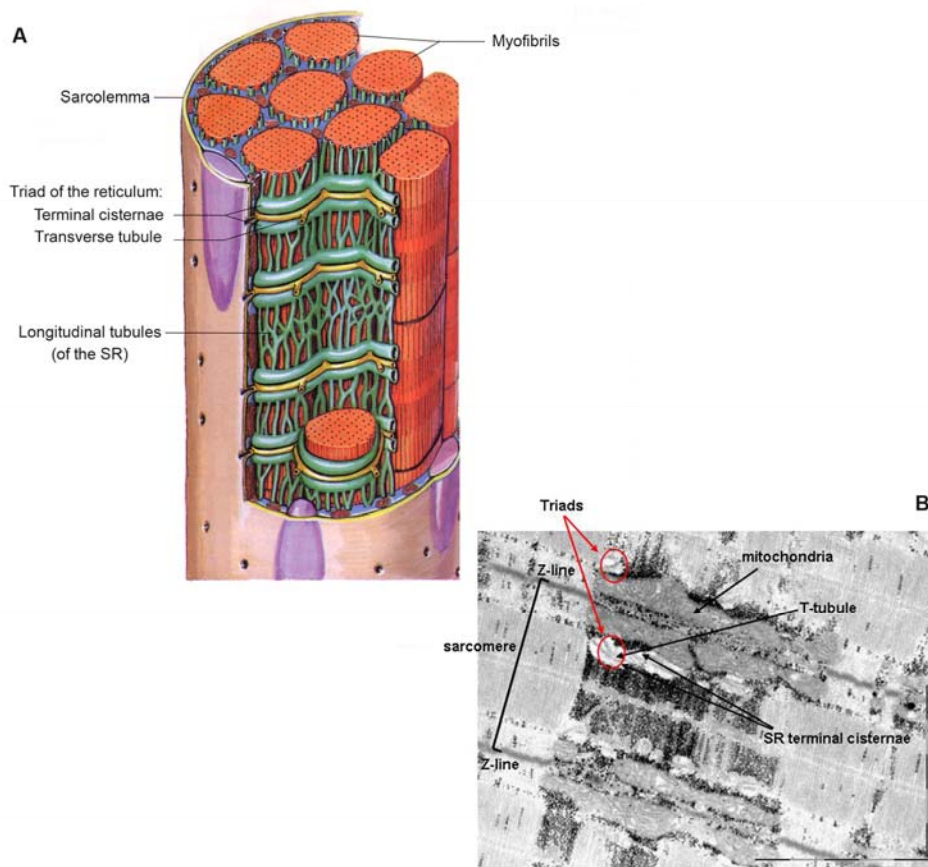


Figure 1.5 Sarcoplasmic reticulum (SR) and transverse tubule (T-tubule) system.

The SR is a membranous network surrounding each myofibril and is composed of two major regions: (i) the terminal cisternae (TC) and (ii) the longitudinal tubules (LT). The TC interacts with the T-tubules, forming a ‘triad’ (where one TC lies to each side of the T-tubule) - this structure is involved in the transmission of the excitatory signal from the surface membrane to the SR, causing SR Ca^{2+} release. The LT, which run parallel to the myofibrils, contain a high density of SR Ca^{2+} pumps (responsible for SR Ca^{2+} re-uptake following stimulation).

A. From Powers & Howley (2001) with modifications. B. Electron microscope image (x 20,000 magnification) of mammalian skeletal muscle (courtesy of Dr Niels Ørtenblad).

Fast-twitch and slow-twitch fibres differ in many structural and functional features relevant to the E-C-R cycle, including the rate of action potential propagation (Stephenson *et al.*, 1998), area/volume of T-tubule system, TC and SR (Bárány *et al.*, 1965; Luff & Atwood, 1971; Dulhunty *et al.*, 1986; Rüegg, 1992), DHPR concentration (Lamb & Walsh, 1987), SR Ca^{2+} concentration (Fryer & Stephenson, 1996), Ca^{2+} cycling kinetics (Fryer & Neering, 1989), SR Ca^{2+} pump concentration (Dulhunty *et al.*, 1987; Everts *et al.*, 1989) and SERCA isoform expression (Brandl *et al.*, 1987; Loukianov *et al.*, 1998; Johansson *et al.*, 2003).

1.3.7 Sliding filament theory

The sliding filament theory (Huxley & Hanson, 1954; Huxley & Niedergerke, 1954) provides the current paradigm for the molecular mechanisms involved in skeletal muscle contraction. According to this mechanical model, myosin heads (i.e. S1 fragments) projecting from the thick filament form a physical link (termed a *cross-bridge*) with actin of the thin filament, and hydrolysis of ATP by myosin induces sliding of the inter-digitating thick and thin filaments of the sarcomere past one another (i.e. sarcomere shortening). Force is developed by a change in the structure of the cross-bridge, usually conceptualised as a change in the angle at which the myosin head binds to actin (Geeves, 1991). As mentioned in Section 1.3.2, this idea is known as the swinging-lever-arm hypothesis, where the major conformational change involves rotation of the myosin neck region driven by more subtle changes in the catalytic domain (Cooke, 1997; Sweeney & Houdusse, 2004).

Figure 1.6 illustrates the kinetic model of the cross-bridge cycle (i.e. actomyosin ATPase reaction) in skeletal muscle (Geeves, 1991; Moss *et al.*, 1995; Cooke, 1997;



Gordon *et al.*, 2000). A cross-bridge cycle is the sequence of events from the binding of the myosin head to actin until the next binding (to repeat the cycle), and this occurs independently of other cross-bridges in the sarcomere. As such, at the conclusion of the previous cross-bridge cycle (see $A + M^* \cdot ATP$ in Figure 1.6), ATP hydrolysis by the myofibrillar ATPase (associated with the myosin head) takes place, resulting in an intermediate state ($A + M \cdot ADP \cdot P_i$) that precedes the formation of an actomyosin complex. When the muscle fibre is next activated by an increase in $[Ca^{2+}]_i$, myosin attaches to actin in a weakly-bound, low-force state ($A \cdot M \cdot ADP \cdot P_i$). The following release of inorganic phosphate (P_i) from the ATPase site on the MHC is coupled to the transition in actomyosin binding from this weakly-bound, low-force state to a strongly-bound, high-force state ($A \cdot M^* \cdot ADP$) and cross-bridge movement/force generation (i.e. structural change in myosin). The actomyosin complex must be broken (i.e. cross-bridge detachment) in order for the myosin head to attach to a new actin monomer, so as to repeat the cross-bridge cycle; this occurs when ATP binds to myosin ($A + M^* \cdot ATP$).

1.3.8 *Parameters describing the isometric contraction of an isolated skeletal muscle*

The pattern of force development that results from neural stimulation or direct activation of a muscle, motor unit or muscle fibre is determined by the number and frequency of stimulations delivered. For *in vitro* muscle preparations, a variety of parameters describing the magnitude and duration of a contraction have been reported, and Table 1.2 lists many of the commonly-used descriptors and what each is proposed to represent from a mechanistic viewpoint.

Table 1.2 Isometric contractile response.

Parameter measured	Functional parameter/s represented by the measured parameter	References
<i>Twitch</i>		
Peak specific force (P_t)	The number of cross-bridges acting in parallel in a strongly-bound, high-force state at submaximal $[Ca^{2+}]_i$ Force per cross-bridge	Moss <i>et al.</i> , 1995; Fitts & Balog, 1996.
Time to peak twitch force (TPT)	Time course of the increase in $[Ca^{2+}]_i$ Rate of Ca^{2+} release from the SR	Close, 1972; Fitts & Widrick, 1996.
Half-relaxation time (1/2RT)	Rate of SR Ca^{2+} uptake Rate of Ca^{2+} dissociation from troponin-C Rate of cross-bridge detachment	Close; 1972; Gillis, 1985; Fitts & Widrick, 1996.
Width at half-amplitude (W_{50})	Time course of the Ca^{2+} transient	Posterino & Lamb, 2003.
<i>Tetanus</i>		
Peak specific force (P_o)	The number of cross-bridges acting in parallel in a strongly-bound, high-force state at high $[Ca^{2+}]_i$ Force per cross-bridge	Moss <i>et al.</i> , 1995; Fitts & Balog, 1996; Fitts & Widrick, 1996.
Peak rate of force development (+dP/dt)	Limited by the rate of cross-bridge transition from a weakly-bound low-force state to the strongly-bound, high-force state Rate of Ca^{2+} release from the SR Rate of Ca^{2+} binding to troponin-C	Fitts & Holloszy, 1977, 1978; Fitts & Widrick, 1996; Gordon <i>et al.</i> , 2000.
Half-relaxation time (1/2RT _{tet})	Rate of SR Ca^{2+} uptake Rate of cross-bridge detachment Ca^{2+} dissociation from troponin-C Rate of Ca^{2+} binding to high affinity Ca^{2+} binding myoplasmic proteins (e.g. parvalbumin)	Close; 1972; Gillis, 1985; Gordon <i>et al.</i> , 2000; Allen <i>et al.</i> , 2007.
Peak rate of relaxation (-dP/dt)	Non-uniform sarcomere behaviour (sarcomere shortening/lengthening)	Edman, 1980; Gillis, 1985; Allen <i>et al.</i> , 1995; Fitts & Widrick, 1996; Telley <i>et al.</i> , 2006.
Rate of linear phase of relaxation	Net rate of cross-bridge detachment	Westerblad & Lännergren, 1991; Gillis, 1985; Allen <i>et al.</i> , 1995.

SR – sarcoplasmic reticulum.

1.3.8.1 Isometric twitch response

The contractile response resulting from a single maximal stimulus is referred to as a *twitch*. There is a short delay from excitation to the first evidence of force development (known as the electromechanical delay) and this occurs due to the time required for T-tubule activation/signal conduction, release of Ca^{2+} from the SR, binding of Ca^{2+} to troponin-C, and initiation of cross-bridge cycling (and, hence, force development). The amount of Ca^{2+} bound to troponin-C depends on the magnitude and duration of the Ca^{2+} transient, thereby determining the number of cross-bridges that participate in force development and the time course of the entire twitch response. Muscle relaxation (that is, the discontinuation of cross-bridge cycling) is then brought about by Ca^{2+} removal from troponin-C and the cytoplasm due to the pumping action of the SR Ca^{2+} -ATPase.

Figure 1.7 shows a representative illustration of an isometric twitch contraction, indicating several commonly used descriptors of the response (Close, 1972; Taylor *et al.*, 1980; Gillis, 1985; Moss *et al.*, 1995; Fitts & Widrick, 1996) such as peak force (P_t), time taken to generate peak twitch force (TPT) [also referred in the literature as *contraction time* (e.g. Taylor *et al.*, 1980)], and time taken for force to decrease from its peak value to 50% of the peak value (1/2RT) (referred to as *half-relaxation time of the twitch*). The duration of the twitch response measured at half amplitude (W_{50}) (Posterino & Lamb, 2003) is also shown.

1.3.8.2 Isometric tetanus response

A muscle, motor unit or muscle fibre that is stimulated repeatedly (such that each stimulus arrives before complete relaxation) experiences a phenomenon known as

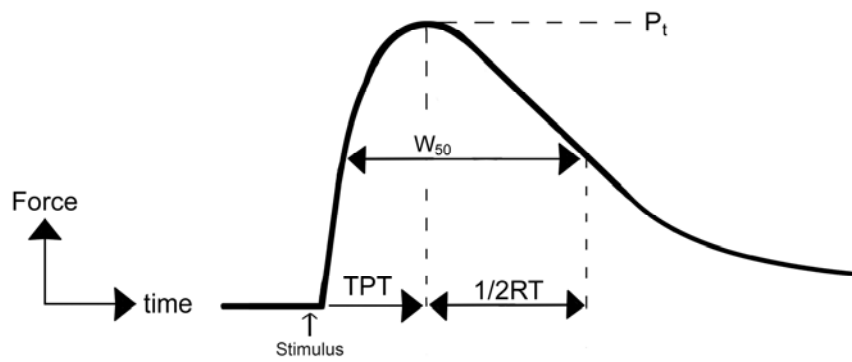


Figure 1.7 Parameters used to describe the isometric twitch response of skeletal muscle. Peak force (P_t); time to peak twitch force (TPT); time for P_t to decay 50% ($1/2RT$); duration of the twitch measured at half amplitude (W_{50}).

force summation, where the force developed is greater than that of a single twitch. With progressively greater stimulation frequencies comes an increase in the amount of force generated, to a point where the frequency of stimulation is high enough that the force curve becomes smooth and greater frequencies do not elicit significant increases in force. This force is commonly called the maximum isometric force (P_o) and the contractile response is referred to as a *tetanus*. Under isometric conditions, these increases in force generated at progressively greater stimulation frequencies, up to that which elicits P_o , can be used to plot a force-frequency relationship, which, in turn, describes the influence that recruitment frequency has on the force generated by a muscle.

Figure 1.8 shows a representative illustration of an isometric tetanus response, indicating several parameters that are commonly used to describe the response (Close, 1972; Gillis, 1985; Allen *et al.*, 1995; Fitts & Widrick, 1996), including peak isometric force (P_o), peak rate of force development ($+dP/dt$), time from the last stimulus to the point where force reached 50% of the peak value ($1/2RT_{tet}$) (referred to as *half-relaxation time of the tetanus*), and peak rate of relaxation ($-dP/dt$). As shown in Figure 1.8, the fall in force during relaxation of the tetanus often displays two distinct phases: (i) the linear (slow) phase, and (ii) the exponential (fast) phase. During the linear phase, there is no change in sarcomere length (Huxley & Simmons, 1970; Gillis, 1985; Allen *et al.*, 1995) and, thus, this phase has been related to the kinetics of isometric cross-bridge detachment (Gillis, 1985; Allen *et al.*, 1995), whereas the exponential phase involves non-uniform changes in sarcomere length (Edman, 1980; Allen *et al.*, 1995; Telley *et al.*, 2006).

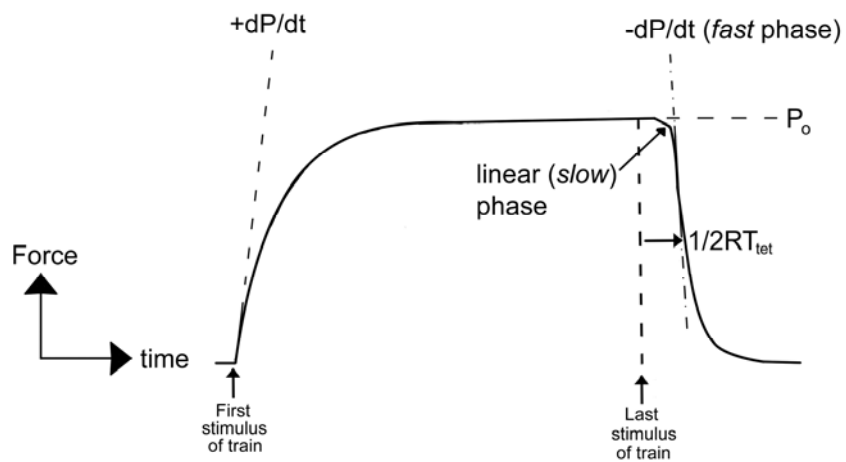


Figure 1.8 Parameters used to describe the isometric tetanus response of skeletal muscle. Peak force (P_o), peak rate of force development ($+dP/dt$), peak rate of relaxation ($-dP/dt$), time for P_o to decay 50% ($1/2RT_{tet}$), slope and duration of the linear phase of relaxation.

It is worth noting that these commonly used parameters for describing the magnitude and the time course of a twitch or tetanus response are dependent on: (i) the species from which the muscle was obtained (Close, 1972; Rome *et al.*, 1988; Pellegrino *et al.*, 2003; Andrucho *et al.*, 2004); (ii) the temperature of the muscle during experimentation (Close, 1972; Taylor *et al.*, 1980; Segal & Faulkner, 1985); and, (iii) the fibre type composition of the muscle under investigation (Close, 1964, 1969, 1972; Bárány & Close, 1971; Salmons & Sréter, 1976; Fitts *et al.*, 1982; Roy *et al.*, 1982; Saltin & Gollnick, 1983; Troup *et al.*, 1986; Brooks & Faulkner, 1988; Mounier *et al.*, 1989; Schluter & Fitts, 1994; Bottinelli *et al.*, 1996; Fitts & Widrick, 1996; Harridge *et al.*, 1996; Pette *et al.*, 1999; Bottinelli, 2001; Pette & Staron, 2001). The influence that fibre type composition has on these contractile parameters (and on the fatigue resistance of a skeletal muscle discussed below) can be attributed to the heterogeneity that exists among fibres with respect to a range of factors, including: (a) myofibrillar protein isoform content (Pette & Staron, 1990; Stevens *et al.*, 2006) and, in particular, MHC_i content (Staron, 1997; Pette *et al.*, 1999; Pette & Staron, 2000; Stephenson, 2001); (b) ATPase activity and tension cost (Bárány *et al.*, 1965; Bárány, 1967; Bottinelli *et al.*, 1994; Schluter & Fitts, 1994; Stienen *et al.*, 1996; Sieck & Prakash, 1997; Han *et al.*, 2003); (c) E-C-R cycle characteristics such as the rate of action potential propagation (Stephenson *et al.*, 1998), area/volume of T-tubule system, TC and SR (Bárány *et al.*, 1965; Luff & Atwood, 1971; Dulhunty *et al.*, 1986; Rüegg, 1992), DHPR concentration (Lamb & Walsh, 1987), SR Ca²⁺ concentration (Fryer & Stephenson, 1996), Ca²⁺ cycling kinetics (Fryer & Neering, 1989), Ca²⁺-ATPase concentration (Dulhunty *et al.*, 1987; Everts *et al.*, 1989) and parvalbumin concentration (Heizmann *et al.*, 1982; Schmitt & Pette, 1991; Rall, 1996); and (d) metabolic parameters (Bass *et al.*, 1969; Essen *et al.*, 1975; Pette *et al.*, 1976;

Reichmann & Pette, 1982; Saltin & Gollnick, 1983; Gollnick *et al.*, 1985; Pette & Staron, 1990; Fitts, 1994). Based on these properties, the velocity of a contractile response for each fibre type increases in the order: type I < type IIA < type IID < type IIB, while the fatigue resistance of each fibre type decreases in the order: type I > type IIA > type IID > type IIB). It is also worth noting that the parameters describing the tetanic force response of a muscle are seen as providing more physiologically meaningful information about its functional status than parameters related to the twitch response (Powers & Howley, 2001; MacIntosh *et al.*, 2006).

1.3.9 *Muscle fatigue*

As mentioned at the beginning of Section 1.3, the predominant function of skeletal muscle is to generate force, but sustained activation is often accompanied by a contraction-induced reduction in this ability. This failure to reproduce equivalent expressions of force generation over time is termed *muscle fatigue*, with P_o being a better indicator of this phenomenon than P_t (Edwards *et al.*, 1977; Fitts & Holloszy, 1977, 1978; Thompson *et al.*, 1992). Fatiguing stimulation also leads to a slowing in the kinetics of contractile responses (i.e. the time for force development and, in particular, relaxation), with these phenomena occurring under voluntary and *in vitro* conditions (Edwards *et al.*, 1977; Fitts and Holloszy, 1977, 1978; Jones, 1981; Fitts *et al.*, 1982; Thompson *et al.*, 1992; Fitts, 1994; Allen *et al.*, 2007). Importantly, a reduction in the ability of a muscle to generate force and/or shorten as required may result in a loss of performance at the whole-organism level; thus, the fatigue resistance of a muscle is an important indicator of its functional status.

Many factors have been implicated in the process of muscle fatigue (Larsson *et al.*, 1991; Westerblad *et al.*, 1991; Fitts, 1994; Stephenson *et al.*, 1995; Williams & Klug, 1995; Chin *et al.*, 1997; Gandevia, 1998; Nielsen & Harrison, 1998; Sahlin *et al.*, 1998; Stephenson *et al.*, 1998; Ward *et al.*, 1998; Westerblad *et al.*, 1998; Allen, 2004; Rowley *et al.*, 2005; Allen *et al.*, 2007), and the contribution of each is dependent on a number of aspects, including: (i) intensity, duration and mode of activity; (ii) training status; and, (iii) muscle fibre type composition. As the command chain for voluntary force production is initiated in the brain and culminates in cross-bridge cycling in the muscle fibre, fatigue may be attributed to any one or more steps in this process. Traditionally, the steps in this chain of command have been partitioned into (i) central (neural) processes, and (ii) peripheral (muscular) processes (Edwards, 1981; Sahlin, 1992; Fitts & Balog, 1996), with a substantial component of fatigue resulting from force failure at the peripheral level (Bigland-Ritchie *et al.*, 1986).

Possible mechanisms of peripheral muscle fatigue include: (i) energy deficiency, where the rate of ATP utilisation exceeds ATP supply, and includes situations of reduced substrate availability; (ii) an accumulation of metabolic products that impair contractile events; (iii) changes in intracellular and extracellular muscle electrolyte concentrations that impair muscle excitability; and, (iv) alterations in SR Ca^{2+} handling properties that limit the activation and relaxation of the contractile apparatus (Dawson *et al.*, 1978; Jones, 1981; Godt & Nosek, 1989; Westerblad *et al.*, 1991; Williams & Klug, 1995; Nielsen & Clausen, 1996; Chin *et al.*, 1997; Sahlin *et al.*, 1998; Stephenson *et al.*, 1998; Westerblad *et al.*, 1998; Allen & Westerblad, 2001; Allen, 2004; Allen *et al.*, 2007). Attention to not only the pattern of activity that elicits

fatigue but also to the recovery phase from fatigue can provide insight into the contribution of each mechanism to the overall etiology of muscle fatigue.

1.3.9.1 Recovery from fatigue

In the quiescent period following fatiguing activity (with the assumption that sufficient substrate is available), muscle gradually restores its maximal force- or power-generating capacity. The time required to do so depends on factors such as: (i) the stimulation protocol employed to induce fatigue; (ii) the training status of the muscle; (iii) muscle fibre type composition; and, (iv) the type of exercise (i.e. concentric, isometric, eccentric) performed in the fatigue protocol (Edwards *et al.*, 1977; Fitts, 1994; Chin & Allen, 1996, 1998; Jones, 1996; Chin *et al.*, 1997; Rijkelijhuizen *et al.*, 2003). Fatigue resulting from continuous high frequency stimulation [termed *high-frequency fatigue* (HFF)] is rapidly reversed by reducing the frequency of stimulation, with a large proportion of force recovery occurring in a few seconds (Jones, 1981; Westerblad *et al.*, 1991; Cairns & Dulhunty, 1995). This type of fatigue is not thought to occur during normal voluntary skeletal muscle activity (Jones, 1981; Westerblad *et al.*, 1991).

The loss in force production resulting from repeated short tetani (i.e. of lesser intensity than that of HFF) is correlated with changes in intracellular ionic and metabolite concentrations. This form of fatigue is often referred to as *metabolic fatigue* and involves decreases in cellular resources (e.g. creatine phosphate, glycogen, ATP), accumulation of metabolic by-products with potential deleterious effects (e.g. P_i , H^+ , lactate), and changes in muscle ion concentrations (e.g. Na^+ , K^+ , Ca^{2+} , Mg^{2+}) (Dawson *et al.*, 1978; Cooke & Pate, 1985; Metzger & Fitts, 1987a; Godt

& Nosek, 1989; Westerblad *et al.*, 1991; Fitts, 1994; Moss *et al.*, 1995; Chin *et al.*, 1997; Westerblad *et al.*, 1997a; Allen & Westerblad, 2001; Allen, 2004). Recovery from metabolic fatigue appears to occur in two phases: (i) a rapid phase lasting a few minutes, involving the normalisation of cellular energy potential and restoration of a normal intracellular/extracellular ionic milieu (Westerblad *et al.*, 1991; Fitts & Balog, 1996; Jones, 1996; Nielsen & Harrison, 1998; Sahlin *et al.*, 1998), and (ii) a slower phase (< 60 min) where pre-exercise force-generating capacity returns (Edwards *et al.*, 1977; Westerblad *et al.*, 1993; Chin & Allen, 1997, 1998; Chin *et al.*, 1997).

In some cases of repeated contractions, a very slow rate of force recovery occurs (i.e. hours or days). The defining characteristic of this form of fatigue is a proportionally greater loss of force-generating ability at low frequencies of stimulation (i.e. ≤ 30 Hz) compared with high frequencies of stimulation (e.g. ≥ 50 Hz). Thus, this phenomenon is referred to as *low-frequency fatigue* (LFF) (Edwards *et al.*, 1977; Westerblad *et al.*, 1993; Chin & Allen, 1996; Jones, 1996; Chin *et al.*, 1997; Allen *et al.*, 2007). This LFF has been observed in isolated single muscle fibres, *in situ* and *in vitro* whole muscle/bundle preparations and human muscle *in vivo* (Edwards *et al.*, 1977; Moxham *et al.*, 1980; Jones *et al.*, 1982; Westerblad *et al.*, 1993; Chin & Allen, 1996; Jones, 1996; Chin *et al.*, 1997; Rijkelijhuizen *et al.*, 2003). It can result from both low (duty cycle ~ 0.1) and high (duty cycle ~ 0.3) intensity stimulation protocols *in vitro* (Chin & Allen, 1998) and from a variety of exercise intensities and modes and types of contraction *in vivo* (Edwards *et al.*, 1977; Ratkevicius *et al.*, 1998). Due to its long lasting nature, LFF is unlikely to have a metabolic/ionic basis (Edwards *et al.*, 1977; Chin *et al.*, 1997), and it occurs in the presence of normal action potentials (Edwards *et al.*, 1977; Westerblad *et al.*, 1993; Allen *et al.*, 2007). The etiology of

LFF remains equivocal, but reductions in SR Ca^{2+} release and alterations in $[\text{Ca}^{2+}]_i$ leading to disturbed E-C coupling have been implicated (Edwards *et al.*, 1977; Edwards, 1981; Westerblad *et al.*, 1993; Lamb *et al.*, 1995; Chin & Allen, 1996; Allen *et al.*, 2007). Furthermore, LFF is more prominent following eccentric exercise than isometric and concentric work, suggesting that mechanical stress/structural damage may also disrupt normal E-C coupling mechanisms (Bruton *et al.*, 1995; Jones, 1996; Rijkeljkhuizen *et al.*, 2003; Allen *et al.*, 2007). The majority of work probing LFF has employed fast-twitch muscles/fibres and, thus, data are sparse regarding the susceptibility of slow-twitch muscles to LFF.

1.3.9.2 Fatigue and muscle metabolism

Metabolic factors play an important role in a muscle's ability to sustain contractile activity, with the metabolic profile of a muscle, in large part, determined by its fibre type composition (Edström & Kugelberg, 1968; Burke *et al.*, 1973; Saltin & Gollnick, 1983; Pette, 1985). These metabolic properties, which refer to the preferred substrate/s and to the metabolic capacities of the anaerobic and aerobic energy pathways, are determined by the content and activity levels of the enzymes involved in these bioenergetic pathways (Bass *et al.*, 1969; Pette, 1985).

The fatigue resistance of a skeletal muscle is positively correlated with its aerobic-oxidative capacity (Burke, 1981; Saltin & Gollnick, 1983; Pette, 1985). This relationship is supported by ample evidence that fatigue-resistant slow-twitch fibres/muscles display greater contents and higher activity levels of aerobic-oxidative enzymes (e.g. enzymes of the tricarboxylic acid cycle, electron transport chain, and β -oxidation) and lower activity levels of glycolytic enzymes, while the more fatigable

fast-twitch fibres/muscles usually present a lower relative aerobic-oxidative-to-anaerobic-glycolytic profile (Bass *et al.*, 1969; Nolte & Pette, 1972; Burke, 1981; Reichmann & Pette, 1982; Pette, 1985). It should be noted, though, that there exists a large degree of heterogeneity among fibres and muscles of the same type with respect to these enzyme activity patterns (Nolte & Pette, 1972; Spamer & Pette, 1980; Reichmann & Pette, 1982).

The metabolic profile of skeletal muscle is qualitatively and quantitatively adjusted to reflect its functional requirements (Pette, 1985). Therefore, the metabolic enzyme pattern may be used as an indicator of change in the functional capacity of a muscle. An increased presence of mitochondrial enzymes would indicate a greater capacity to synthesise ATP by aerobic-oxidative pathways, while an increase in the capacity for glycogenolysis, glycolysis and lactate fermentation would reflect a greater anaerobic-glycolytic potential (Bass *et al.*, 1969; Pette, 1985).

1.3.9.3 Lactate dehydrogenase (LDH) as a marker of metabolic capacity/phenotype

LDH plays a critical role in glycolytic metabolism, as it catalyses the reversible reaction:



This reaction is vital for the maintenance of intracellular levels of NAD^+ . LDH provides an avenue for tissues to generate a temporary oxygen debt in the form of accumulated lactate, to be later removed by the re-oxidation of lactate to pyruvate in the presence of oxygen (Markert, 1984).

LDH exists in different molecular forms (isoenzymes). In skeletal muscle, there are five isoenzymes, and these are tetramers generated by different associations of two different subunits (Dawson *et al.*, 1964; Markert, 1984) that are coded for by two different genes (Tsuji *et al.*, 1994; Rossignol *et al.*, 2003). The nomenclature for these subunits, and subsequent isoenzymes, differs in the literature. The two subunits have been termed: (i) M (muscle) and H (heart) (Dawson *et al.*, 1964; Thorling & Jensen, 1966; Leberer & Pette, 1984; Acosta *et al.*, 2005) in recognition of the tissues in which they are predominant, or (ii) A and B (Markert, 1984; Tsuji *et al.*, 1994; Andrade & McMullen, 2006). The resulting five combinations that form the LDH tetramers (i.e. isoenzymes) have been dubbed (in the same respective order): (i) M₄, HM₃, H₂M₂, H₃M and H₄ (Dawson *et al.*, 1964; Thorling & Jensen, 1966; Acosta *et al.*, 2005); (ii) A₄, A₃B, A₂B₂, AB₃ and B₄ (Markert, 1984); (iii) LDH5, LDH4, LDH3, LDH2 and LDH1 (Vesell & Yielding, 1966; Dietz & Lubrano, 1967; Prochazka *et al.*, 1970; Leberer & Pette, 1984; Otis *et al.*, 2004; Acosta *et al.*, 2005); (iv) LD5, LD4, LD3, LD2 and LD1 (Wilkinson & Withycombe, 1965; Rosalki, 1970). This order represents the migration pattern (from least to greatest distance travelled) of the five isoenzymes when separated by gel electrophoresis. For the purposes of the present work, the five isoenzymes will be referred to as: LDH5-M₄, LDH4-HM₃, LDH3- H₂M₂, LDH2-H₃M and LDH1-H₄.

The different LDH isoenzymes have been associated with different modes of metabolism, with LDH5-M₄ maintaining activity at relatively high pyruvate concentrations, while LDH1-H₄ becomes inhibited in such conditions (Dawson *et al.*, 1964). This inhibition of LDH1-H₄ by pyruvate favours oxidative metabolism. As a consequence, the LDH5-M₄ isoenzyme predominates in fast-twitch skeletal muscle,

while the predominance of the H subunit characterises the LDH isoenzyme profile of slow-twitch muscle, with all five LDH isoenzymes being often present (Dawson *et al.*, 1964; Briand *et al.*, 1981; Leberer & Pette, 1984; Pette, 1985; Otis *et al.*, 2004). Therefore, the proportional LDH isoenzyme distribution of a skeletal muscle may be used as a marker of its normal anaerobic-glycolytic and aerobic-oxidative capacity, and for monitoring changes in its metabolic profile when subjected to altered pathological/physiological conditions.

1.4 Obesity and skeletal muscle

Data exist to indicate that obesity is associated with alterations in the structure of skeletal muscle (Kelley & Storlien, 2004), especially in rodent models of obesity (see below). It has been suggested that these alterations, which may arise as a consequence of obesity, may contribute to the pathogenesis of, and the pathologies associated with, obesity (Mrad *et al.*, 1992; Simoneau & Kelley, 1998; Mercier *et al.*, 1999; Ryder *et al.*, 2001). Importantly, alterations to the structure and composition of skeletal muscle may influence its contractile performance. Therefore, in this section is addressed the current knowledge regarding the structure and functional status of skeletal muscle in rodent models of obesity.

1.4.1 Structural alterations in skeletal muscle as a contributor to the pathogenesis of/pathologies associated with obesity

It has been proposed (Lillioja *et al.*, 1987; Wade *et al.*, 1990; Hickey *et al.*, 1995; Helge *et al.*, 1999) that muscles from obese individuals contain a greater proportion of type II fibres than muscles from non-obese controls, and that this difference in fibre type composition may contribute to the pathogenesis of/pathologies associated with

obesity (Simoneau & Kelley, 1998; Ryder *et al.*, 2001). This is because, compared with type I fibres and type I fibre-rich muscles, type II fibres and type II fibre-rich muscles have a lower insulin binding capacity, insulin-stimulated glucose uptake, glucose transport protein (GLUT-4) content (Bonen *et al.*, 1981; Henriksen *et al.*, 1990; Marette *et al.*, 1992; Megeney *et al.*, 1993) and capacity for fatty acid metabolism (uptake, oxidation, storage) (Essen *et al.*, 1975; Dyck *et al.*, 1997; Bonen *et al.*, 1998; Malenfant *et al.*, 2001).

It is worth noting that there are marked discrepancies among studies concerned with the fibre type/MHC_i composition of skeletal muscles from obese rodents. Thus, across a range of diverse skeletal muscles:

- (i) type I fibre/MHC I isoform proportions have been reported to increase (Farkas *et al.*, 1994; Powers *et al.*, 1996; Tankersley *et al.*, 1998) and decrease (Torgan *et al.*, 1989; Mrad *et al.*, 1992; He *et al.*, 1995);
- (ii) type IIA fibre/MHC IIa isoform proportions have been reported to increase (Farkas *et al.*, 1994; Powers *et al.*, 1996; Tankersley *et al.*, 1998; Warmington *et al.*, 2000) and decrease (Powers *et al.*, 1996);
- (iii) type IIB fibre/MHC IIb isoform proportions have been reported to decrease (Almond & Enser, 1984; Powers *et al.*, 1996; Tankersley *et al.*, 1998; Warmington *et al.*, 2000);
- (iv) type IID fibre/MHC II_d isoform proportions have been reported to decrease (Powers *et al.*, 1996; Tankersley *et al.*, 1998);
- (v) no alterations in fibre type/MHC_i proportions have been reported (Burbach *et al.*, 1985; Torgan *et al.*, 1989; Stickland *et al.*, 1994; He *et al.*, 1995).

Some of the aforementioned studies (Almond & Enser, 1984; Burbach *et al.*, 1985; Torgan *et al.*, 1989; Mrad *et al.*, 1992; Farkas *et al.*, 1994; Stickland *et al.*, 1994; He *et al.*, 1995; Warmington *et al.*, 2000) used histochemistry-based methods for identifying fibre type composition, and, as discussed in Section 1.3.4, such methods cannot accurately identify hybrid fibres. So far, there have been no reports of the fibre composition of skeletal muscles from obese animals based on MHC isoform analysis at the single fibre level.

1.4.2 Structural alterations in skeletal muscle as a consequence of obesity

It is well-established that skeletal muscles of obese animals, across a variety of obesity models (e.g. genetic; chemically-induced; dietary-induced) and species (e.g. mouse; rat), are smaller than those of control (lean) animals (Shapira *et al.*, 1980; Trostler *et al.*, 1982; Durschlag & Layman, 1983; Almond & Enser, 1984; Champion *et al.*, 1984; Smith & Romsos, 1984; Burbach *et al.*, 1985; Wardlaw *et al.*, 1986; Stickland *et al.*, 1994; Warmington *et al.*, 2000; Bruton *et al.*, 2002). The mechanisms that underlie this phenomenon are poorly defined, as is the contribution of single muscle fibre morphology to the reduced whole muscle size (Almond & Enser, 1984; Champion *et al.*, 1984; Torgan *et al.*, 1989; Stickland *et al.*, 1994; He *et al.*, 1995; Warmington *et al.*, 2000).

In *ob/ob* mice, the reductions in skeletal muscle mass do not appear to be related to delayed maturity (Almond & Enser, 1984). Therefore, it has been proposed that the persistent metabolic aberrations associated with obesity may alter the balance between protein synthesis and breakdown in skeletal muscle (Trostler *et al.*, 1979; Almond & Enser, 1984). As briefly mentioned in Section 1.2.2, *elevated glucocorticoid* levels

play a key role in the development of obesity in rodent models (York & Hansen, 1998), but glucocorticoids are also implicated in muscle atrophy (Goldberg & Goodman, 1969; Polla *et al.*, 1994; Hasselgren, 1999; Seene *et al.*, 2003). In *ob/ob* mouse, circulating levels of the glucocorticoid corticosterone are raised (Dubuc, 1976b; Smith & Romsos, 1984; Bray *et al.*, 1989; Tsai & Romsos, 1991), as is its sensitivity to the hormone (Tokuyama & Himms-Hagen, 1987). In fact, when circulating concentrations of corticosterone were lowered by adrenalectomy, *ob/ob* mice displayed improvements in muscle mass gain (Smith & Romsos, 1985). Furthermore, glucocorticoids up-regulate myostatin expression (Ma *et al.*, 2001), a growth factor that acts as a negative regulator of skeletal muscle mass (Zimmers *et al.*, 2002; Glass, 2003; Rennie *et al.*, 2004; Sartorelli & Fulco, 2004). Increased myostatin expression in rats via dexamethasone administration has been shown to lead to muscle atrophy (Ma *et al.*, 2003), while in *ob/ob* mice lacking the myostatin gene, muscle mass was twice that of conventional *ob/ob* mice at three months of age (McPherron & Lee, 2002). Taken together, these data suggest that an amplified glucocorticoid presence may be involved in the smaller skeletal muscle mass common to obese rodents.

Elevated levels of pro-inflammatory *adipokines* (see Section 1.1.1) have also been implicated in accelerated muscle protein degradation and are linked to the marked skeletal muscle atrophy of several physiological/pathological states, including cancer-induced cachexia, sepsis, rheumatoid arthritis and sarcopenia (Goodman, 1991; Llovera *et al.*, 1994; Rall *et al.*, 1996; Tisdale, 1997; Guttridge *et al.*, 2000; Li & Reid, 2000; Roubenoff, 2000; Pedersen *et al.*, 2003a; Dirks & Leeuwenburgh, 2006; Gea *et al.*, 2006). In animals treated with exogenous TNF- α (Fong *et al.*, 1989;

Goodman, 1991; Buck & Chojkier, 1996) or expressing a transgene (Cheng *et al.*, 1992), losses in muscle mass are observed. In differentiated skeletal muscle myotubes treated with TNF- α , specific losses in myosin heavy chain (MHC) were observed without increases in synthesis, indicating that, in the absence of other exogenous anabolic factors, TNF- α induces MHC proteolysis (Li *et al.*, 1998). Furthermore, Buck & Chojkier (1996) reported structural irregularities consisting of smaller fibres in skeletal muscles from mice receiving exogenous TNF- α . TNF- α and other adipokines (e.g. IL-1 β and IL-6) are also reported to decrease the expression of skeletal muscle insulin-like growth factor 1 (IGF-1) (Lang & Frost, 2002), a hormone central to postnatal muscle growth (Rennie *et al.*, 2004). Therefore, with elevated levels of TNF- α present in obese mice (Hotamisligil *et al.*, 1993; Nakao *et al.*, 2000; Hotamisligil, 2006), this adipokine may also be a contributor to obesity-related decrements in skeletal muscle mass.

It is also noteworthy that increases in the activity of myofibril-bound protease in skeletal muscles of *ob/ob* mouse, which may lead to increased protein catabolism, have been reported (Trostler *et al.*, 1982). In this study, Trostler *et al.* (1982) showed protease activity to be related to reductions in muscle mass, with both being greatest in skeletal muscles containing higher proportions of fast-twitch fibres and lowest in soleus. The mechanism responsible for this increased myofibril-bound protease activity was not reported.

The overall function of skeletal muscles is determined not only by the muscle size but also by ultra-structural properties such as myofibrillar diameter, T-tubule dimensions and lattice spacing (Fitts *et al.*, 2001). However, to the author's knowledge, there exist

no published data addressing ultra-structural changes in skeletal muscles of *ob/ob* mouse.

1.4.3 Obesity and skeletal muscle contractility

The smaller size of skeletal muscles in obese animals (above) raises the possibility of contractile alterations that may affect the organism as a whole. Currently available data on the contractile function of skeletal muscle in rodent models of obesity are scarce and often conflicting. For example, there are only two studies that have addressed this issue in *ob/ob* mice (Warmington *et al.*, 2000; Bruton *et al.*, 2002). These studies have generated conflicting data with respect to the force-generating capacity and the fatigue resistance of EDL muscle from obese mice. Moreover, only one of these two studies (Bruton *et al.*, 2002) used single fibre preparations to gain further insight into mechanisms underlying observed alterations at the whole muscle level.

1.5 The aims of this study

The overall aim of this study was to further knowledge and understanding of the functional status of skeletal muscle in *ob/ob* mouse, a commonly used model of obesity. The working hypothesis was that skeletal muscles of obese mice undergo muscle-specific alterations that can be detected by using biochemical and physiological methods and a combination of whole muscle and single fibre approaches. The animals were used at an age where there is no evidence of hyperglycemia or hypertension, and the muscles examined included two hind limb muscles (EDL – predominately locomotor; SOL – predominately postural) and one

trunk muscle (SM – involved in head/neck motion and respiratory assistance). The specific aims of the study were as follows:

- (1) To investigate the morphological and biochemical characteristics [muscle/fibre size; protein content; MHC_i/fibre type composition] of EDL, SM and SOL muscles of *ob/ob* mice and controls (*Chapter 3*);
- (2) To investigate the contractile characteristics [twitch and tetanic force-generating capacity; kinetics of twitch and tetanic responses; force-frequency relationship] of isolated EDL, SM and SOL muscles of *ob/ob* mice and controls (*Chapter 4*);
- (3) To explore mechanisms underlying alterations of contractile characteristics observed at the whole muscle level using mechanically skinned single fibre preparations (*Chapter 5*);
- (4) To investigate the fatigability characteristics of isolated EDL, SM and SOL muscles of *ob/ob* mice and controls, and characteristics related to energy consumption (as indicated by myofibrillar ATPase activity) and energy supply (as indicated by LDH isoenzyme profile) of the muscles from the two mouse groups (*Chapter 6*);
- (5) To integrate the findings reported in Chapters 3-6 and discuss them in the context of the well-being of the obese animal (*Chapter 7*).

Chapter 2

General Methods

2.1 *Animals*

In this study, a total of 36 male (obese) C57BL/6J-*ob/ob* (B6.V-*Lep^{ob}*) and 53 male lean C57BL/6J (?/+) mice, aged 18-22 weeks, were used. As previously stated in Section 1.2.2, at this age, obesity is well-developed in the C57BL/6J-*ob/ob* mouse and euglycaemia is present (Coleman & Hummel, 1973; Leiter, 1992; Dong *et al.*, 2006). This provides an experimental tool to study the pathogenesis of obesity (Coleman, 1978; Martins & Redgrave, 2004) without the co-existence of hyperglycaemia. The mice were housed in a temperature-controlled environment (21-22 °C) on a 12:12 hr light:dark cycle, with access to water and standard chow *ad libitum*. Prior to experimentation, the animals were euthanised by halothane overdose in accordance with Victoria University Animals Experimentation Committee procedures. Following death (2.5 min of deep halothane inhalation), animals were weighed to the nearest 10 mg using an electronic balance (A&D model FX-320, Japan).

2.2 *Muscle dissection, handling and storage*

Immediately following sacrifice and weighing, the animal was placed on a bed of ice. Muscle dissection was carried out under stereomicroscope (Nikon SMZ645) with light source (Meiji Techno FL-150), using a range of Dumont Inox forceps, Vannas style iris spring scissors and fine iris scissors (Fine Science Tools, North Vancouver). In obese organisms, skeletal muscle morphology/biochemistry may vary among diverse muscles (see Section 1.3) and, thus, measurements were performed on three muscles [extensor digitorum longus (EDL); sternomastoid (SM); soleus (SOL)] that

differ with respect to anatomical location and physiological function. EDL is a hind limb muscle important to locomotion (Hennig & Lømo, 1987), SM is located in the neck and assists in head/neck rotation and respiration (Campbell, 1970; Moxham *et al.*, 1980, 1981; Gandevia *et al.*, 1990), and SOL is a hind limb muscle involved in postural support (Hennig & Lømo, 1987; Fitts *et al.*, 2001; Hitomi *et al.*, 2005).

The muscles of interest – EDL, SM and SOL – were carefully dissected, avoiding any cutting or stretching of the muscle. For EDL, an incision was made in the skin at the base of the lower limb and the muscle was dissected from its origin to insertion, ensuring that as much tendon as possible was preserved at each end of the muscle belly. SM originates directly from the outer surface of the mastoid process and inserts into the superior aspect of the sternum (Paul, 2001) such that there is little tendon at both ends. As this creates a problem for the tying of surgical thread (required for whole muscle contractile work – see Section 4.2.3.2), a small section of bone at the point of origin and insertion was removed with the muscle (see Figure 2.1). Briefly, the dissection of SM involved (a) a longitudinal incision along the midline of the sternum and an incision across the clavicle to provide a bone segment at SM insertion, and (b) the removal of a section of the mastoid process at SM origin. The removal of bone along with tendons has been recommended and used with other muscles that also present limited tendon (Goldberg *et al.*, 1975). For SOL, an incision was made posteriorly in the skin at the base of the hind limb. The Achilles tendon, which includes the inserting tendon of SOL (Goldberg *et al.*, 1975) was severed, allowing for other muscles to be moved aside to expose SOL. Dissection was completed by carefully cutting the proximal tendon

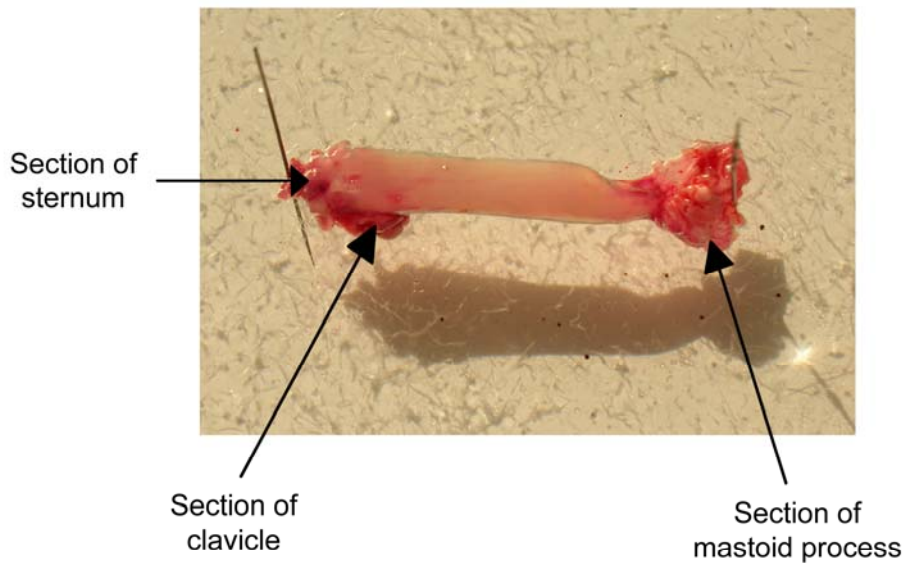


Figure 2.1 Sternomastoid muscle dissected from mouse.

Dissection of the sternomastoid muscle with small segments of bone still attached, from sternum and clavicle at the point of origin and from mastoid process at the point of insertion. Note: these sections of bone were further trimmed prior to the tying of suture silk for subsequent contractility experiments.

originating at the proximal tibia, fibula and interosseus membrane (Paul, 2001), being careful to retain as much intact proximal and distal tendon as possible.

Following dissection, a muscle was handled in one of three ways depending on its subsequent experimental use:

(a) For whole muscle homogenate analyses (Chapter 3), a muscle was immediately placed in a Petri dish layered with Sylgard 184 transparent resin (Dow Corning) covered with liquid paraffin oil (AJAX Chemicals) which allowed for the careful excision of tendon (and bone, in the case of SM) under stereomicroscope. The muscle was then blotted dry on Whatman 1 filter paper, weighed to the nearest 0.1 mg using an electronic balance (A&D model HM-200, Japan) and stored at -84°C for future homogenisation and biochemical analyses (see Section 3.2.4).

(b) A muscle to be used for single fibre dissection (Chapters 3, 5 and 6) was immediately blotted dry on Whatman 1 filter paper and also placed in a Petri dish layered with Sylgard 184 transparent resin (Dow Corning) covered with liquid paraffin oil (AJAX Chemicals). Entomological pins were inserted through the tendons of the muscle in order to secure the muscle to the layer of Sylgard resin and hold it submerged in the liquid paraffin oil. At periods when not undergoing single fibre isolation at room temperature ($22-26^{\circ}\text{C}$), muscles were refrigerated (4°C) in the Petri dish.

(c) For whole muscle contractility and fatigue experiments (Chapters 4 and 6), a muscle was immediately pinned in a Petri dish (with a Sylgard 184 base) containing

carbogen bubbled (95% oxygen, 5% carbon dioxide) Krebs solution (pH 7.4) (see Section 4.2.3.1 for composition of solution and other details).

2.3 *Determination of muscle width*

Muscle width was measured for studies on contractile (Chapter 4) and fatigue (Chapter 6) characteristics of EDL, SM and SOL muscles from *ob/ob* and lean mice. The measurements were performed following the muscle contractility/fatigue experiments and prior to the excision of tendons and subsequent weighing of muscles. To do so, a muscle was removed from the *in vitro* chamber by severing the suture silk that tied it to the mounting rod and isometric force transducer, leaving the tendons intact. The muscle was immediately transferred to a Petri dish containing Krebs solution (with a Sylgard 184 base). The Petri dish was placed on graph paper, under stereomicroscope, with the muscle being pinned at L_0 (the length at which the muscle generates peak twitch force) (see also Section 4.2.4). The muscle width was measured at the midpoint of L_0 using a video monitoring system (Sony PVM-14N5A) and a pair of precision (0.05 mm) calipers (Mitutoyo, Japan). Actual muscle width was then calculated using the magnification conversion factor for the stereomicroscope.

2.4 *Dissection of single muscle fibres and mechanical removal of the surface membrane (skinning)*

The dissection of single muscle fibre segments was performed at RT (22-26 °C) with the aid of a dissecting microscope, light source and video monitoring system. Two different set-ups were employed interchangeably for this procedure:

(a) Olympus (SZPT) dissecting microscope and Meiji Techno FL-150 light source, with Panasonic WV-BP100 CCD camera and Panasonic WV-BM900 video monitor.

(b) Olympus (SZ61) dissecting microscope and Meiji Techno FL-150 light source, with Panasonic SDII WV-CP474 CCTV camera and Sony PVM-14N5A video monitor.

Single muscle fibre segments were isolated randomly with fine jeweler forceps (Dumont Inox forceps no. 5 and no. 55) and Vannas style iris spring scissors under liquid paraffin oil. Briefly: (i) at one end of the muscle, the tendon was freed from its entomological pin; (ii) an incision was made in the epimysium at this end of the muscle to allow access to fibre bundles; (iii) the incision was continued along the length of the muscle from the free end towards the end secured by an entomological pin so that a bundle of 5 to 20 fibres was partially dissected from the muscle belly; (iv) with the free end of the bundle secured with forceps, a second pair of forceps was used to tease single fibres, one by one, from the bundle.

While still attached to the muscle belly, a single fibre was mechanically skinned (i.e. the surface membrane was removed). To achieve this, the free end of the single fibre was held to the Sylgard resin base with forceps while a second pair of forceps carefully pinched the surface membrane of the fibre. From here, the membrane was slowly separated from the fibre and rolled back along the entire length of the fibre segment so that a 'cuff' was formed as the membrane was peeled away (see Figure 2.2). Skinning of fibres was performed for two primary reasons: (i) the formation of the 'cuff' was evidence that the fibre segment teased from the muscle belly was indeed only one fibre, and (ii) the skinned fibre preparation allowed direct activation of the myofibrillar apparatus by the solutions utilised in the experiments of Chapters 5 and 6.

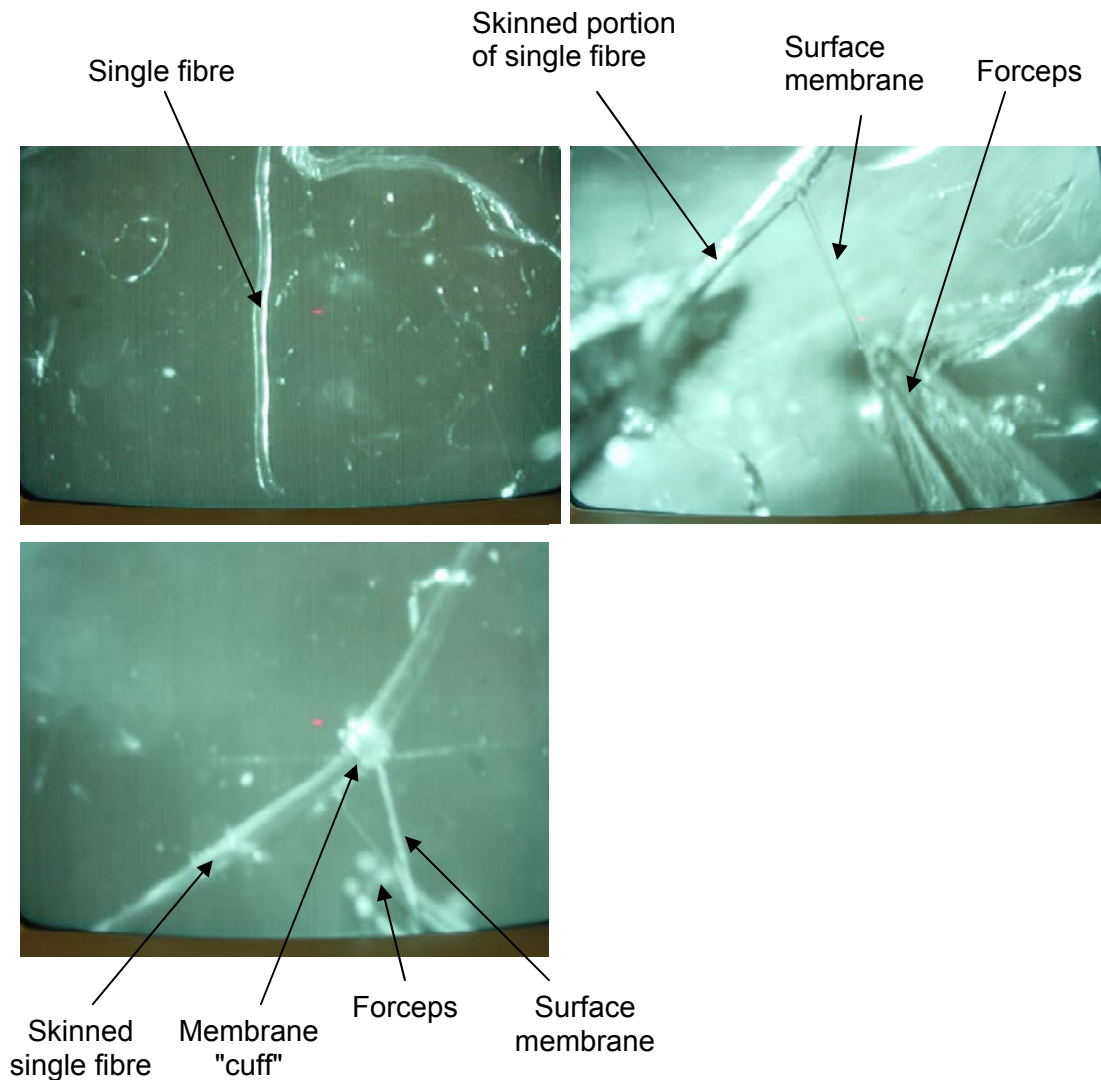


Figure 2.2 Mechanical skinning of a single muscle fibre. In a Petri dish layered with Sylgard 184 transparent resin covered by liquid paraffin oil, a single muscle fibre segment was isolated with fine jeweler forceps. The single fibre was then mechanically skinned (i.e. the surface membrane was removed) by slowly separating the membrane from the fibre and rolling it back along the entire length of the fibre so that a ‘cuff’ was formed as the membrane was peeled away.

2.5 *Determination of single fibre diameter, cross-sectional area (CSA) and volume*

The length and the diameter (taken as the mean of at least three values measured at different positions along the length) of the skinned fibre segment were measured using a video monitoring system (described above) and a pair of precision ($50 \mu\text{m}^2$) calipers (Mitutoyo, Japan) (see Figure 2.3).

Single fibre CSA was calculated from the mean diameter (with the assumption that the fibre was cylindrical) using the formula:

$$\text{fibre CSA } (\mu\text{m}^2) = \pi \times (d/2 \times a)^2$$

where **d** is fibre diameter (μm) and **a** is the magnification conversion factor for diameter.

The volume of each single fibre segment was calculated from the mean diameter and length using the formula:

$$\text{fibre volume (nl)} = \pi \times (d/2 \times a)^2 \times L \times b$$

where **d** is the average diameter of the fibre (μm), **L** is the length of the fibre segment (μm), **a** is the magnification conversion factor for diameter and **b** is the magnification conversion factor for length.

2.6 *Single fibre preparation for analysis of MHC isoform (MHC_i) composition by SDS-PAGE*

The preparation of single fibre samples for SDS-PAGE analysis of MHC_i composition is described here as it is relevant to Chapters 3, 5 and 6. Preparation of whole muscle

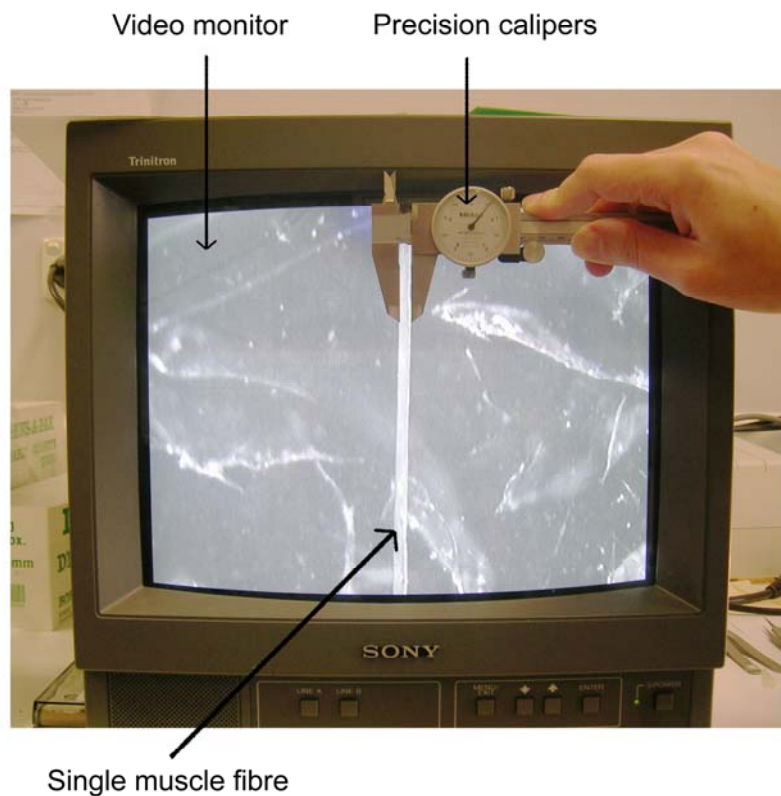


Figure 2.3 Measurement of single muscle fibre diameter. During single muscle fibre dissection, a stereomicroscope and video monitoring system provides an on-screen image of the single fibre. A pair of precision calipers was then used to assess the diameter of the fibre from at least three sites along its length, with the mean of these measurements taken as fibre diameter.

homogenates for SDS-PAGE analysis of MHC_i composition is described in detail in Section 3.2.6.

Briefly, each fibre was placed in SDS-PAGE solubilization buffer which contained 80 mM Tris-HCl (pH 6.8), 2.3% w/v SDS, 5% w/v β-mercaptoethanol, 10 mM dithiothreitol, 12.5% v/v glycerol, 13.6% w/v sucrose, 0.01% w/v bromphenol blue, 0.1 mM phenylmethylsulfonyl fluoride, 0.002 mM leupeptin and 0.001 mM pepstatin. Samples (0.4 nl fibre volume/1 µl solubilization buffer) were left for approximately 24 hours at RT, then were boiled for 5 min and stored at -84 °C until SDS-PAGE analysis of MHC isoforms.

2.7 *SDS-PAGE analyses of MHC_i composition in whole muscle homogenate and single fibre samples*

SDS-PAGE was used for determining the MHC_i composition of whole muscle tissue homogenates and single muscle fibre samples. All gels were manually prepared at RT from stock solutions (stored at 4 °C). Gels were cast in a Mighty Small SE245 Dual Gel Caster (Hoefer Scientific Instruments, San Francisco) (see Figure 2.4A) using 10 x 10.5 cm glass plates and 0.75 cm spacers.

MHC isoforms were separated using the glycine-SDS-PAGE protocol of Talmadge and Roy (1993) with modifications. The separating gel [T = 7.6%, C = 2%] contained 200 mM Tris-HCl (pH 8.8), 100 mM glycine, 30% (v/v) glycerol, 0.4% (w/v) SDS, 0.1% (w/v) ammonium persulfate and 0.05% (v/v) *N,N,N',N'*-tetramethylethylenediamine (TEMED), whilst the stacking gel [T = 4%, C = 2%] contained 70 mM Tris-HCl (pH 6.7), 4 mM ethylenediamine-tetraacetic acid,

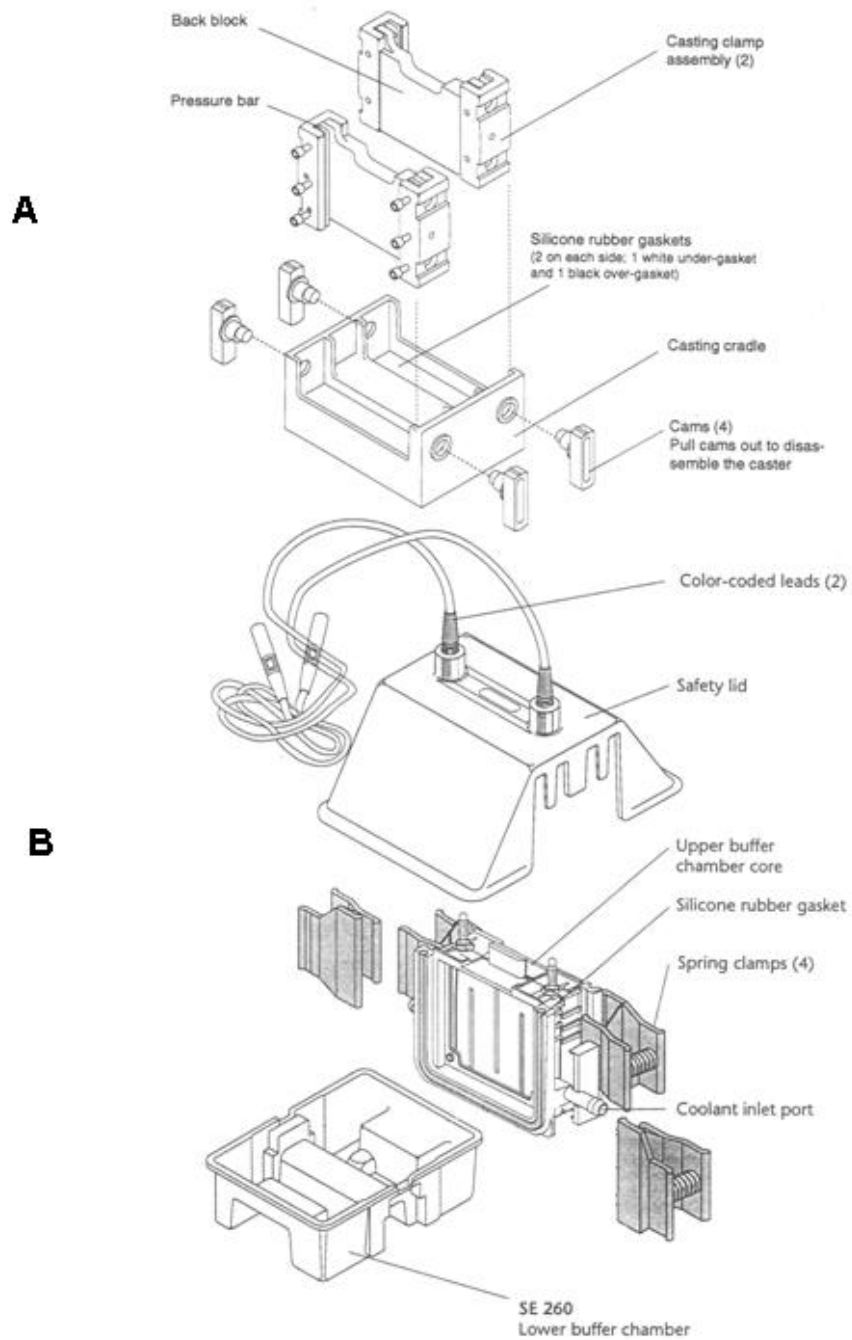


Figure 2.4 Apparatus employed for SDS-PAGE experiments. (A) Hoefer Mighty Small SE245 Dual Gel Caster. (B) Hoefer SE 260 Gel Set-up Unit. (Modified from *Hoefer Gel Electrophoresis Unit Instructions*. San Francisco: Hoefer Scientific Instruments).

30% (v/v) glycerol, 0.4% (w/v) SDS, 0.1% (w/v) ammonium persulfate and 0.05% (v/v) TEMED.

The separating gel was prepared first by mixing all gel ingredients in a conical flask, with the polymerising agents ammonium persulfate and TEMED added to the flask immediately before pouring. The solution was then poured between two glass plates (clamped together in the Hoefer Dual Gel Caster) to a height of 7.6 cm. A 0.5-cm deep layer of milli-Q water was added above the separating gel immediately following pouring to minimise exposure to atmospheric oxygen, an inhibitor of polymerisation (Hepworth *et al.*, 1999). The separating gels were allowed to polymerise for 60 minutes.

Following polymerisation of the separating gel, all components of the stacking gel (except ammonium persulfate and TEMED) were combined and mixed in a conical flask. At this point, the layer of water atop the separating gel was carefully removed with Whatman 1 filter paper. Ammonium persulfate and TEMED were then added to the stacking gel solution and the mixture was poured between the two glass plates to form a 2 cm-high stacking gel above and in contact with the separating gel. A 15-pronged well comb was immediately inserted into the stacking gel solution so that during polymerisation, 15 electrophoretic wells were formed within the stacking gel (thereby accommodating up to 15 samples). The stacking gel was allowed to polymerise for 50 min.

Once the stacking gel was polymerised, the 15-pronged comb was carefully removed so as to maintain the integrity of the electrophoretic wells. Each well was immediately

cleansed of unpolymerised acrylamide by the insertion and removal of filter paper (Whatman 1) strips cut to a width of the wells. Pre-chilled upper chamber running buffer (150 mM glycine, 100 mM Tris, 0.1% (w/v) SDS, 10 mM β -mercaptoethanol) was then added to each well.

The pairs of glass plates in which each gel slab resided were transferred to a Hoefer SE260 Gel Set-Up Unit (Hoefer Scientific Instruments, San Francisco) (see Figure 2.4B). Once clamped in place, further running buffer was added to the upper chamber of the set-up to a level where the stacking gel was completely submerged. At this point, samples to undergo electrophoretic separation (i.e. either whole muscle homogenate or single fibre samples) were applied to the electrophoretic wells using an Eppendorf pipette (Hamburg) and gel loading pipette tips (Quality Scientific Plastics, USA).

For MHC_i analysis of whole muscle homogenates, 6 μ l samples (containing 3 μ g of protein) were applied to each electrophoretic well, whilst for single muscle fibre analysis, 4 μ l samples (containing 1.6 nl of fibre) were applied to each well. A laboratory MHC_i marker (containing the MHC I, MHC IIa, MHC IIc and MHC IIb isoforms of mouse skeletal muscle) was also applied to gels to allow for the identification of the individual MHC isoforms in each sample when stained for visualisation.

Once all electrophoretic wells were loaded with sample, pre-chilled lower chamber running buffer (75 mM glycine, 50 mM Tris, 0.05% (w/v) SDS) was added to the lower chamber of the set-up. The lid of the set-up was then fitted and connected to a

power supply (VoKam 2541) for the commencement of electrophoresis. Electrophoresis was carried out at constant voltage (150 V) at 5 °C in a Contherm Digital Series Cooled Incubator (model 1100C) for 27 hr.

Upon cessation of electrophoresis, gel set-ups were dismantled, pairs of glass plates separated and the stacking gel discarded. The separating gel was then gently removed from the glass plates and placed in a solution specific to the staining procedure required for visualisation of proteins of interest.

2.8 *Protein visualisation on SDS-polyacrylamide gels*

The stain used for the visualisation of MHC isoforms in whole muscle homogenate samples was Coomassie Brilliant Blue (CBB). The staining solution contained 45% methanol, 10% acetic acid, 0.1% w/v CBB and the gels were incubated for at least two hours (without agitation). Following this process, gels were transferred to a destaining solution (5% methanol, 7.5% acetic acid) and left overnight (without agitation). The following day, the gels were twice transferred to fresh destaining solution for one hour each time. Finally, gels were transferred to 200 ml milli-Q water for at least five min prior to laser densitometry (see Section 2.9).

For the visualisation of MHC isoforms in single fibre samples, the Bio-Rad Silver Stain Plus kit was used and the protocol is outlined in Figure 2.5. Note that all steps prior to incubation in the stopping solution were performed with agitation. Also, the ingredients of the silver reaction solution were mixed immediately before use.

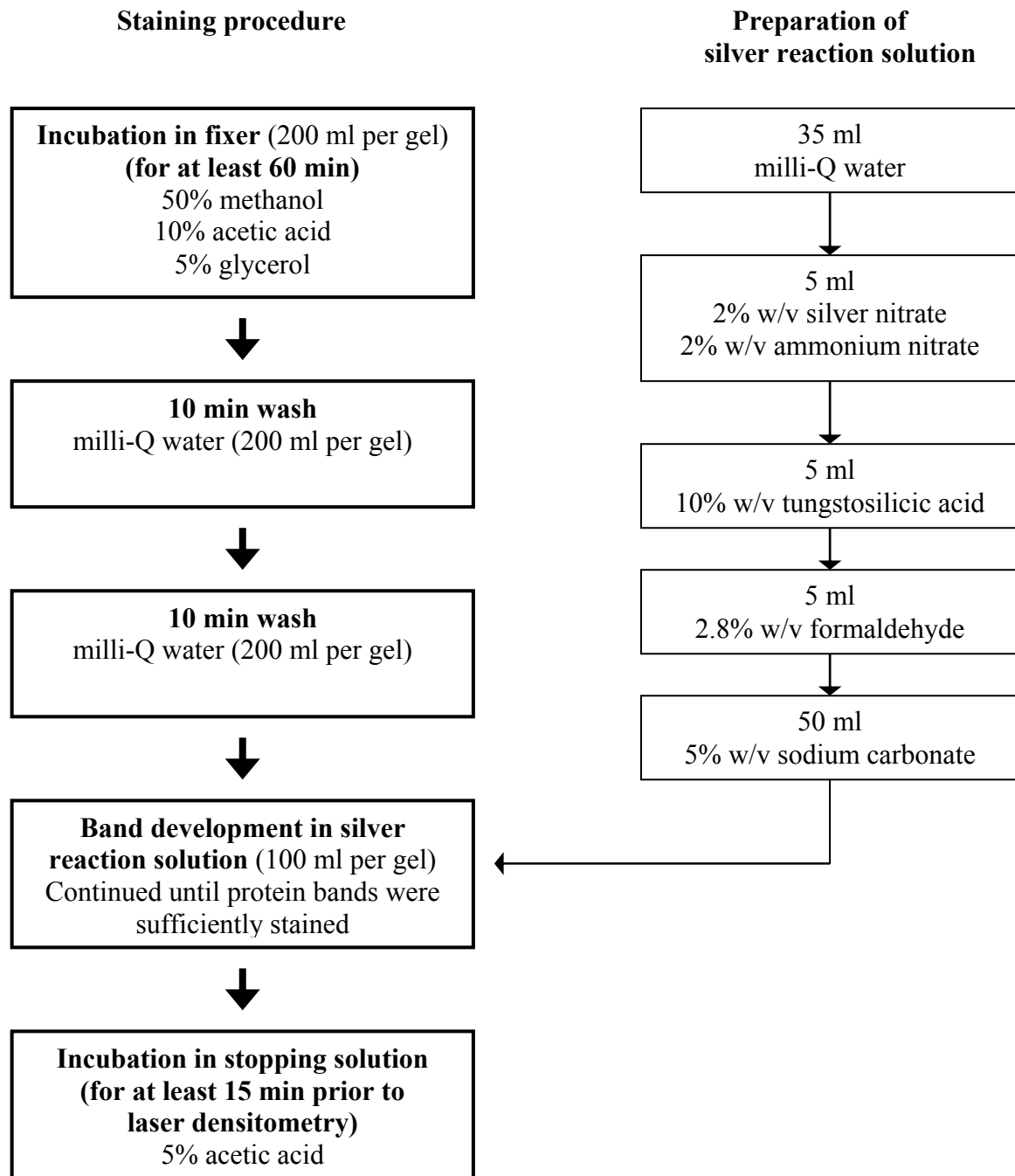


Figure 2.5 Bio-Rad silver staining procedure. This silver staining procedure was used for visualisation of proteins in single muscle fibres on glycine-SDS-PAGE gels. The left hand column represents the sequential order in which the silver staining procedure was performed. At each step, gels were removed from the previous solution and placed in the following solution. The right hand column represents the sequential order in which the components of the silver reaction solution were introduced during its preparation.

2.9 *Laser densitometry for quantitation of protein bands on SDS-polyacrylamide gels*

Volumetric quantitation of electrophoretic bands was carried out using a Molecular Dynamics Personal Densitometer (Molecular Dynamics, Sunnyvale). Background correction was performed using the *object average* background correction method supplied by ImageQuaNT V5.2 software (Molecular Dynamics, Sunnyvale) which provided a measure of optical density (OD) for each MHC isoform.

Chapter 3

Morphological and biochemical characteristics of EDL, SM and SOL muscles from *ob/ob* mouse

Section 3.1 INTRODUCTION

The C57BL/6J-*ob/ob* (B6.V-*Lep^{ob}*) mouse, described in Section 1.2.2, is a widely used animal model for exploring the pathophysiology of obesity. A noticeable morphological trait in these mice is a markedly reduced mass of skeletal muscles, similar to that described in other murine models of obesity (Shapira *et al.*, 1980; Durschlag & Layman, 1983; Burbach *et al.*, 1985; Wardlaw *et al.*, 1986). Interestingly, the degree to which this morphological alteration takes place appears to be muscle-type related. Thus, predominantly fast-twitch hind limb muscles of *ob/ob* mice have been consistently reported to exhibit decrements in mass (Almond & Enser, 1984; Champion *et al.*, 1984; Smith & Romsos, 1984; Bruton *et al.*, 2002). In contrast, for slower hind limb muscles, such as SOL, both the presence (Trostler *et al.*, 1982; Champion *et al.*, 1984; Smith & Romsos, 1984) and absence (Cuendet *et al.*, 1976; Le Marchand-Brustel *et al.*, 1978; Grundleger *et al.*, 1980; Almond & Enser, 1984) of lower muscle mass associated with obesity have been reported. It is worth noting that most of the studies on skeletal muscle of obese mice published to date were performed on animals aged less than 16 weeks and, therefore, a cognitive gap still exists regarding the morphological and biochemical characteristics of skeletal muscles in adult mice of this model.

Skeletal muscle function is closely related not only to its size, but also to its fibre type composition. Surprisingly, studies on the fibre type composition of skeletal muscles from obese mice has produced, so far, inconsistent results. Thus, in one study, the authors (Almond & Enser, 1984) reported that the biceps brachii of young C57BL/6J-

ob/ob mouse contains fewer fast-twitch white fibres than its counterpart in the lean controls. In muscles from *ob/ob* mice of different background strain to that of the C57BL/6J-*ob/ob* mouse, Warmington *et al.* (2000) reported an increase in the proportion of type IIA fibres at the expense of type IIB fibres in EDL muscle and a decrease in the type IIB proportion in SOL. In contrast, Stickland *et al.* (1994) showed no change in the fibre type composition of biceps brachii or SOL muscles.

It is important to note that in the three aforementioned studies, the authors determined fibre type composition using myosin ATPase-based (Almond & Enser, 1984; Stickland *et al.*, 1994; Warmington *et al.*, 2000), succinate dehydrogenase-based (Almond & Enser, 1984; Stickland *et al.*, 1994; Warmington *et al.*, 2000) and phosphorylase-based (Almond & Enser, 1984; Stickland *et al.*, 1994) histochemistry. As stated in Section 1.3.4, knowledge of fibre type composition produced by histochemistry-based techniques is limited because they cannot reliably identify hybrid fibres. The strategy that allows for the detection of hybrid fibres is based on the electrophoretic separation of MHC isoforms expressed in single fibres under denaturing conditions (i.e. single fibre SDS-PAGE) (Pette & Staron, 2000; Stephenson, 2001).

In this study, a range of morphological and biochemical characteristics (including muscle size and MHC_i-based fibre type composition) were used to compare skeletal muscles from adult C57BL/6J-*ob/ob* mice with those from lean (control) mice. Comparisons were made for three muscles, EDL, SM and SOL, which differ with respect to anatomical location and/or physiological function.

Section 3.2 METHODS

3.2.1 Animals and muscle preparations

In this chapter are presented morphological data on body, whole muscle and single fibre size as well as a range of biochemical characteristics of whole muscles and single muscle fibres from *ob/ob* and lean mice. The data describing body size for *ob/ob* and lean mice were derived from a representative sample of *ob/ob* (n=25) and lean (n=31) mice.

The morphological and biochemical data for whole muscles and single fibres were collected from a total of 178 muscles dissected from 86 mice. It must be noted that the muscle fibres employed for the acquisition of single fibre data were not dissected from the muscles used to collect whole muscle mass data. This is because the conditions required for the accurate assessment of muscle mass (where tendons are carefully removed from the isolated muscle) were not compatible with the techniques used for the dissection of single fibres (where intact tendons of the isolated muscle are retained – see Section 2.4).

3.2.2 Measurement of body size and whole muscle morphology characteristics

Body mass was determined as described in Section 2.1. The procedures of whole muscle dissection and muscle mass measurement are described in Section 2.2. The measure used in this study to represent the muscle length (L_0) was assessed as described in Section 4.2.4 and whole muscle CSA was estimated using the calculations described in Section 4.2.5.

3.2.3 Measurement of single fibre size

The dissection of single muscle fibres and the mechanical removal of their surface membrane are described in Section 2.4 and the procedures undertaken for single fibre size measurements are described in Section 2.5.

3.2.3.1 Estimation of fibre number

The equation (E) below, relating CSA data for whole muscle (CSA_m) and single fibre (CSA_{sf}), was used to assess whether the lower values obtained for the whole muscle CSA for EDL, SM and SOL muscles of *ob/ob* mice were due to a decrease in the total fibre area (CSA_{sf}) or in the number of fibres (N_f).

$$\frac{N_f^{ob}}{N_f^{le}} = \frac{1}{1 - A} \left(\frac{CSA_m^{ob}}{CSA_m^{le}} - A \right) \times \frac{CSA_{sf}^{le}}{CSA_{sf}^{ob}} \quad (E3.1)$$

where: N_f^{ob} = number of fibres in the muscle of *ob/ob* mouse; N_f^{le} = number of fibres in the muscle of lean mouse; A = mean CSA of the ‘extra-myofibre’ or ‘non-fibre’ space expressed as a proportion of the CSA of the muscle from the lean mouse (CSA_m^{le}) = mean CSA of the extra-myofibre space in the muscle of the *ob/ob* mouse expressed as a proportion of CSA_m^{le} ; CSA_m^{ob} = mean CSA of the muscle from the *ob/ob* mouse; CSA_m^{le} = mean CSA of the muscle from the lean mouse; CSA_{sf}^{le} = mean CSA of single fibres (regardless of fibre type) from the lean mouse; CSA_{sf}^{ob} = mean CSA of single fibres from the *ob/ob* mouse.

The derivation of this equation is as follows:

$$CSA_m = CSA_{\text{total fibre area}} + CSA_{\text{non-fibre area}} \quad (E3.2)$$

where $CSA_{\text{total fibre area}} = CSA_{sf} \times N_f$

$$CSA_m^{le} = CSA_{totalfibre}^{le} + CSA_{nonfibre}^{le} \quad (E3.3)$$

$$CSA_m^{ob} = CSA_{totalfibre}^{ob} + CSA_{nonfibre}^{ob} \quad (E3.4)$$

Assumption: $\frac{CSA_{nonfibre}^{le}}{CSA_m^{le}} = \frac{CSA_{nonfibre}^{ob}}{CSA_m^{le}} = A$ (proportion of ‘non-fibre’ area expressed as a proportion of the muscle area in a control animal)

Both sides of E3.3 and E3.4 are divided by CSA_m^{le} :

$$1 = \frac{CSA_{totalfibre}^{le}}{CSA_m^{le}} + A \quad (E3.5) \longrightarrow \frac{CSA_{totalfibre}^{le}}{CSA_m^{le}} = 1 - A \quad (E3.6)$$

$$\frac{CSA_m^{ob}}{CSA_m^{le}} = \frac{CSA_{totalfibre}^{ob}}{CSA_m^{le}} + A \quad (E3.7) \longrightarrow \frac{CSA_{totalfibre}^{ob}}{CSA_m^{le}} = \frac{CSA_m^{ob}}{CSA_m^{le}} - A \quad (E3.8)$$

From E3.6 and E3.8 it follows:

$$\frac{CSA_{totalfibre}^{le}}{CSA_{totalfibre}^{ob}} = \frac{1 - A}{\frac{CSA_m^{ob}}{CSA_m^{le}} - A} \longrightarrow \frac{CSA_{sf}^{le} \times N_f^{le}}{CSA_{sf}^{ob} \times N_f^{ob}} = \frac{1 - A}{\frac{CSA_m^{ob}}{CSA_m^{le}} - A}$$

$$\longrightarrow \frac{N_f^{le}}{N_f^{ob}} = \frac{1 - A}{\frac{CSA_m^{ob}}{CSA_m^{le}} - A} \times \frac{CSA_{sf}^{ob}}{CSA_{sf}^{le}} \quad (E3.9)$$

Reciprocal of both sides:

$$\frac{N_f^{ob}}{N_f^{le}} = \frac{1}{1 - A} \left(\frac{CSA_m^{ob}}{CSA_m^{le}} - A \right) \frac{CSA_{sf}^{le}}{CSA_{sf}^{ob}} \quad (E3.10)$$

3.2.4 Muscle homogenisation for biochemical analyses

Whole muscles were placed in 6 volumes [note: 1 volume (ml) \approx wet muscle mass g] of relaxing solution and homogenised manually, on ice, with a glass/glass

homogeniser. The relaxing solution contained 90 mM HEPES, 126 mM K⁺, 36 mM Na⁺, 1 mM Mg²⁺, 50 mM EGTA_{total}, 8 mM ATP_{total} and 10 mM CrP (pH 7.10).

3.2.5 Protein determination in muscle homogenates

Following homogenisation, protein concentration of whole muscle homogenates was determined by the Bradford protein assay (Bradford, 1976). Bovine serum albumin (BSA) was employed as the protein standard from which a standard curve was plotted and muscle homogenate protein concentrations derived.

3.2.6 Preparation of whole muscle homogenates for electrophoretic analysis of MHC content and MHC_i composition

Following protein determination, the remaining muscle homogenate sample was diluted in SDS-PAGE solubilization buffer (for composition see Section 2.6). Samples were then immediately boiled for 5 min and stored at -84 °C. For determination of MHC content (see below) and MHC_i composition, these samples were further diluted to a final concentration of 0.5 µg protein/1 µl solubilization buffer prior to SDS-PAGE analysis.

3.2.7 Electrophoretic determination of MHC content in whole muscle homogenates

The MHC content in whole muscle homogenate samples was determined electrophoretically using SDS-PAGE, under conditions in which the MHC isoforms co-migrated as a single band (see Figure 3.1A), and purified rabbit MHC [Sigma M7659] as a standard. The separating gel [T=12%, C=2.6%] contained 750 mM Tris-HCl (pH 9.3), 10% (v/v) glycerol, 0.1% (w/v) SDS, 0.04% (w/v) ammonium

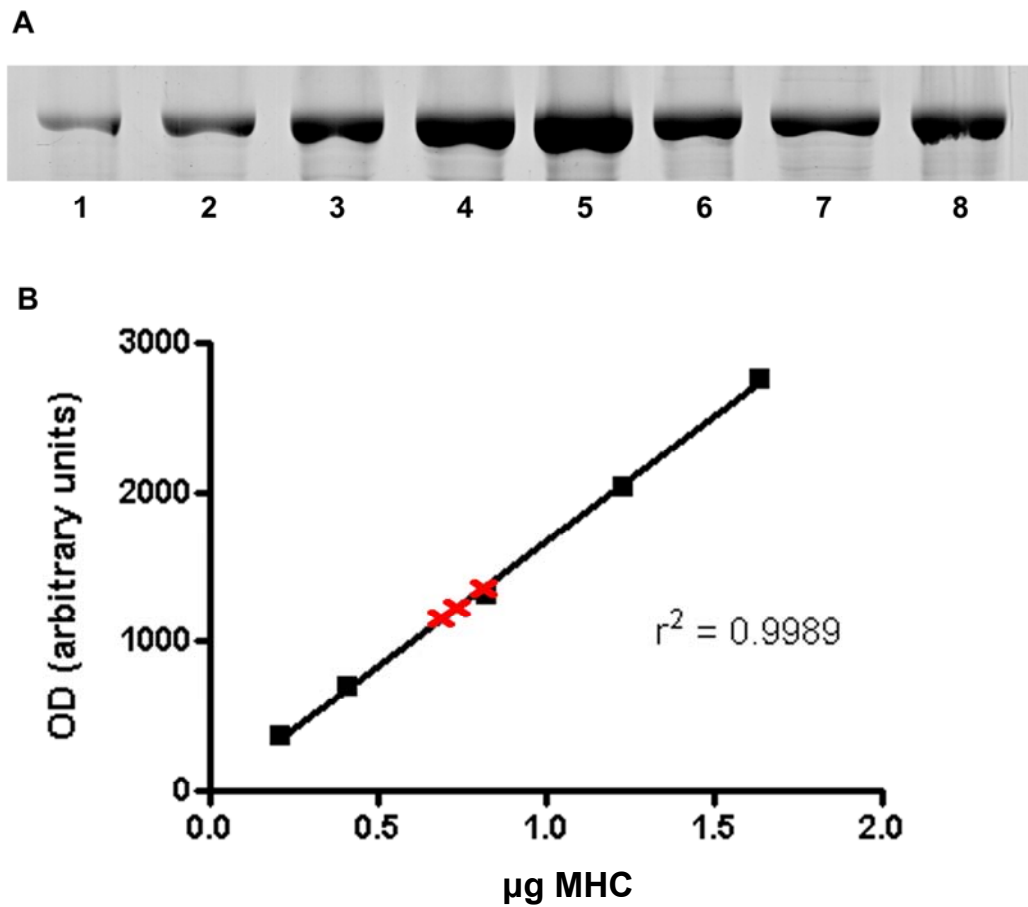


Figure 3.1 Representative electrophoretogram and standard curve used to determine the MHC content of skeletal muscles from adult *ob/ob* and lean mice.
 A. Representative electrophoretogram. Known concentrations of MHC were prepared from purified rabbit MHC [Sigma M7659] and applied to electrophoretic wells: Lane 1 – 0.204 µg MHC; lane 2 – 0.408 µg MHC; lane 3 – 0.817 µg MHC; lane 4 – 1.225 µg MHC; lane 5 – 1.633 µg MHC. Alongside, whole muscle homogenate samples of unknown MHC content were applied with protein separation performed by SDS-PAGE: lane 6 – sample prepared from EDL of lean mouse (3 µg protein applied); lanes 7 & 8 – samples prepared from SM of lean mouse (3 µg protein applied). B. Standard curve prepared from the optical density (OD) of samples of known MHC content (■ - i.e. lanes 1-5 above). The OD of lanes 6-8 (x) are plotted on the regression line.

persulfate and 0.1167% (v/v) TEMED, and the stacking gel [T=4%, C=4.76%] contained 125 mM Tris-HCl (pH 6.8), 10% (v/v) glycerol, 0.1% (w/v) SDS, 0.1% (w/v) ammonium persulfate and 0.1% (v/v) TEMED. The manual preparation of the separating and stacking gels followed the procedures described in Section 2.7 with some modifications. Specifically, once the separating gel had been poured, a 0.5-cm layer of milli-Q water was added above the separating gel for 20 min. After this time, the water layer was replaced by a 2-cm layer of 0.2% (w/v) SDS to minimise the loss of gel components and the separating gel was left to polymerise overnight. The following morning, the stacking gel was prepared, poured atop the separating gel and allowed to polymerise for 50 min. All procedures following polymerisation were carried out as described in Section 2.7. This experiment used the same running buffer (380 mM glycine, 50 mM Tris, 0.1% (w/v) SDS) for both the upper and lower chambers of the Hoefer SE260 Gel Set-Up Unit (see Figure 2.4B). Electrophoresis was conducted at constant current (20 mA) at RT for 4 hr. The MHC band in each whole muscle homogenate sample was stained with Coomassie Brilliant Blue (see Section 2.8 for protocol) and quantified by laser densitometry as described in Section 2.9.

The whole muscle homogenate samples (6 μ l samples containing 3 μ g of protein) of unknown MHC concentrations were run on the same gel with a series of known concentrations of MHC standard in the range of 0.204 to 1.633 μ g. This standard range was chosen based on published estimates of myofibrillar protein as a proportion of total muscle protein (60%; Yates & Greaser, 1983; Ohtsuki *et al.*, 1986; Perry, 1996), myosin as a proportion of myofibrillar protein (43%; Yates & Greaser, 1983; Ohtsuki *et al.*, 1986) and MHC as a proportion of myosin (85%; Lowey & Risby,

1971; Bagshaw, 1993; Geiger *et al.*, 2000; Stevens *et al.*, 2006). A linear relationship between the OD of the MHC bands produced by the standards and their known MHC content provided a standard calibration curve based on which the MHC content of the mouse samples on each gel was determined (see lanes 1-5 in Figure 3.1A and Figure 3.1B). Note that the MHC concentration of the Sigma [M7659] stock suspension was verified in the laboratory by the Biuret method (Gornall *et al.*, 1949; Layne, 1957), in accordance with the manufacturer's certificate of analysis (Sigma-Aldrich, <http://www.sigmaaldrich.com>).

To ensure that the variability in MHC content reflected inter-muscle differences rather than experimental error (i.e. variability in the volume applied to electrophoretic wells), a control experiment was carried out. This involved the application, in triplicate, of 6 μ l samples from mouse skeletal muscle homogenates to the same gel. Following electrophoresis, protein staining and laser densitometry, the OD values within each set of triplicate samples were compared and the coefficient of variation (CV) derived. For five sets of triplicate samples, the mean CV \pm S.E. was 2.85 \pm 0.6%.

3.2.8 *Determination of MHC_i composition in whole muscle homogenate and single fibre samples*

The SDS-PAGE protocol and associated procedures used for determining the MHC_i composition in whole muscle tissue homogenate and single muscle fibre samples are described in Sections 2.7-2.9.

3.2.9 *Statistical analysis*

All results are presented as mean \pm standard error of the mean (S.E.), unless otherwise stated. One way analysis of variance (ANOVA) with Tukey HSD *post hoc* testing was used to detect differences among values for EDL, SM and SOL muscles from lean mice. Student's independent *t* test (two-tailed) was used to detect differences between *ob/ob* and lean mouse groups. To test for differences in the proportions of pure and hybrid fibres between *ob/ob* and lean mouse groups, a chi-square test was employed. Statistical significance was accepted as $p \leq 0.05$. Sample size is denoted by *n*.

Section 3.3 RESULTS

3.3.1 *Body size and whole muscle morphology*

At 18-22 weeks of age, the mean body mass of *ob/ob* mice (53.03 ± 0.66 g, $n=25$) was 81% greater ($p<0.0001$) than that of their lean counterparts (29.22 ± 0.36 g, $n=31$). As seen in Table 3.1, which displays muscle morphology data, the mean mass of muscles from *ob/ob* mice was consistently smaller than that of control muscles, but the magnitude of the difference was muscle-specific. Thus, EDL, SM and SOL were 21% ($p<0.0001$), 30% ($p<0.0001$) and 13% ($p=0.045$) smaller, respectively.

Given the body size differences between the two groups of animals, when muscle mass was normalised to body mass, the values obtained for all three muscles from *ob/ob* mice were markedly lower than those obtained for the lean counterparts (EDL: -56%; SM: -62%; SOL: -52%), and were statistically significant ($p<0.0001$). In a subpopulation of these muscles, which was used for the contractility experiments described in Chapter 4, it was found that mean length of muscles (represented by the mean length, L_o , at which muscles generated peak twitch force) from *ob/ob* mice, was not statistically different from that of the respective muscles from lean mice for EDL ($p=0.349$), SM ($p=0.310$) or SOL ($p=0.582$). Assuming that muscles from *ob/ob* and lean mice possess the same length of tendons, the similar L_o infers that bone lengths are similar between the two animal groups.

Table 3.1: Muscle morphology data for EDL, SM and SOL from adult *ob/ob* and lean mice.

	EDL		SM		SOL	
	<i>ob/ob</i>	lean	<i>ob/ob</i>	lean	<i>ob/ob</i>	lean
Muscle mass (mg)	9.9 ± 0.3 ^c (n=13)	12.5 ± 0.5 (n=15)	17.2 ± 0.5 ^c (n=11)	24.7 ± 1.0 (n=13)	8.8 ± 0.4 ^a (n=6)	10.1 ± 0.4 (n=6)
Muscle-to-body mass (mg/g)	0.19 ± 0.01 ^c (n=13)	0.43 ± 0.01 (n=15)	0.32 ± 0.01 ^c (n=11)	0.85 ± 0.03 (n=13)	0.16 ± 0.01 ^c (n=6)	0.33 ± 0.01 (n=6)
L_o (mm)	11.2 ± 0.2 (n=8)	11.5 ± 0.3 (n=8)	9.6 ± 0.3 (n=6)	10.0 ± 0.2 (n=6)	11.0 ± 0.3 (n=6)	10.7 ± 0.4 (n=6)
CSA (mm²)	0.84 ± 0.04 ^b (n=8)	1.11 ± 0.06 (n=8)	1.77 ± 0.09 ^b (n=6)	2.52 ± 0.14 (n=6)	0.76 ± 0.04 ^a (n=6)	0.89 ± 0.03 (n=6)

All values are mean ± S.E. Significantly different from lean counterpart at ^ap<0.05, ^bp<0.005 and ^cp<0.0001. L_o was defined as the length at which the muscle generates peak twitch force (see Section 4.2.4); CSA – whole muscle cross-sectional area; EDL – extensor digitorum longus; SM – sternomastoid; SOL – soleus.

The muscle mass and muscle length values given in Table 3.1 were used to calculate the cross-sectional area (CSA) of EDL, SM and SOL muscles from *ob/ob* and lean mice, as described in Section 4.2.5(ii), and these values are also given in Table 3.1. As expected, the lower whole muscle CSA for EDL (-24%), SM (-30%) and SOL (-15%) muscles from *ob/ob* mice was quantitatively consistent with the decrement observed in muscle mass.

3.3.2 Single fibre size

To address the possibility that the smaller size of EDL and SM muscles from *ob/ob* mice is related to smaller fibre sizes, measurements were made of the diameters of single fibres randomly dissected from these muscles. From these measurements, single fibre CSA values were calculated assuming the fibres are cylindrical. Figure 3.2 shows the frequency distribution of calculated fibre CSA values (partitioned into 300 μm^2 increments) for obese (open bars) and lean (solid bars) mice.

As shown by the distribution of fibre areas in Figure 3.2, the smaller muscle size of EDL and SM from *ob/ob* mice was paralleled by smaller fibre sizes. This figure highlights that the 81.2% of fibres from EDL of *ob/ob* mice displayed CSA values below 1200 μm^2 , whilst 63.1% of fibres from EDL of lean mice had CSA values above 1200 μm^2 . Similarly, 68.2% of fibres from SM of *ob/ob* mice displayed CSA values below 1200 μm^2 , whilst 66.7% of fibres from SM of lean mice exhibited CSA values above 1200 μm^2 . By comparison, the CSA values for single fibres from SOL of *ob/ob*

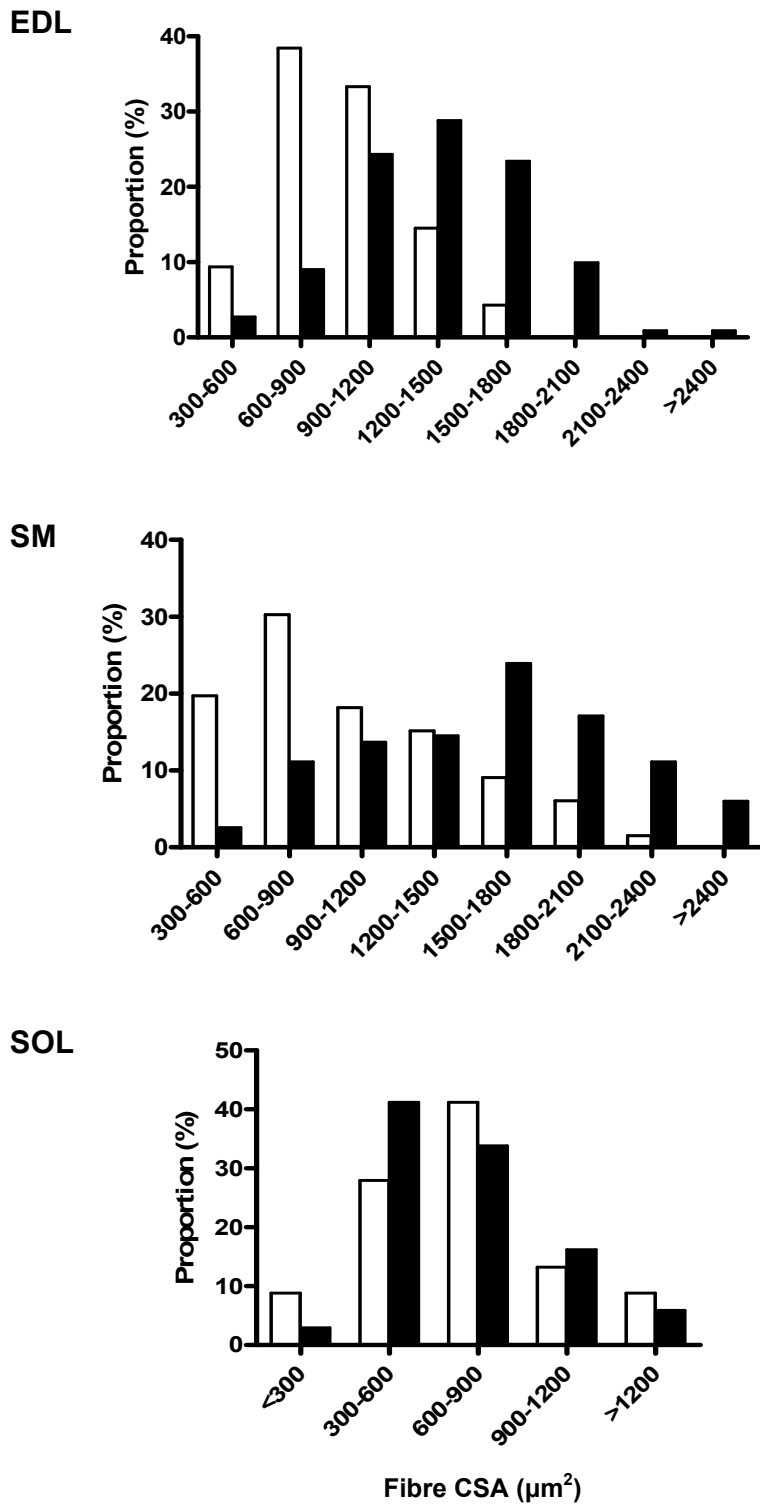


Figure 3.2 Frequency distribution of CSA values for single muscle fibres randomly dissected from EDL (□ n=117; ■ n=111), SM (□ n=66; ■ n=117) and SOL (□ n=68; ■ n=68) muscles of *ob/ob* (□) and lean (■) mice.

mice displayed a similar size distribution to those of lean mice, with over 69.1% of fibres from both groups falling between 300 and 900 μm^2 .

In Figure 3.3 are presented the mean fibre CSA values for the single fibre populations from EDL, SM and SOL muscles of *ob/ob* and lean mice. Consistent with the smaller CSA of EDL and SM muscles from *ob/ob* mice, the mean fibre CSA for fibres from EDL and SM muscles of *ob/ob* mice was 30% ($p < 0.0001$) and 35% ($p < 0.0001$) smaller than that of lean mice, respectively. In contrast, no statistical difference was found between the mean fibre CSA for SOL muscles from *ob/ob* and lean mice, despite a significant difference in whole muscle CSA (Table 3.1).

In order to assess whether differences in the mean fibre CSA in EDL and SM muscles from *ob/ob* and lean mice could quantitatively explain the differences observed between the respective values of whole muscle CSA, the equation (E3.1) in Section 3.2.3.1 was used on the assumption that the mean CSA of the ‘non-fibre’ space in both muscle groups represents ~20% of the mean CSA of control muscles (Burr & McLennan, 1960; Goldspink, 1966; Lin *et al.*, 1981; Clausen *et al.*, 2004). For the EDL and SM muscles, the values obtained for the ratio between the number of fibres in the muscle of *ob/ob* mouse and that in the muscle of lean mouse ($\frac{N_f^{ob}}{N_f^{le}}$) were greater than 0.97. This result indicates that the number of fibres in the two muscle groups was similar and, therefore, the decrease in the mean fibre CSA fully accounted for the smaller CSA of EDL and SM muscles from *ob/ob* mice.

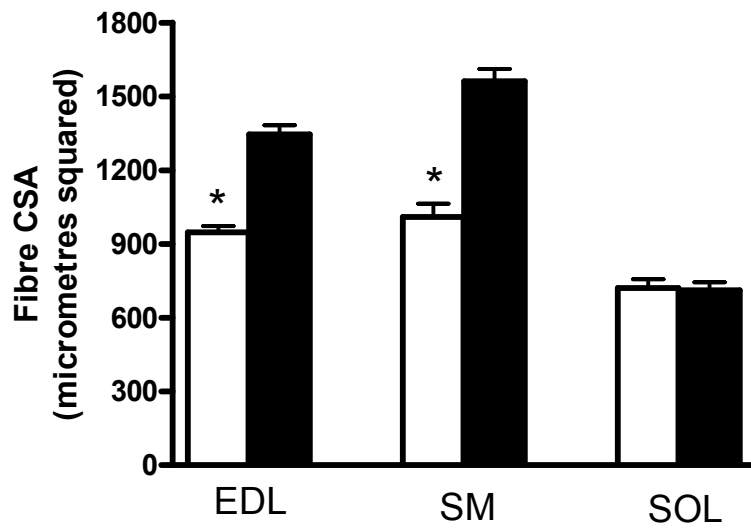


Figure 3.3 Mean fibre CSA (μm^2) for the single fibre populations of muscle fibres randomly dissected from EDL (\square n=117; \blacksquare n=111), SM (\square n=66; \blacksquare n=117), and SOL (\square n=68; \blacksquare n=68) muscles of *ob/ob* (\square) and lean (\blacksquare) mice. *Significantly different from lean counterpart at $p < 0.0001$. S.E. bars are shown.

It is worth noting that when the equation in Section 3.2.3.1 was applied to SOL muscles from the two mouse groups, the value for $(\frac{N_f^{ob}}{N_f^{le}})$ was 0.8, indicating that the number of fibres in muscles of *ob/ob* mice was about 20% smaller than that in muscles of lean mice. To extend these findings, the mean values for fibre CSA were related to the MHC composition (fibre type) of the fibres dissected from the two muscle groups.

In Table 3.2 are provided the data grouped according to fibre type and muscle of origin. As it will be reported in detail in Section 3.3.6, the single fibre population dissected from the EDL, SM and SOL muscles of *ob/ob* and lean mice comprised four types of pure fibres (I, IIA, IID and IIB) and nine types of hybrid fibres (I+IIA, IIA+IIB, IIA+IID, IIB+IID, I+IIA+IIB, I+IIA+IID, I+IIB+IID, IIA+IIB+IID and I+IIA+IIB+IID). As seen in Table 3.2, not all fibre types were detected in the fibre populations dissected from each muscle group, and not all data were obtained from a large enough sample size to allow statistical analysis. Notwithstanding these limitations, the values presented in Table 3.2 lead to two important conclusions. First, a large difference (~30%) in CSA between fibres from *ob/ob* and lean mice was observed for type IIB and type IIB+IID fibres. This was valid for both EDL and SM muscles, with the CSA of type IIB and IIB+IID fibres from EDL of *ob/ob* mice being 30% ($p<0.0001$) and 25% ($p=0.033$) smaller, respectively, and the CSA of type IIB and type IIB+IID fibres from SM of *ob/ob* mice being 28% ($p<0.0001$) and 33% ($p=0.002$) smaller, respectively. Second, type IIB fibres were not detected in the SOL muscle (from either *ob/ob* or lean mouse) and type IIB+IID fibres were only detected in SOL muscles of the lean group. However, of the fibre type groups detected in the population

Table 3.2 Cross-sectional area (CSA) of electrophoretically-defined singles fibres randomly dissected from EDL, SM and SOL muscles of *ob/ob* and lean mice.

Fibre Type	EDL <i>ob/ob</i> CSA (μm^2)	EDL lean CSA (μm^2)	SM <i>ob/ob</i> CSA (μm^2)	SM lean CSA (μm^2)	SOL <i>ob/ob</i> CSA (μm^2)	SOL lean CSA (μm^2)
PURE						
Type I					752.8 \pm 71.9 (n=25)	727.4 \pm 60.5 (n=25)
Type IIA			575.1 \pm 47.2 (n=2)		525.9 \pm 61.1 (n=8)	651.1 \pm 77.5 (n=10)
Type IIB	962.0 \pm 29.8* (n=96)	1355.0 \pm 36.8 ^{a,b} (n=106)	1182.0 \pm 72.0* ^d (n=38)	1636.0 \pm 55.2 ^{a,b,c} (n=97)		
Type IID			680.5 \pm 125.5 (n=5)			745.0 \pm 112.2 (n=6)
HYBRID						
I+IIA					630.5 \pm 58.4 (n=18)	644.7 \pm 22.4 (n=3)
IIA+IIB	1000.0 \pm 88.3 (n=2)		527.9 (n=1)	993.3 \pm 41.37 (n=2)		622.3 (n=1)
IIA+IID					830.1 \pm 53.2 (n=5)	690.7 \pm 105.4 (n=8)
IIB+IID	867.7 \pm 49.0 [§] (n=19)	1157.0 \pm 170.5 ^a (n=5)	815.6 \pm 82.3 [#] (n=18)	1226.0 \pm 94.8 ^{a,b} (n=17)		884.0 \pm 128.9 (n=7)
I+IIA+IIB					858.3 \pm 116.2 (n=7)	527.9 (n=1)
I+IIA+IID						624.0 \pm 65.5 (n=2)
I+IIB+IID						624.0 \pm 65.5 (n=2)
IIA+IIB+IID			962.7 \pm 202.5 (n=2)	1165.28 (n=1)	760.2 (n=1)	710.6 \pm 241.3 (n=2)
I+IIA+IIB+IID					923.1 \pm 85.1 (n=4)	527.9 (n=1)

All values are mean \pm S.E. Significantly different from LEAN counterpart at * $p < 0.0001$, # $p < 0.005$ and § $p < 0.05$; Significantly different from ^alean SOL type I and IIA ($p < 0.001$), ^blean SOL type IID fibres ($p < 0.05$), ^clean EDL type IIB fibres ($p < 0.0001$) and ^bobese EDL type IIB fibres ($p \leq 0.001$). [NB: statistical comparisons not performed on fibre type samples of $n < 3$]. EDL – extensor digitorum longus; SM – sternomastoid; SOL – soleus.

of SOL fibres (I, IIA, I+IIA and IIA+IID) that satisfied the sample size requirement ($n \geq 3$), none displayed CSA differences between *ob/ob* and lean mice.

3.3.3 Muscle total protein content

Total protein content in whole muscle homogenates was determined by Bradford (1976) assay using bovine serum albumin (BSA) as the protein standard. The protein content of EDL, SM and SOL muscles from *ob/ob* and lean mice expressed as absolute values (mg) and as values normalised to muscle mass (mg protein/mg muscle) are given in Table 3.3.

Among the EDL, SM and SOL muscles from lean mice only, absolute protein content was significantly different ($p < 0.0001$), with SM displaying the highest content and SOL the lowest. However, when normalised to muscle mass, there was no longer a difference among the three muscle types ($p = 0.087$), despite SOL being approximately 12% lower than both EDL and SM. When comparisons were made between *ob/ob* and lean mice, the absolute protein content of all three muscles from *ob/ob* mice was lower than that of controls, with EDL being 22% lower ($p = 0.0013$), SM being 36% lower ($p < 0.0001$) and SOL being 23% lower ($p = 0.0259$). When these values were normalised to muscle mass, differences between *ob/ob* and lean mice were no longer statistically significant, though there was a trend for lower concentrations in all three muscles from *ob/ob* mice (-10% for EDL, $p = 0.067$; -9% for SM, $p = 0.225$; -14% for SOL, $p = 0.101$).

Table 3.3 Protein and MHC content in EDL, SM and SOL muscles from adult *ob/ob* and lean mice.

	EDL		SM		SOL	
	<i>ob/ob</i> (5)	lean (7)	<i>ob/ob</i> (5)	lean (7)	<i>ob/ob</i> (5)	lean (8)
Total protein (mg)	1.648 ± 0.110 [#]	2.113 ± 0.043 ^a	2.726 ± 0.086 ^{&}	4.234 ± 0.163 ^a	1.049 ± 0.061 [*]	1.364 ± 0.087 ^a
Total protein (mg/mg muscle)	0.168 ± 0.006	0.186 ± 0.006	0.168 ± 0.008	0.184 ± 0.009	0.140 ± 0.009	0.163 ± 0.008
MHC (mg/mg protein)	0.252 ± 0.019	0.239 ± 0.006	0.282 ± 0.010	0.265 ± 0.015	0.300 ± 0.022	0.269 ± 0.010
MHC (mg/mg muscle)	0.042 ± 0.003	0.044 ± 0.002	0.047 ± 0.003	0.048 ± 0.001	0.042 ± 0.003	0.044 ± 0.002

All values are mean ± S.E. Significantly different from lean counterpart at ^{*}p<0.05, [#]p<0.005 and ^{\$}p≤0.0001. Significantly different from other lean muscles at ^ap<0.001. The number of muscles assessed is indicated in parentheses. EDL – extensor digitorum longus; SM – sternomastoid; SOL – soleus; MHC – myosin heavy chain.

3.3.4 MHC content

As stated in Section 1.3.2, MHC plays a key role in muscle contractility as it contains both the catalytic site of ATPase and the actin binding site. In this study, the MHC content in whole muscle homogenates from EDL, SM and SOL muscles was determined electrophoretically using SDS-PAGE and a commercial MHC preparation as a standard. A representative electrophoretogram displaying five known concentrations of commercial MHC (lanes 1-5) and three mouse samples of unknown MHC concentration (lanes 6-8) is presented in Figure 3.1A (see Section 3.2.7). In Figure 3.1B is shown the standard curve produced by plotting the OD values of the MHC bands ν the concentrations of the five MHC standards; note that on the graph are also shown the OD values for the three unknown samples.

Among the EDL, SM and SOL muscles from lean mice only, there was no significant difference in MHC concentration expressed either per mg protein ($p=0.134$) or per mg muscle mass ($p=0.206$). When comparisons were made between muscles of *ob/ob* and lean mice, there were no statistically significant differences in MHC concentration expressed per mg protein, though there was a trend in all three muscles from *ob/ob* mice for greater values (+5% for EDL, $p=0.458$; +6% for SM, $p=0.425$; +12% for SOL, $p=0.155$). No significant differences in MHC concentration between muscles of *ob/ob* and lean mice were found when MHC concentration was expressed per mg muscle mass (EDL: $p=0.543$; SM: $p=0.785$; SOL: $p=0.632$).

3.3.5 MHC_i composition

The contractile characteristics of a muscle depend not only on MHC content but also on its MHC_i/fibre type composition. The MHC_i composition of EDL, SM and SOL

muscles from *ob/ob* and lean mice was determined electrophoretically using whole muscle homogenates, and representative electrophoretograms are shown in Figure 3.4. The 'MHC_i marker' (Lane 1 in this figure) displays the four MHC isoforms detected in skeletal muscles from 18-22 wk old mouse and identified according to their electrophoretic mobility (IIa < IId < IIb < I).

As seen in the bar graphs presented in Figure 3.5, marked differences in MHC_i composition were observed between EDL, SM and SOL muscles of lean mice, with EDL containing only MHC IIb and IId, SM containing MHC IIb, IId and IIa, and SOL containing all four MHC isoforms. When comparisons were made between the data for EDL, SM and SOL muscles from *ob/ob* mice and their controls (Figure 3.5) the following results were obtained: (i) the EDL from *ob/ob* mice contained a lower proportion of MHC IIb (-8.6%; p<0.0001) and a greater proportion of MHC IId (+7.7%; p<0.0001), as well as a small amount of MHC IIa; (ii) the SM from *ob/ob* mice contained a lower proportion of MHC IIb (-12.4%; p<0.0001) and a greater proportion of MHC IId (+6.5%; p=0.0002) and MHC IIa (+5.9%; p<0.0001); (iii) the SOL from *ob/ob* mice displayed a lower proportion of MHC IId (-9.1%; p=0.0005) and a greater proportion of MHC I (+6.9%; p=0.0006), whilst no significant differences were detected in the proportions of MHC IIa (p=0.1067) or MHC IIb (p=0.3687) between the two mouse groups. Taken together, these data suggest that in *ob/ob* mice, all three muscles contain a significantly *lower* proportion of the 'faster' MHC isoforms (IIb for EDL and SM; IId for SOL) and a significantly *higher* proportion of the 'slower' MHC isoforms (IId for EDL; IId and IIa for SM; I for SOL) than their counterparts from the lean mice.

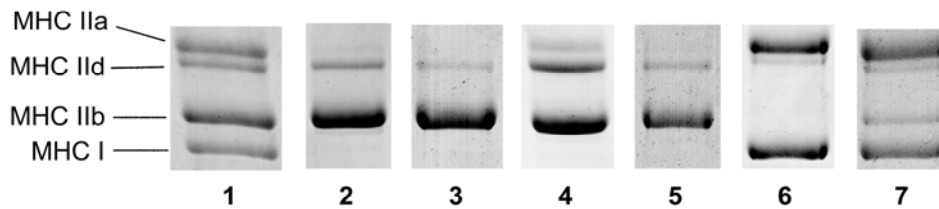


Figure 3.4 Representative electrophoretograms of MHC isoform profiles of EDL, SM and SOL muscles from adult *ob/ob* and lean mice. Whole muscle homogenate samples were prepared from EDL, SM and SOL muscles. MHC isoform separation was performed by SDS-PAGE with 3 μ g of protein applied per electrophoretic well. Lane 1 – MHC_i marker; lane 2 – EDL from *ob/ob* mouse; lane 3 – EDL from lean mouse; lane 4 – SM from *ob/ob* mouse; lane 5 – SM from lean mouse; lane 6 – SOL from *ob/ob* mouse; lane 7 – SOL from lean mouse.

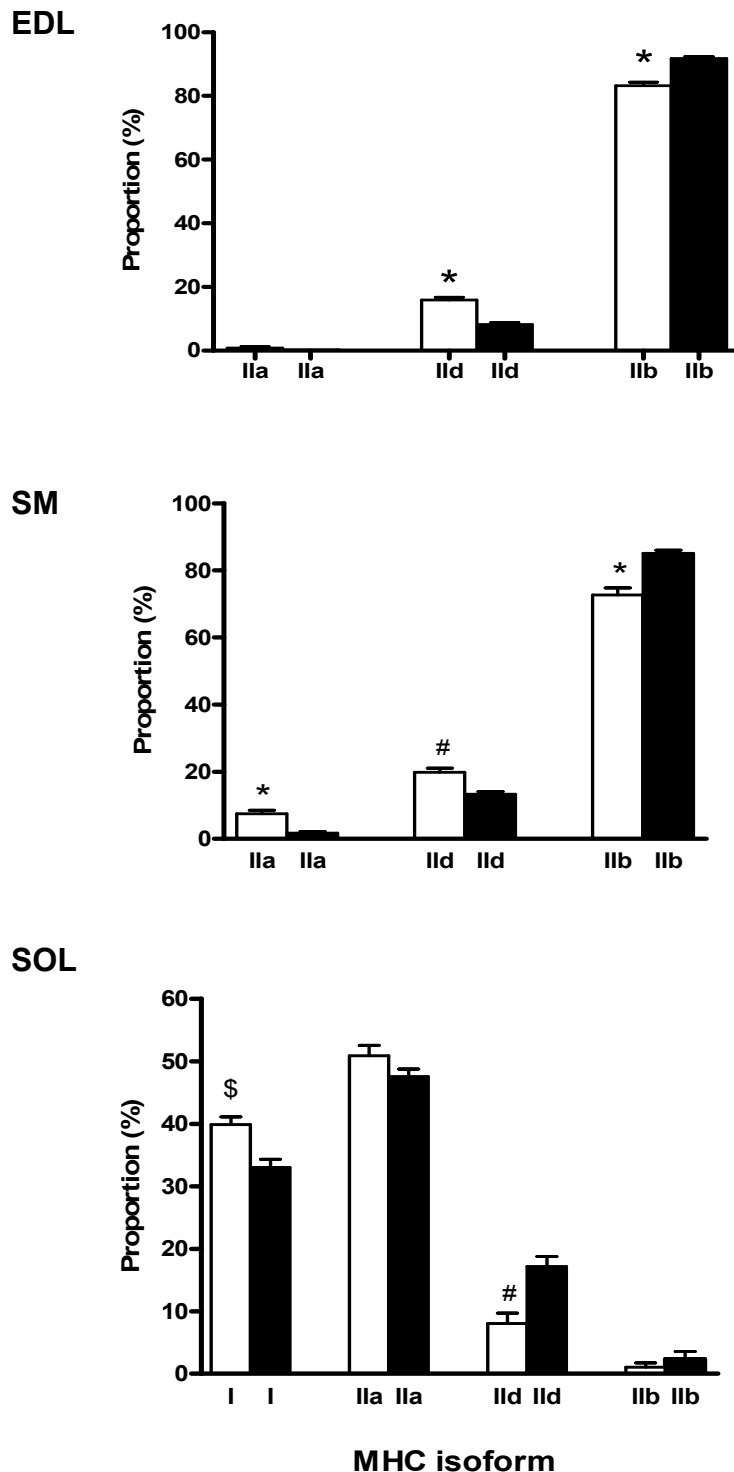


Figure 3.5 MHC isoform composition of whole muscles from adult *ob/ob* and lean mice. Whole muscle homogenates from *ob/ob* (□) and lean (■) mice underwent electrophoresis at constant voltage (150 V) for 27 hr at 5 °C for MHC isoform separation in EDL (□ n=11; ■ n=14), SM (□ n=12; ■ n=11) and SOL (□ n=14; ■ n=15). Significantly different proportion to lean counterpart with respect to the same MHC isoform at $^{\$}p < 0.001$, $^{\#}p \leq 0.0005$ and $^*p < 0.0001$. S.E. bars are shown.

3.3.6 Fibre type composition

In Figure 3.6 are shown representative electrophoretograms of the 13 MHC_i-based fibre types [four pure fibre types (lanes 2-5) and nine hybrid fibre types (lanes 7-15)] detected among the single fibres dissected from the EDL, SM and SOL muscles from *ob/ob* and lean mice.

The relative proportions of the pure and hybrid fibre types detected in the populations of fibres dissected from EDL, SM and SOL muscles of *ob/ob* and lean mice are shown in Figure 3.7. The fibre populations dissected from EDL (111 fibres from 20 muscles), SM (117 fibres from 20 muscles) and SOL (68 fibres from 14 muscles) muscles of lean mice contained 4.5%, 17.1% and 42.7% hybrid fibres, respectively. By comparison, the fibre populations dissected from EDL (117 fibres from 23 muscles), SM (66 fibres from 6 muscles) and SOL (68 fibres from 9 muscles) muscles of *ob/ob* mice produced consistently a higher proportion of hybrid fibres: four times higher for EDL ($p < 0.001$), 1.9 times higher for SM ($p < 0.001$) and 1.3 times higher for SOL ($p = 0.060$).

In Figure 3.8 are shown the relative proportions of individual fibre types in the single fibre populations dissected from the EDL, SM and SOL muscles of *ob/ob* and lean mice. In Table 3.4 are shown obesity-related changes in the proportion of each fibre type in the EDL and SM muscles of *ob/ob* mouse, while in Table 3.5 are shown the proportion of each fibre type in the SOL muscle of *ob/ob* and lean mice, expressed as per cent of total number of fibres in the SOL muscle of lean mice (N_f^{le}), and the obesity-related changes in the proportion of each fibre type in the SOL muscle of *ob/ob* mouse.

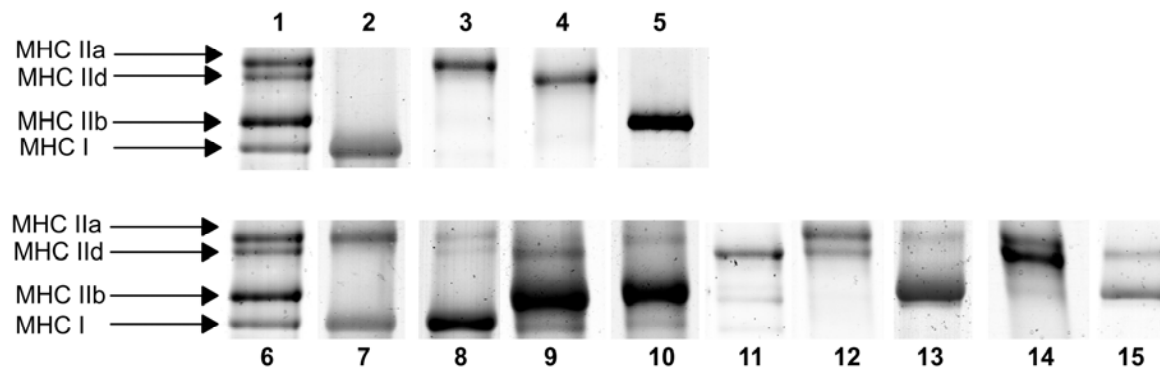


Figure 3.6 Representative electrophoretograms of the 13 MHC isoform-based fibres types found in a population of single fibres randomly dissected from EDL, SM and SOL muscles of adult *ob/ob* and lean mice. Single fibre samples were prepared and MHC isoform separation was performed by SDS-PAGE with 1.2 nl of fibre applied per electrophoretic well Lane 1,6 – MHC_i marker; lane 2 – fibre type I; lane 3 – fibre type IIA; lane 4 – fibre type IID; lane 5 – fibre type IIB; lane 7 – fibre type I+IIA; lane 8 – fibre type I+IIA+IID; lane 9 – fibre type I+IIA+IIB+IID; lane 10 – fibre type I+IIA+IIB; lane 11 – fibre type I+IIB+IID; lane 12 – fibre type IIA+IID; lane 13 – fibre type IIA+IIB; lane 14 – fibre type IIA+IIB+IID; lane 15 – fibre type IIB+IID. [Note that the scanning and printing resolution may make some faint bands that are clear to the naked eye difficult to see in this diagram].

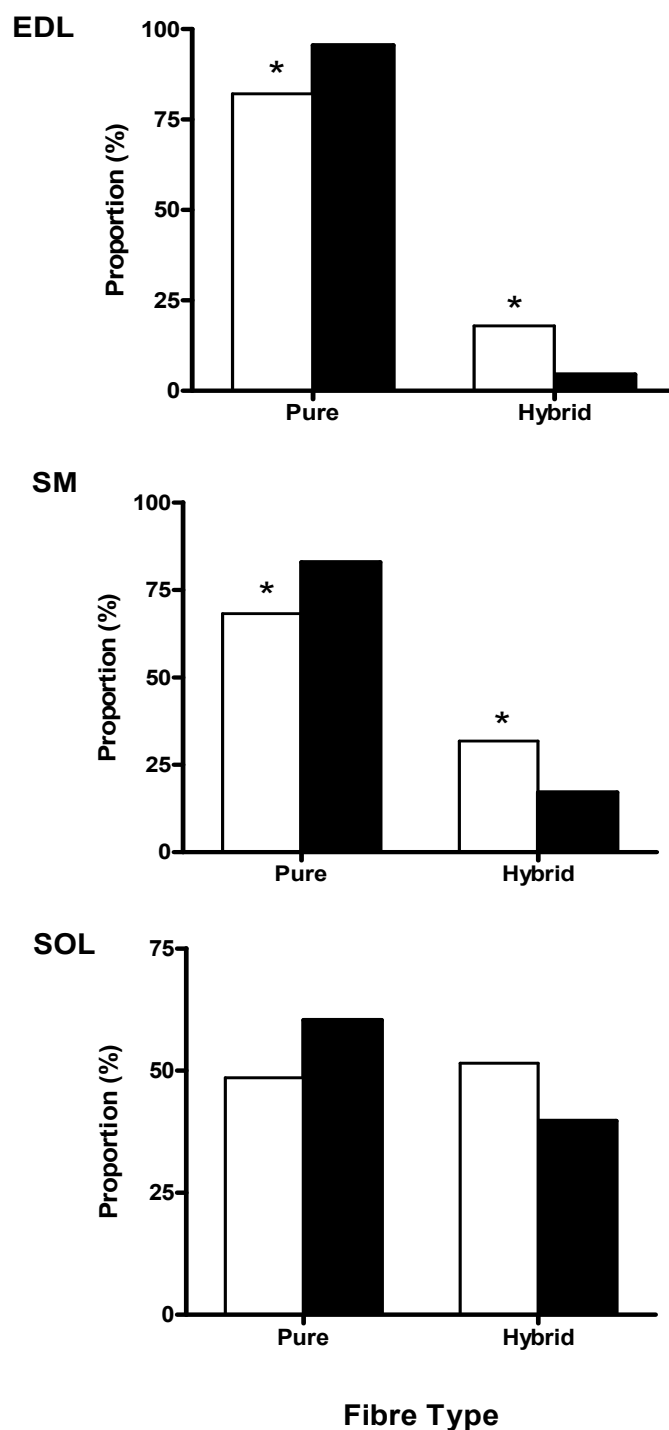


Figure 3.7 Proportion of pure and hybrid fibres in populations of single fibres randomly dissected from muscles of adult *ob/ob* (□) and lean (■) mice. Single fibre samples from EDL (□ n=117; ■ n=111), SM (□ n=66; ■ n=117) and SOL (□ n=68; ■ n=68) muscles underwent electrophoresis at constant voltage (150 V) for 27 hr at 5 °C for MHC_i separation. *significantly different at p<0.001 (using a chi-square test for differences between proportions)

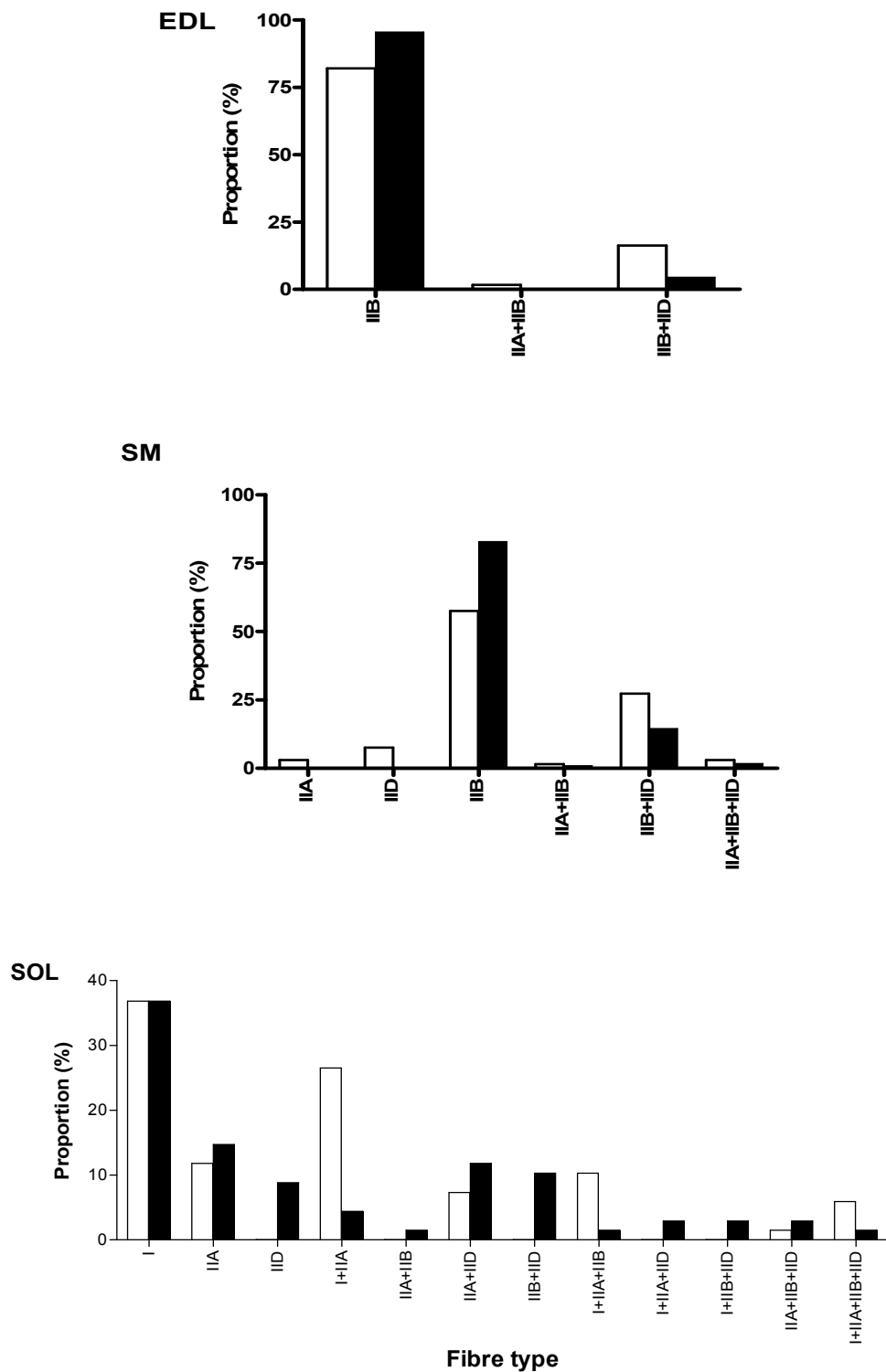


Figure 3.8 Fibre type proportions in populations of single fibres randomly dissected from muscles of adult *ob/ob* (□) and lean (■) mice. Single fibre samples from EDL (□ n=117; ■ n=111), SM (□ n=66; ■ n=117) and SOL (□ n=68; ■ n=68) muscles underwent electrophoresis at constant voltage (150 V) for 27 hr at 5 °C for MHC_i separation.

Table 3.4: Obesity-related changes in the proportion of each fibre type detected in populations of single fibres dissected from EDL and SM muscles of adult *ob/ob* and lean mice.

Fibre type	EDL (% change)	SM (% change)
I	–	–
IIA	–	+3.0
IIB	-13.4	-25.3
IID	–	+7.6
I+IIA	–	–
IIA+IIB	+1.7	+0.6
IIA+IID	–	–
IIB+IID	+11.7	+12.8
I+IIA+IIB	–	–
I+IIA+IID	–	–
I+IIB+IID	–	–
IIA+IIB+IID	–	+1.3
I+IIA+IIB+IID	–	–

Values represent the obesity-related difference (expressed as percentage change from control muscle) in the proportion of each fibre type in the muscles of *ob/ob* mouse. ‘–’ indicates that the fibre type was not detected in the muscle of interest. EDL – extensor digitorum longus; SM – sternomastoid.

A closer look at Figure 3.8 and Table 3.4 shows that the single fibre population dissected from EDL of *ob/ob* mice contained a smaller proportion of type IIB fibres, a larger proportion of type IIB+IID fibres and an additional fibre type group viz. type IIA+IIB fibres; this detection of a small number of type IIA+IIB fibres is consistent with the appearance of a small amount of MHC IIa isoform in EDL muscle homogenate samples from *ob/ob* mice. The single fibre population dissected from SM of *ob/ob* mice also contained a smaller proportion of type IIB fibres and a larger proportion of type IIB+IID fibres; in addition it contained as a larger proportion of type IIA+IIB and IIA+IIB+IID fibres and two ‘new’ groups of fibre types (type IIA

Table 3.5: The proportion of each fibre type in the SOL muscle of adult *ob/ob* and lean mice, expressed as per cent of total number of fibres in the SOL muscle of lean mice (N_f^{le}), and the obesity-related changes in the proportion of each fibre type in the SOL muscle of *ob/ob* mouse.

Fibre type	<i>ob/ob</i> (%)*	lean (%)	Obesity-related change (% change)
I	29.4	36.8	-7.4
IIA	9.4	14.7	-5.3
IID	–	8.8	-8.8
I+IIA	21.2	4.4	+16.8
IIA+IIB	–	1.5	-1.5
IIA+IID	5.8	11.8	-6.0
IIB+IID	–	10.3	-10.3
I+IIA+IIB	8.2	1.5	+6.7
I+IIA+IID	–	2.9	-2.9
I+IIB+IID	–	2.9	-2.9
IIA+IIB+IID	1.2	2.9	-1.7
I+IIA+IIB+IID	4.7	1.5	+3.2

*expressed as per cent of total number of fibres in the SOL muscle of lean mice (N_f^{le}). “Obesity-related change” values represent the obesity-related difference (expressed as percentage change from control muscle) in the proportion of each fibre type in SOL muscles of *ob/ob* mice. ‘–’ indicates that the fibre type was not detected in the SOL muscles from *ob/ob* mice. SOL – soleus.

and IID) that were not detected in the fibre population dissected from SM of lean mice.

As seen in Figure 3.8, the population of fibres dissected from SOL of *ob/ob* mice yielded seven types of fibres while that from SOL muscles of lean mice produced 12 fibre types. As seen in Table 3.5, there was an obesity-related decrease in type II-only fibres (33.6%), a 7.4% decrease in type I fibres and a 20.9% increase in type I+II-containing hybrids. If one considers that the 20.9% increase in type I+II hybrids is

equivalent with a 10.45% increase in type I fibres and a 10.45% increase in type II fibres, one would obtain a net increase of 3.05% in type I fibres and a net decrease of 23.15% in type II fibres in SOL muscle of *ob/ob* mouse.

Section 3.4 DISCUSSION

The data produced by the present study indicate that skeletal muscles of genetically obese mice differ significantly from those of lean controls with respect to muscle mass and CSA, fibre CSA and fibre type composition. While these differences were observed in all three muscles examined (EDL – hindlimb, locomotor; SM – upper trunk-neck, accessory in respiration; SOL – hindlimb, postural support), regardless of their location or main function, the extent of these differences was found to be muscle-specific.

Fibre type composition

In this study, the fibre type composition of muscles from the *ob/ob* and lean mice was established by electrophoretic analysis of MHC isoforms in whole muscle homogenates and in randomly dissected, single muscle fibres. The results obtained using the two approaches (lower MHC IIB/IId ratio in homogenates and lower proportion of IIB fibres in fibre populations from EDL and SM of obese mice; greater MHC I/II ratio in homogenates and higher proportion of fibres containing MHC I fibre populations from SOL of obese mice) are consistent with the idea that, in mice, genetic obesity is associated with a slower skeletal muscle phenotype. An increase in the proportions of MHC I and IIa isoforms and a decrease in the proportion of the MHC IId and IIB isoforms were also reported for the diaphragm from C57BL/6J-*ob/ob* mice by Tankersley *et al.* (1998) in a study in which the authors examined, electrophoretically, muscle proteins from whole muscle homogenates. To date, there

have been only two investigations of fibre type composition in limb muscles of adult *ob/ob* mice and in both these investigations, the authors used histochemical methods for determining fibre types. In one of these studies, Warmington *et al.* (2000) reported an obesity-related decrease in the proportion of type IIB fibres in EDL (matched by an increase in the proportion of type IIA fibres) and in SOL, but the data illustrating this phenomenon are not very convincing because in their study, where the effects of leptin treatment were explored, evidence for obesity-related fibre type alterations was produced from leptin- and non-leptin-treated mice data grouped together. When the fibre type proportions of these muscles are compared using non-leptin-treated *ob/ob* and lean mice only, the data suggest little difference in fibre type composition. In the other study, Stickland *et al.* (1994) reported no evidence of a fibre type shift in either SOL or biceps brachii muscles of *ob/ob* mice.

The difference in fibre type composition between muscles from *ob/ob* and lean mice could have arisen if these muscles followed a different developmental pattern. Consistent with this idea is the finding that, in *ob/ob* mice, skeletal muscles have a smaller mass from an early age (Grundleger *et al.*, 1980; Almond & Enser, 1984; Champion *et al.*, 1984). Alternatively, muscles from *ob/ob* mice could have undergone a process of structural remodeling associated with the obese condition. This possibility is supported by the finding that EDL, SM and SOL of *ob/ob* mice contain a greater proportion of hybrid fibres [a marker of structural remodeling (Pette *et al.*, 1999; Pette & Staron, 2000; Stephenson, 2001, 2006)] than their respective counterparts in the lean controls. Specifically, in EDL and SM muscles from *ob/ob* mice, the proportion of hybrid fibres was four and 1.9 times greater, respectively, than that in control muscles. For EDL from *ob/ob* mice, this resulted from a greater

proportion of type IIB+IID fibres, with an additional fibre type group, IIA+IIB, also being identified. For SM from *ob/ob* mice, the greater proportion of hybrid fibres was primarily due to a greater proportion of type IIB+IID fibres. By comparison with EDL and SM, the proportion of hybrid fibres in SOL muscles from *ob/ob* mice was only 1.3 times greater than in SOL muscles from lean mice, and this difference did not reach statistical significance ($p=0.060$).

The greater proportion of hybrid fibres detected in EDL and SM muscles of *ob/ob* mice, and the range of combinations of MHC isoforms co-expressed in these fibres, could indicate that in these muscles, a process of fibre type transition is taking place in the direction IIB→IID→IIA. In the fibre population dissected from SOL muscles of *ob/ob* mice, there was a markedly greater proportion of hybrid fibres co-expressing the MHC I isoform than in fibres from lean mice (82.9% *v* 42.7%), as well as a greater proportion of the total hybrid fibre count made up of type I+IIA fibres (51.5% *v* 11.1%). Together these data suggest that in SOL muscles of *ob/ob* mice, an active process of fibre type transition in the direction IIB→IID→IIA→I is taking place.

Interestingly, SOL muscles from lean (control) mice displayed a much larger proportion of hybrid fibres (42.7%) than has been reported for SOL muscles from rat (11% – Bortolotto *et al.*, 2000). It has been suggested that the presence of a large proportion of hybrid fibres in a ‘normal’ (or ‘non-transforming’) muscle is related to the muscle’s ability to perform a greater repertoire of activities (Stephenson, 2006). In this context, the physiological functions performed by the SOL muscle of the mouse may be more diverse than that of rat, involving more than just a postural role (Hennig & Lomo, 1987; Fitts *et al.*, 2001; Hitomi *et al.*, 2005). The fibre type population from

SOL of lean mice also exhibited a more diverse pattern of MHC co-expression, with nine combinations identified, as compared to only five hybrid fibre types in the population from *ob/ob* mice. This finding challenges current dogma which asserts that both the proportion of hybrid fibres and the diversity of MHC co-expression are greater in transforming muscles (Pette *et al.*, 1999; Stephenson, 2001). The level of molecular complexity found here in mouse SOL muscle, in conjunction with the EDL and SM data of the present study and other reports of ‘unusual’ fibre types in rodent skeletal muscle (Bortolotto *et al.*, 2000; Picquet *et al.*, 2002; O’Connell *et al.*, 2004), suggest that MHC co-expression in single fibres is not constrained by the ‘nearest-neighbour rule’ formulated by Pette *et al.* (1999).

What factors could contribute to the slower fibre type profile of skeletal muscles from obese mice? One potential factor (considered also in relation to the smaller skeletal muscle size in *ob/ob* mice; see Section 1.4.2) is the higher level of circulating glucocorticoids in *ob/ob* mice (Dubuc, 1976b; Smith & Romsos, 1984; Bray *et al.*, 1989). Indeed, fibre type changes in the direction discussed above have been associated with elevated glucocorticoid concentrations (Falduto *et al.*, 1990; Polla *et al.*, 1994; Seene *et al.*, 2003). For example, in EDL and plantaris of adult rat, elevated glucocorticoid concentrations lead to alterations that are similar to those obtained for obese mice EDL and SM in the present study, viz. decreases in the MHC Iib and increases in MHC Iia and MHC Iid isoform proportions (Seene *et al.*, 2003). Polla *et al.* (1994) also reported decreases in type IIB and increases in type IIA fibre proportions in EDL, diaphragm and parasternal intercostal muscles of rats administered glucocorticoids, with SOL showing evidence of lower type IIA and greater type I fibre proportions.

The observed alteration in muscle fibre composition phenotype is also likely to result from a combination of mechanical, neural and metabolic changes that accompany genetic obesity. One such change is the dramatically reduced muscle mass-to-body mass ratio of EDL, SM and SOL muscles from *ob/ob* mice, which in this study showed decreases of 56%, 62% and 52%, respectively, when compared to values for lean mice. This reduction in the normal muscle-to-body mass ratio may be viewed as an increase in the functional demand on postural muscles (e.g. SOL) that are required to support a proportionally greater mass against gravity and locomotor muscles (e.g. EDL) that must overcome the proportionally greater inertia of the limbs during movement. Studies employing compensatory overload by synergist ablation (Ianuzzo *et al.*, 1976; Timson *et al.*, 1985; Yamaguchi *et al.*, 1996) or load addition (Awede *et al.*, 1999) also display shifts in muscle fibre phenotype towards a slower profile, while another mouse model, the kyphoscoliotic (*ky/ky*) mouse, that experiences a reduced muscle mass-to-body mass ratio *in vivo* in response to an inability of skeletal muscle to hypertrophy, displays a slower muscle phenotype in both EDL and SOL muscles (Maréchal *et al.*, 1995; Maréchal *et al.*, 1996; Blanco *et al.*, 2001). Therefore, it is proposed that a chronic increase in work load may act as a stimulus to drive a fibre type/MHC_i transition in skeletal muscles of *ob/ob* mice in the direction observed in the present study, especially for the weight-bearing muscles (i.e. EDL and SOL).

When placed under greater relative load, skeletal muscle normally hypertrophies (Goldberg, 1967; Ianuzzo *et al.*, 1976; James, 1976; Baldwin *et al.*, 1982; Roy *et al.*, 1982; Timson *et al.*, 1985; Frischknecht & Vrbová, 1991; Frischknecht *et al.*, 1995; Yamaguchi *et al.*, 1996; Awede *et al.*, 1999). However, it is apparent that this adaptive ability is stifled in skeletal muscles of *ob/ob* mice. Without this adaptive

hypertrophy to increased load demands, it is further hypothesised that the neuromuscular system must employ other means to maintain typical muscle performance under greater load, namely a greater degree of activation to recruit more motor units and to stimulate them more frequently – that is, an increase in neuromuscular activity. This suggests that the obese mouse not only represents a model where postural and locomotor muscles *in vivo* are adapting to an endogenously generated overload but also to increased neuromuscular activity. Models of increased neuromuscular activity, including CLFS (Simoneau & Pette, 1988; Termin *et al.*, 1989; Leeuw & Pette, 1993; Jaschinski *et al.*, 1998; Peuker *et al.*, 1999), endurance training (Andersen & Henriksson, 1977; Jansson & Kaijser, 1977; Green *et al.*, 1984; Baumann *et al.*, 1987) and spontaneous hyperactivity resulting from a genetic defect (Asmussen *et al.*, 2003), also display shifts towards a slower muscle fibre profile, as observed in the present study.

For SM, its anatomical location likely renders the stress of an increased body mass minimal; however, SM did display a significantly ‘slower’ MHC_i/fibre type composition. With this muscle considered an accessory muscle of ventilation (Campbell, 1970; Moxham *et al.*, 1980; 1981; Gandevia *et al.*, 1990), the transition observed in its MHC_i/fibre type profile may signify an adaptation to the increased work of breathing associated with obesity (Sharp, 1985; Tankersley *et al.*, 1996, 1998). In *ob/ob* mice, this manifests itself as an increased respiratory rate (Tankersley *et al.*, 1996, 1998), which would imply a greater neural activation history for respiratory muscles. Previous work investigating respiratory muscles from genetically obese rodents supports the findings of a shift towards a slower MHC phenotype, with diaphragm from adult *ob/ob* mice (Tankersley *et al.*, 1998) and costal diaphragm,

crural diaphragm and parasternal intercostal muscles from adult Zucker obese rat (Powers *et al.*, 1996) displaying transitions of this nature in whole muscle MHC_i composition.

Fibre CSA and muscle mass

The predominance of type IIB and IIB+IID fibres in EDL (98%) and SM (85%) muscles of *ob/ob* mice is likely to be a major contributing factor to the smaller mass (and CSA) of these muscles, as compared to their respective controls, because the CSA of the fibres from these fibre type groups was significantly lower than that of their respective controls. Thus, the mean mass of EDL muscles from *ob/ob* mice was 21% smaller than that of the corresponding muscles from lean mice and, consistent with this difference, the mean CSA of type IIB and IIB+IID fibres from EDL muscles of *ob/ob* mice was 30% and 25% smaller, respectively, than the control IIB and IIB+IID fibres. Similarly, the mean mass of SM muscles from *ob/ob* mice was 30% smaller than that of the corresponding muscles from lean mice and, again, consistent with this difference, the mean CSA of type IIB and IIB+IID fibres from SM muscles of *ob/ob* mice was 28% and 33% smaller, respectively, than the control IIB and IIB+IID fibres. By comparison, the CSA area of the predominant fibre types in SOL muscle, viz. type I, IIA, I+IIA and IIA+IID fibres (82% in *ob/ob* mouse), displayed similar values between *ob/ob* and lean mice and, consistent with this, SOL muscles from *ob/ob* mice demonstrated smaller decrements in mass than the decrements observed for EDL and SM muscles. Therefore, these data suggest that the magnitude of muscle mass attenuation experienced by skeletal muscles of *ob/ob* mice is strongly influenced by fibre type composition, with single fibres expressing the MHC IIB isoform being most susceptible to decrements in size.

The significant reductions observed in the size of type IIB and IIB+IID fibres, but not in the size of type I, IIA, I+IIA and IIA+IID fibres, from muscles of *ob/ob* mice in the present study are in agreement with data from a variety of obese rodent models (Almond & Enser, 1984; Burbach *et al.*, 1985; He *et al.*, 1995). For example, Almond & Enser (1984) showed that muscle mass decrements in biceps brachii from *ob/ob* mice were accounted for solely by reductions in the CSA of the larger, more glycolytic fibres (i.e. fast white and intermediate white fibres) rather than the fast red fibres. Similarly, in diaphragm of aspartic acid-treated obese rats, fast glycolytic (to the greatest extent) and fast oxidative-glycolytic fibres displayed reductions in fibre diameter when compared to control rats, with no differences observed in slow oxidative fibre diameter (Burbach *et al.*, 1985). Taken together, these data support the proposition that, in obese animals, fast fibres are more susceptible to reductions in size and, as such, fibre type composition plays a determining role in the morphological alterations observed in skeletal muscles of the *ob/ob* mouse.

The decrements in mass of EDL and SM muscles from *ob/ob* mice reported here are in agreement with results from other studies investigating predominantly fast-twitch skeletal muscles from these animals. The masses of the EDL, gastrocnemius and rectus femoris hind limb muscles from *ob/ob* mice have been reported to be more than 20% smaller than those from lean mice (Almond & Enser, 1984; Champion *et al.*, 1984; Smith & Romsos, 1984; Stickland *et al.*, 1994; Warmington *et al.*, 2000; Bruton *et al.*, 2002), a figure consistent with the 21% smaller mass of EDL in this study. Also, the 30% lower mass for SM found in this study is in close agreement with the 33% lower SM mass reported by Stickland *et al.* (1994).

The greater resistance of SOL from *ob/ob* mice to decrements in mass observed in this study agrees with previous work investigating the C57BL/6J-*ob/ob* strain of a similar age (15-16 weeks) (Grundleger *et al.*, 1980; Champion *et al.*, 1984). However, two other studies of adult *ob/ob* mice have reported large decrements (~33%) in SOL mass (Stickland *et al.*, 1994; Warmington *et al.*, 2000), but these works used mice in which the *ob/ob* mutation was maintained on different genomic backgrounds. As mentioned in Section 1.2.1, there is evidence that the interaction of the background genome with the mutant gene itself can influence the phenotype of the genetically obese animal (Herberg & Coleman, 1977; Coleman, 1978; Haluzik *et al.*, 2004). In agreement, with this, the degree of attenuation in SOL mass associated with the genetically obese condition appears to vary with the genetic background of the mouse strain used, with SOL muscles of C57BL/6J-*ob/ob* mice being more resistant to reductions in size.

Protein content

Despite the differences in skeletal muscle morphology between *ob/ob* and lean mice recorded in the present study, no statistically significant differences were observed between the two groups with respect to protein concentration. This finding agrees with the bulk of previous work on genetically obese rodents, including *ob/ob* mice (Trostler *et al.*, 1982; Smith & Romsos, 1984) and Zucker obese rats (Shapira *et al.*, 1980; Durschlag & Layman, 1983). The total protein concentrations for EDL, SM and SOL muscles from lean (and obese) mice are consistent with previously published values for mammalian skeletal muscle (Bárány *et al.*, 1965; Yates & Greaser, 1983; Lawrie, 1991; Geiger *et al.*, 2000) and, specifically, with values for C57BL/6J mice (Cuendet *et al.*, 1976; Smith & Romsos, 1984). It should be noted that Cuendet *et al.* (1976) reported a significantly lower protein concentration in SOL from *ob/ob*

compared to lean mice, but this may be attributed to the fact that in the study of Cuendet *et al.* (1976), muscles were weighed with tendons intact, which would add variability to the measurement.

The values reported here for MHC content are the first in the literature for *ob/ob* mice and, similar to total protein data, normalised values (i.e. MHC content per gram muscle mass) showed no statistically significant differences from lean mice. Again, the normalised values reported here for MHC content are in close agreement with other work examining mammalian skeletal muscle (Bárány & Close, 1971; Geiger *et al.*, 2000; Tikunov *et al.*, 2001).

In conclusion, EDL, SM and SOL muscles of *ob/ob* mice displayed significant alterations in MHC_i composition, fibre type distribution and hybrid fibre content as compared to control muscles, with EDL muscle being the most affected. In particular, skeletal muscles of *ob/ob* mice displayed a greater proportion of hybrid fibres and a shift in their MHC_i/fibre type composition towards a slower phenotype. These structural changes are suggested to reflect a different pattern of development followed by these muscles and/or an active process of fibre type transformation resulting from a combination of mechanical, neural and hormonal/metabolic stimuli associated with the *ob/ob* milieu. EDL, SM and SOL muscles of *ob/ob* mice also displayed significant attenuations in size, with EDL and SM being most affected. The predominating presence of type IIB and IIB+IID fibres in EDL and SM muscles contributed to the markedly smaller size of these two muscles from *ob/ob* mice, because these fibre types from *ob/ob* mice were significantly smaller than the same fibre types from lean mice.

In other physiological/pathological conditions that display decrements in skeletal muscle mass and muscle fibre size, impairments in normal contractile function are also observed (Fitts *et al.*, 1986; Seene, 1994; Maréchal *et al.*, 1995; Larsson *et al.*, 1997; Grinspoon *et al.*, 1999; Thompson & Brown, 1999; Roubenoff, 2000; Greiwe *et al.*, 2001; D'Antona *et al.*, 2003; Villareal *et al.*, 2004; Gea *et al.*, 2006). This can raise a number of questions related to the contractile status of skeletal muscles from *ob/ob* mice. The questions addressed in the following chapters are: (i) What are the contractile characteristics of these markedly smaller muscles from obese mice? (ii) Do the observed differences in muscle morphology translate to differences in contractile function? (iii) Is the fibre type transition towards a slower muscle fibre profile reflected in the contractile performance of the muscles from *ob/ob* mouse?

Chapter 4

Contractile characteristics of EDL, SM and SOL muscles from *ob/ob* mouse

Section 4.1 INTRODUCTION

As stated in Section 1.4.2, skeletal muscles of obese animals, including those of *ob/ob* mouse, are often significantly smaller than those of their respective control animals (Shapira *et al.*, 1980; Durschlag & Layman, 1983; Almond & Enser, 1984; Campion *et al.*, 1984; Smith & Romsos, 1984; Burbach *et al.*, 1985; Stickland *et al.*, 1994; Warmington *et al.*, 2000; Bruton *et al.*, 2002). This phenomenon has been also observed in the 18-22 wk-old *ob/ob* mice examined in the present study (see Section 3.3.1). In other conditions where the size of skeletal muscles is diminished, impairments in contractile function also occur (Fitts *et al.*, 1986; Maréchal *et al.*, 1995; Larsson *et al.*, 1997; Grinspoon *et al.*, 1999; Thompson & Brown, 1999; Roubenoff, 2000; Greiwe *et al.*, 2001; D'Antona *et al.*, 2003; Villareal *et al.*, 2004; Gea *et al.*, 2006). This raises questions as to the contractile performance of skeletal muscle in obese animals, whose larger body mass must be managed by the smaller skeletal muscles.

To date there have been only two studies concerned with the contractile characteristics of skeletal muscles from *ob/ob* mice (Warmington *et al.*, 2000; Bruton *et al.*, 2002). These two studies were limited to two hind limb muscles (EDL and SOL - Warmington study; EDL - Bruton study) and neither study produced data on both the force-generating capacity and contractile kinetics of the twitch and tetanus responses. The findings reported in these studies cannot be easily compared because the strain of the *ob/ob* mice used in the study of Warmington *et al.* (2000) (Aston strain) differs from that used by Bruton *et al.* (2002) (C57BL/6J strain). One notes,

though, that the muscle mass values for EDL and SOL from *ob/ob* and control mice reported by Warmington *et al.* (2000) are markedly smaller than those reported in studies examining C57BL/6J-*ob/ob* mice of similar age (Grundleger *et al.*, 1980; Almond & Enser, 1984; Campion *et al.*, 1984; Bruton *et al.*, 2002) and that the force generating-capacity of muscles in the studies of Warmington *et al.* (2000) and Bruton *et al.* (2002) are markedly different.

In addition to questions raised by the limited and seemingly inconsistent data available for hind limb skeletal muscles of *ob/ob* mice, there is the question of whether skeletal muscles of different anatomical location and/or physiological function from these animals experience comparative alterations in contractility. Sternomastoid muscle, a rotator and flexor of the head and neck (Gandevia *et al.*, 1990), exhibits obesity-related decrements in size (Stickland *et al.*, 1994; the present study) but is not subjected to the locomotor and/or weight-bearing forces experienced by hind limb muscles. However, SM acts also as an accessory muscle of ventilation (Campbell, 1970; Moxham *et al.*, 1980; 1981; Gandevia *et al.*, 1990) and, as such, may be affected by the respiratory complications known to develop in *ob/ob* mice due to obesity (Tankersley *et al.*, 1996, 1998).

Within this context, the aim of this study was to explore the possibility that alterations in the size and work demands of skeletal muscles of different locations and/or function from *ob/ob* mice are accompanied by muscle-specific changes in their contractile performance. To this end, parameters describing the twitch and tetanus responses (see Section 1.3.8) of EDL, SM and SOL muscles from C57BL/6J-*ob/ob* and lean mice were assessed *in vitro* using isolated whole muscle preparations.

Section 4.2 METHODS

4.2.1 *Animals and muscles*

A pool of forty muscles was used in the experiments designed to assess contractile function at a whole muscle level. This pool comprised EDL (8 per animal group), SM (6 per animal group) and SOL (6 per animal group) muscles from 20 *ob/ob* and 20 lean mice. Animal care and handling are described in Section 2.1 and the procedures followed with respect to muscle dissection and handling are described in Section 2.2.

4.2.2 *Determination of muscle mass*

For the study described in this chapter, muscle mass was determined, as described in Section 2.2(a), immediately after the completion of measurements of contractile parameters (see Section 4.2.4) and determination of muscle width (see Section 2.3). Muscles were then stored at -84°C for future homogenisation (see Section 3.2.4).

4.2.3 *Set-up for whole muscle contractility experiments*

4.2.3.1 *Solution used for whole muscle contractility experiments*

Following dissection, muscles were pinned in a Petri dish (with a Sylgard 184 base) and incubated for 30 min in a Krebs solution bubbled with carbogen (95% oxygen, 5% carbon dioxide). The solution contained 122 mM NaCl, 2.8 mM KCl, 1.3 mM CaCl_2 , 1.2 mM MgSO_4 , 1.2 mM KH_2PO_4 , 25 mM NaHCO_3 , 10 mM D-glucose and 10 μM tubocurarin (pH 7.4) (modified from Pedersen *et al.*, 2003b). The neuromuscular paralysing agent tubocurarin was added to the solution to prevent any contribution to

force production coming from motor nerve stimulation. All operations involved in whole muscle contractility testing were performed at 25.0 ± 0.5 °C.

4.2.3.2 Mounting of the whole muscle in the system for isometric contractile testing

For all dissected muscles, Deknatel suture silk 5-0 (Genzyme Biosurgery, Falls River) was secured around the tendon at the point of muscle-tendon junction, under stereomicroscope. Two further loops of suture silk were tied immediately behind the initial loop to prevent muscle loosening or slipping. This was repeated on the opposing tendon.

The muscle was then mounted in the *in vitro* system for whole muscle contractile experiments (see Figures 4.1 and 4.2). This mounting process involved fixing the tissue at one end by tying it (with the suture silk) to an immovable mounting rod and then attaching it in a similar manner at the other end to an isometric force transducer (Grass force-displacement transducer, model FT03; Grass Instruments, Quincy) mounted on a micro-manipulator (Prior, UK).

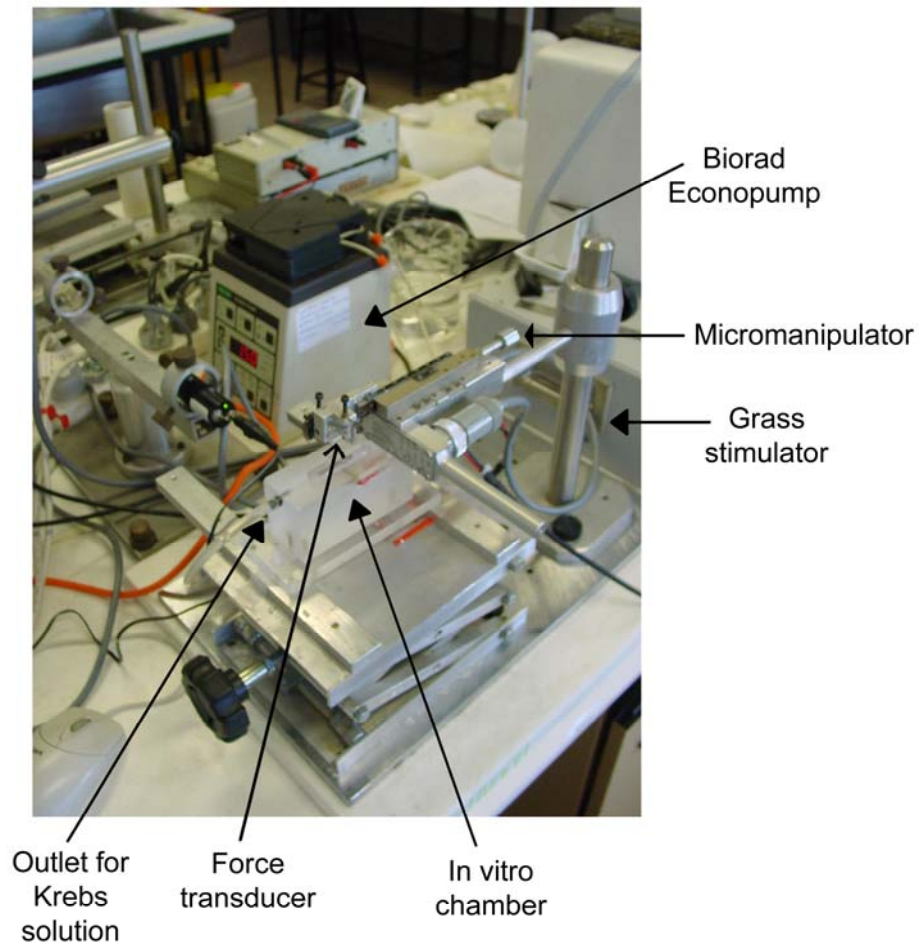


Figure 4.1 Apparatus for *in vitro* whole muscle contractility experiments. An isolated whole muscle was mounted to a force transducer and immovable mounting rod and lowered into the *in vitro* chamber between two platinum electrodes, with stimulation delivered by a Grass stimulator (display not shown). The micromanipulator was used to adjust muscle length. A Biorad Econopump maintained a constant flow of oxygenated Krebs solution.

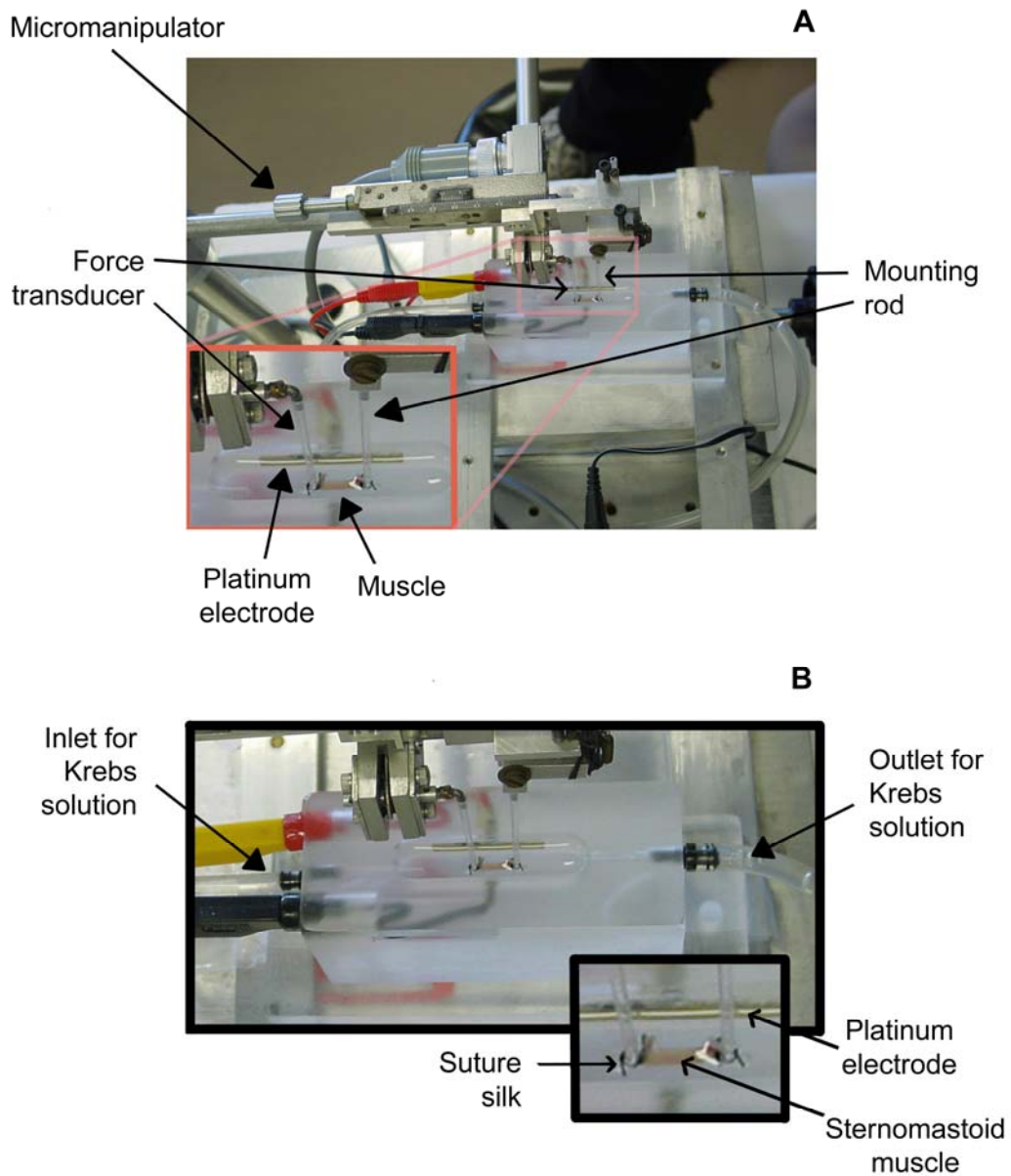


Figure 4.2 *In vitro* chamber for whole muscle contractility experiments.
 A. *In vitro* chamber with micromanipulator, force transducer and a constant flow of Krebs solution. *Inset:* Muscle in place for contractility experiments between platinum electrodes. B. *In vitro* chamber with muscle in place for contractility experiments. *Inset:* Sternomastoid muscle tied by silk suture to force transducer and immovable mounting rod.

4.2.3.3 Calibration of the force transducer

The micromanipulator with the force transducer was rotated by 90° and weights ranging from 5.9 to 356.7 mN (0.6 to 36.4 g) were sequentially hung from the force transducer. The response from each weight was recorded by a computerised data acquisition system using Powerlab software (ADInstruments, Colorado Springs), which included a 12-bit A/D converter and bridge amplifier, at a sampling rate of 1 kHz. A curve was constructed with displacement on the Powerlab software represented on the ordinate axis and force on the abscissa (Figure 4.3). The sensitivity of the transducer was 4.467 mV/1 N.

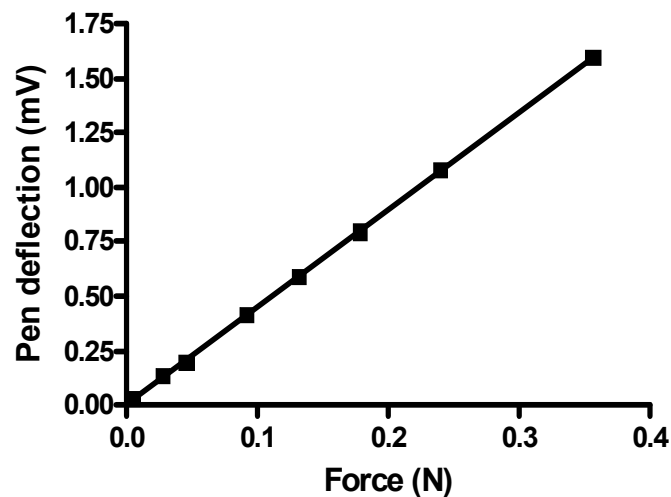


Figure 4.3 Calibration curve of force transducer employed in isolated whole muscle contractility experiments. A series of weights were suspended vertically from the force transducer and the resulting signal was recorded by a computerised data acquisition system. $r^2=0.9998$.

4.2.4 Measurements of the isometric contractile characteristics of whole muscles

In experiments used to assess the contractile characteristics in isolated whole muscle preparations (i.e. in the absence of a circulatory system), it is important to ensure that all fibres are adequately oxygenated throughout the experiment. Goldberg *et al.* (1975) reported that muscles whose wet weight did not exceed 30 mg remained viable in physiological studies at 37 °C *in vitro*. Segal & Faulkner (1985) showed that in contractile studies at 25 °C, muscles of 70-90 mg, with a muscle radius not exceeding ~1.0 mm, maintained stability in the contractile properties of the twitch and tetanus over a 60-min period. For the whole muscle contractile work performed in this study, no muscle exceeded a wet weight of 30 mg.

Two subpopulations of muscles, one from *ob/ob* (n=17) and one from lean (n=13) mice, were used to collect data on muscle width, as described in Section 2.3. For *ob/ob* mice, mean muscle width measured at the midpoint of L_o for EDL (n=6) was 1.51 ± 0.05 mm, for SM (n=5) was 1.72 ± 0.07 mm and for SOL (n=6) was 1.32 ± 0.05 mm. For lean mice, mean width was 1.73 ± 0.09 mm for EDL (n=4), 1.92 ± 0.03 mm for SM (n=5) and 1.39 ± 0.07 mm for SOL (n=4). Therefore, none of these muscles exceeded the critical radius of 1.0 mm. Taken together, these data indicate that the sizes of the EDL, SM and SOL muscles used in this study satisfied both the width-based and the mass-based criteria for testing the contractility of whole muscle preparations *in vitro*.

After the 30-minute equilibration period in oxygenated Krebs solution, the muscle was mounted to the *in vitro* system (described in Section 4.2.3), positioned horizontally between the two platinum plate electrodes in the *in vitro* chamber (see

Figure 4.2B) and then exposed to supramaximal field stimulation [13 V/cm (verified with an oscilloscope); 0.2 ms pulse duration] delivered by a Grass Telefactor Square Pulse Stimulator, model S48K (Grass Instruments, Quincy). Krebs solution flowed through the chamber at 1.6 ml/min, controlled by a Biorad Econopump (model EP1). Contractile responses were recorded simultaneously by a chart recorder (Rikedanki, Tokyo) and by the computerised data acquisition system. The data were analysed using Chart V4.1.2 software (ADInstruments, Colorado Springs) and data points selected by the computerised system for generating each parameter value were verified by the experimenter by way of observing each relevant data trace.

First the muscle was adjusted to its optimal length (L_o), defined as the length at which the muscle generates peak twitch force. This process involved a stepwise increase in muscle length (recorded by the micro-manipulator mounted on the force transducer) at one minute intervals. At each new length, the muscle was given a single pulse. This continued until P_t was achieved. All subsequent measurements of twitch and tetanic parameters were performed at this muscle length (i.e. L_o).

In Table 1.2 are given details of the functional parameters represented by the experimental parameters listed in the following sections.

4.2.4.1 Twitch characteristics

A single supramaximal pulse was administered to the muscle to generate a single twitch response. Two twitches at L_o , separated by one minute of rest, were conducted to verify the stability of the response. No differences between the two responses were found for any of the muscles used in this study. For all muscles, the value of the

second twitch was used when calculating the following experimental parameters (see also Figure 1.7; page 32):

- peak twitch force (P_t) (mN)
- time to peak force (TPT) (ms), defined as the time from onset of contraction to the point where peak force was achieved
- half-relaxation time ($1/2RT$) (ms), defined as the time taken for force to decrease from its peak value to 50% of the peak value
- 50-50 duration of the twitch (W_{50}) (ms), defined as the time taken from the point where 50% of the peak force had developed to the point where 50% of the peak force had decayed (i.e. duration of the twitch measured at half amplitude) (Posterino & Lamb, 2003)

4.2.4.2 Force-frequency relationship

Force-frequency responses were determined using stimulation trains of 500 ms. Muscles were sequentially stimulated at the following frequencies, with three minutes of rest between each train:

- EDL – 5 Hz, 10 Hz, 30 Hz, 50 Hz, 70 Hz, 90 Hz, 110 Hz
- SM – 5 Hz, 10 Hz, 30 Hz, 50 Hz, 70 Hz, 80 Hz, 90 Hz
- SOL – 5 Hz, 10 Hz, 30 Hz, 50 Hz, 70 Hz, 80 Hz, 90 Hz

Note: The stimulation rate that elicited peak tetanic force (P_o) for each muscle (EDL 110 Hz; SM 90 Hz; SOL 90 Hz) was determined during preliminary force-frequency experiments.

4.2.4.3 Tetanic characteristics

Preliminary experiments showed no difference between the amplitude of the P_o response performed as part (i.e. the last response) of the force-frequency relationship and that of a P_o response performed 3 min prior to commencement of force-frequency testing. Consequently, P_o responses obtained at 110 Hz for EDL and 90 Hz for SM and SOL, as part of force-frequency testing, were used to calculate the following parameters associated with the tetanic characteristics of the three muscles from *ob/ob* and lean mice (see Figure 1.8; page 34):

- peak tetanic force (P_o) (mN)
- peak rate of force development, normalised to peak tetanic force ($+dP/dt.P_o^{-1}$) (s^{-1})
- half-relaxation time of the tetanus ($1/2RT_{tet}$) (ms), measured from the last stimulus to the point where force reached 50% of the peak value (Gillis, 1985; Bruton *et al.*, 2003; Clark & Peters, 2006)
- peak rate of relaxation, normalised to peak tetanic force ($-dP/dt.P_o^{-1}$) (s^{-1})
- slope of the linear phase of the relaxation response, normalised to peak tetanic force (s^{-1})
- duration of the linear phase of the relaxation response (ms)

4.2.5 Data analysis

(i) For the force-frequency relationship, values were normalised by expressing the force response at each frequency as a percentage of P_o .

(ii) Specific force (for P_t and P_o) was calculated in $kN.m^{-2}$ of muscle cross-sectional area (CSA). CSA was estimated using the formula (Fitts & Holloszy, 1977, 1978):

$$\text{CSA (mm}^2\text{)} = \frac{\text{muscle mass (mg)}}{1.06 \text{ (mg}\cdot\text{mm}^{-3}\text{)} \times L_o \text{ (mm)}}$$

where 1.06 mg.mm⁻³ represents muscle density for mammalian muscle (Méndez & Keys, 1960);

(iii) The CSA calculation in part (ii) above may underestimate the true sum of the cross-sectional areas of all the fibres in a muscle (Close, 1972; Witzmann *et al.*, 1982) because, due to each muscle particular architecture, single fibres may not run the entire length of the muscle and/or may not run parallel to its long axis (Close, 1964, 1972; Gans, 1982; Brooks & Faulkner, 1988). Therefore, P_t and P_o were also normalised to the estimated physiological CSA (PCSA) of the muscle (Witzmann *et al.*, 1982; Wickiewicz *et al.*, 1983; Narici & Maganaris, 2006) as follows:

$$\text{PCSA (mm}^2\text{)} = \frac{\text{muscle mass (mg)} \times \cos(\text{pennation angle in degrees})}{1.06 \text{ (mg}\cdot\text{mm}^{-3}\text{)} \times L_o \times \frac{L_{\text{fibre}}}{L_{\text{muscle}}}}$$

where pennation angle and fibre length/muscle length ratio were estimated from values reported in the literature (outlined in Table 4.1 in Section 4.3.1; page 126).

(iv) For the calculation of the parameters used to describe the twitch and tetanic characteristics, Chart V4.1.2 software was used.

- (a) For the calculation of *peak force* of a response, a least-squares parabola was fitted to the data. From this, P_t and P_o were reported as the peak amplitude of the parabola relative to the baseline.

- (b) For the calculation of *peak rate of force development* and *peak rate of relaxation* for the force curve of P_t or P_o , data points were smoothed across a time period of 5 ms and fitted with a least-squares straight line with the slope of the line taken as the slope at the centre data point. This process was then shifted one point to the right and repeated. The peak slope in this iteration was reported as the peak rate of force development (or peak rate of relaxation).
- (c) The *slope of the linear (slow) phase of the relaxation curve* of P_o (see Figure 1.8; page 34) was calculated as the least-squares line of best fit (i.e. the average of the regression lines fitted to each point making up the linear phase).

4.2.6 Statistical analysis

All results are presented as mean \pm S.E., unless otherwise stated. One way ANOVA with Tukey HSD *post hoc* testing was used to detect differences among values for EDL, SM and SOL muscles from lean mice. Student's independent *t* test (two-tailed) was used to detect differences between *ob/ob* and lean mouse groups. These statistical techniques were also employed when comparing the force-frequency relationships of muscles, in that comparisons were made at each frequency of stimulation among muscles from lean mice (ANOVA) and between *ob/ob* and lean mouse groups (*t*-test). Statistical significance was accepted as $p \leq 0.05$. Sample size is denoted by *n*.

Section 4.3 RESULTS

4.3.1 Parameters describing the force-generating capacity of EDL, SM and SOL muscles of *ob/ob* and lean mice

NOTE: Representative twitch and tetanic traces produced by the EDL, SM and SOL muscles from *ob/ob* and lean mice are displayed in Figure 4.4 and the values of the parameters describing the twitch and tetanic responses for the three muscles from the two animal groups are shown in Table 4.1.

4.3.1.1 Twitch force

As seen in Table 4.1, there was a significant difference among the three skeletal muscles from lean mice with respect to P_t ($p=0.001$), with EDL and SM generating 66% ($p<0.01$) and 72% ($p<0.01$) greater twitch forces than SOL, respectively. When comparisons were made for force normalised to muscle CSA (sP_t), a significant difference still existed among the three skeletal muscles ($p<0.0001$), but the values decreased in the order EDL > SOL > SM. More specifically, the mean EDL value was 33% and 120% higher than that for SOL ($p<0.05$) and SM ($p<0.001$), respectively, and the mean SOL value was 39% higher than that for SM ($p<0.05$). Greater sP_t values for EDL compared to SOL have been reported previously (Fitts *et al.*, 1982; Brooks & Faulkner, 1988), but to this author's knowledge, the data obtained in this study allow, for the first time, comparison of sP_t in isolated whole mouse SM, EDL and SOL muscles tested under the same conditions. It is worth noting that the sP_t

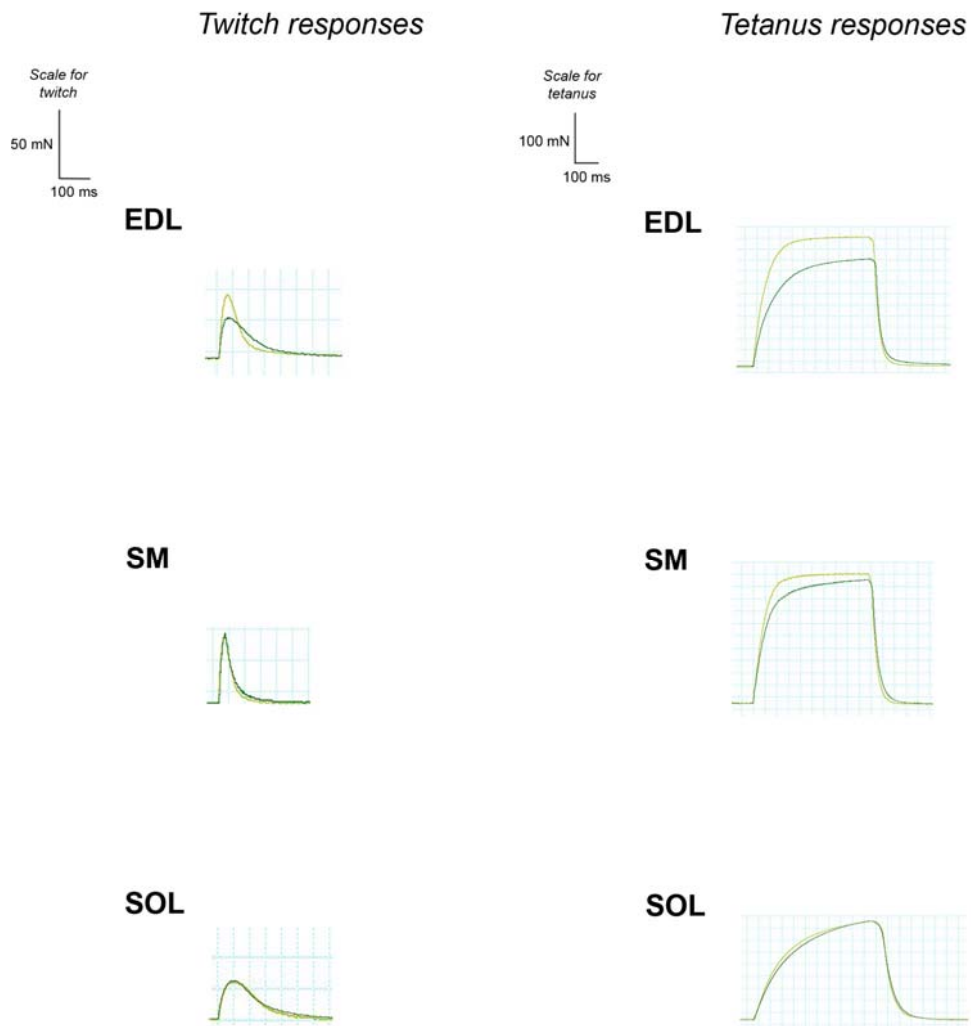


Figure 4.4 Representative data traces of twitch and peak tetanus responses for whole EDL, SM and SOL muscles from adult *ob/ob* and lean mice. For *twitch responses* (left hand column), muscle from *ob/ob* (—) and lean (—) mice were exposed to supramaximal field stimulation and given a single pulse at L_0 . For *tetanus responses* (right hand column), muscles were given stimulation trains of 500 ms at a stimulation frequency of 110 Hz for EDL, 90 Hz for SM and 90 Hz for SOL. Isometric force responses (as shown above) were recorded and displayed by a computerised data acquisition system.

Table 4.1 Parameters describing the force-generating capacity of EDL, SM and SOL muscles of *ob/ob* and lean mice.

Parameter	EDL		SM		SOL	
	<i>ob/ob</i> (8)	lean (8)	<i>ob/ob</i> (6)	lean (6)	<i>ob/ob</i> (6)	lean (6)
P_t (mN)	31.6 ± 2.1*	41.9 ± 3.3	44.5 ± 2.4	43.6 ± 3.7	28.2 ± 0.6	25.3 ± 1.2 ^a
sP_t (kN.m⁻²)	38.0 ± 2.9	38.0 ± 2.9 ^a	25.2 ± 1.1*	17.4 ± 1.4 ^a	37.7 ± 1.7*	28.6 ± 1.6 ^a
P_o (mN)	206.6 ± 14.4	247.0 ± 20.5 ^b	195.1 ± 15.8	198.2 ± 9.2	186.2 ± 8.0	178.4 ± 6.9
sP_o (kN.m⁻²)	250.2 ± 22.2	224.9 ± 18.9	110.9 ± 9.7*	79.1 ± 2.6 ^a	247.9 ± 10.9*	202.1 ± 10.9
s-P_o (mN.g⁻¹ body mass)	4.0 ± 0.3*	8.6 ± 0.6	3.6 ± 0.3*	6.7 ± 0.3	3.4 ± 0.1*	5.8 ± 0.2
Mass (mg)	9.9 ± 0.4	13.5 ± 0.7	17.9 ± 0.8	26.6 ± 1.6	8.8 ± 0.4	10.1 ± 0.4
L_o (mm)	11.2 ± 0.2	11.5 ± 0.3	9.6 ± 0.3	10.0 ± 0.2	11.0 ± 0.3	10.7 ± 0.4
L_{fibre}/L_{muscle}	?	0.47 [§]	?	1.0 ^{&}	?	0.68 [§]
Fibre pennation angle (degrees)	?	3.5 [@]	?	0 [#]	?	5 [@]
CSA (mm²)		1.11 ± 0.06 ^a		2.52 ± 0.14 ^a		0.89 ± 0.03 ^a
PCSA (mm²)		2.35 ± 0.12 ^b		2.52 ± 0.14 ^b		1.30 ± 0.04
psP_t (kN.m⁻²)		17.9 ± 1.4		17.4 ± 1.4		19.6 ± 1.1
psP_o (kN.m⁻²)		105.9 ± 8.9 ^a		79.1 ± 2.6 ^a		138.0 ± 7.5 ^a

Values are mean ± S.E. Significantly different from *lean counterpart, ^aother lean muscles and ^blean SOL (see text for significance levels). The number of muscles assessed is indicated in parentheses. [@]value from Close (1964); [#]value from Young *et al.* (2000); [§]value from Brooks & Faulkner (1988); [&]value based on the assumption that SM single fibres run from muscle origin to insertion (Paul, 2001; Young *et al.*, 2000). Note that the mean muscle mass values listed in the table are derived from the muscles used in the contractility experiments only. EDL – extensor digitorum longus; SM – sternomastoid; SOL – soleus; L_o – optimal length (muscle length providing peak twitch force); L_{fibre}/L_{muscle} – fibre length/muscle length ratio; CSA – whole muscle cross-sectional area; PCSA – physiological cross-sectional area; P_t – peak twitch force; P_o – peak tetanic force; sP_t – peak twitch force, normalised to muscle CSA; sP_o – peak tetanic force, normalised to muscle CSA; s-P_o – peak tetanic force, normalised to body mass; psP_t – peak twitch force, normalised to the estimated muscle PCSA; psP_o – peak tetanic force, normalised to the estimated muscle PCSA.

values recorded for mouse SM muscles in the present study were similar to those ($21.7 \pm 1.2 \text{ kN.m}^{-2}$) reported for fibre bundles dissected from rat SM by Luff (1985).

When comparing P_t for muscles from *ob/ob* and lean mice, differences between the two mouse groups were found only for EDL, with muscles from *ob/ob* mice producing 25% less force than those from lean mice ($p=0.021$). When P_t was normalised to muscle CSA, the EDL value for *ob/ob* mice was not significantly different from that for lean mice ($p=0.994$), while SM and SOL values for *ob/ob* mice were 45% ($p=0.001$) and 32% ($p=0.003$) greater, respectively, than the values for lean mice.

4.3.1.2 Tetanic force

A comparison of the P_o values for EDL, SM and SOL muscles from lean mice (see Table 4.1) showed a significant difference between EDL and SOL ($p<0.05$), with EDL generating a 38% greater absolute tetanic force. When P_o was normalised to muscle CSA, this difference between EDL and SOL was no longer present. Instead, a significant difference was found between SM and both EDL and SOL ($p<0.001$), with SM producing lower sP_o values than both the other two muscles. The differences in tetanic force production among the three muscles of interest from lean mice are similar, in part, to the differences observed in twitch force, with the most noticeable finding being the much smaller sP_o generated by the SM in comparison to the EDL and SOL muscles.

When comparing P_o values for muscles from *ob/ob* and lean mice, no differences were found between the two groups for EDL ($p=0.129$), SM ($p=0.870$) or SOL

($p=0.478$) muscles. When P_o was normalised to muscle CSA, all three muscles from *ob/ob* mice produced greater sP_o than muscles from lean mice, with values for EDL being 11% ($p=0.399$), SM being 40% ($p=0.01$) and SOL being 23% ($p=0.014$) greater than those for lean mice. These data would suggest that the capacity of all three muscles from *ob/ob* mice to produce tetanic force is not diminished despite their smaller size. However, when P_o was normalised to body mass ($s-P_o$), all three muscles from *ob/ob* mice produced significantly smaller $s-P_o$ than muscles from lean mice ($p<0.0001$), with values for EDL being 54%, SM being 46% and SOL being 41% smaller than those for lean mice.

4.3.1.3 Aspects of muscle architecture relevant to force generation by EDL, SM and SOL muscles from ob/ob and lean mice

Specific forces (twitch and tetanic) produced by a muscle depend not only on the cross-sectional area, calculated from the mass, density and length of the muscle, but also on aspects of muscle architecture that include fibre length (Close, 1972; Witzmann *et al.*, 1982; Brooks & Faulkner, 1988) and fibre pennation angle (Close, 1964; Gans, 1982; Brooks & Faulkner, 1988). With specific force values for the twitch and tetanic responses found to be markedly lower in SM than in EDL and SOL from control (lean) mice, it was deemed appropriate to assess the role that architectural differences among these three skeletal muscles may play with respect to this finding.

The value of the physiological cross-sectional area (PCSA) of a muscle takes into consideration the typical architectural characteristics of the muscle and represents the sum of cross-sectional areas of all muscle fibres within it (Gans, 1982; Lieber, 2002;

Narici & Maganaris, 2006). Therefore, sP_t and sP_o data described in Table 4.1 for EDL, SM and SOL from lean mice were re-calculated as described in Section 4.2.5(iii), taking into account published values for pennation angles and fibre length/muscle length ratios. The data for peak twitch and tetanic forces, normalised to the estimated PCSA (psP_t , psP_o) for EDL, SM and SOL muscles of lean mice, are also shown in Table 4.1. It is worth pointing out that, while the mean psP_t value for SM is no longer statistically different from the psP_t values for EDL and SOL, psP_o still displays significant differences among muscles ($p<0.001$), with the SM value being smaller than those for EDL ($p=0.027$) and SOL ($p<0.001$). However, it should be noted that psP_o for SM is only 1.3 times smaller than that for EDL, as compared to 2.8 times smaller when specific tetanic force was normalised to the more commonly used CSA value. The difference between SM and SOL muscles for specific tetanic force was also greatly reduced when normalised to PCSA, with the SM value being 1.7 times smaller than that for SOL, as compared to being 2.6 times smaller when specific tetanic force was normalised to CSA. Clearly, muscle architecture has a marked influence on the magnitude of the differences found with respect to sP_t and sP_o among the three muscles from lean mouse examined in this study.

Inter-muscle differences in architectural characteristics could also explain the statistically significantly larger sP_o values recorded for SM and SOL muscles from *ob/ob* mice as compared to those for SM and SOL from lean mice (see Table 4.1), if one considered:

(i) the relationship between CSA and the ratio $\frac{L_{fibre}}{L_{muscle}}$ ($CSA \approx PCSA \times \frac{L_{fibre}}{L_{muscle}}$; see

Section 4.2.5);

(ii) the finding that the length of SM and SOL muscles does not differ between *ob/ob* and lean mice (see Section 3.3.1);

(iii) the possibility that in SM and SOL muscles from *ob/ob* mouse, the fibre length is smaller than that in the respective muscles from the lean mouse. In this context, it is interesting to note that in mice transfected with TNF- α , an adipokine that is elevated in *ob/ob* mice (Hotamisligil *et al.*, 1993; Uysal *et al.*, 1997; Nakao *et al.*, 2000; Hotamisligil, 2006) and implicated in skeletal muscle mass decrements (Fong *et al.*, 1989; Goodman, 1991; Cheng *et al.*, 1992; Li *et al.*, 1998) (see Sections 1.2.2 and 1.4.2), the structure of skeletal muscle consists of multiple smaller fibres (Buck & Chojkier, 1996).

Based on the experimentally determined differences in the mean sP_o values between the SM muscles (and between the SOL muscles) from the *ob/ob* and lean mice, and using the mathematical strategy described below, it was estimated that a 30% and 20% reduction in the fibre length of SM and SOL muscles from *ob/ob* mice, respectively, could fully account for the difference in sP_o values found in this study between SM muscles (and between SOL muscles) from *ob/ob* and lean mice.

Estimation of fibre length reduction in SM (and SOL) of obese mouse.

$$\frac{sP_{tet}^{ob}}{sP_{tet}^{le}} = 1.40 = \frac{\frac{P_{tet}^{ob}}{CSA^{ob}}}{\frac{P_{tet}^{le}}{CSA^{le}}} \quad (E4.1)$$

From the equation relating PCSA and CSA (see Section 4.2.5), where cosine (pennation angle in degrees) ≈ 1 :

$$CSA^{ob} = PCSA^{ob} \times \frac{L_{fibre}^{ob}}{L_{muscle}^{ob}} \quad (E4.2)$$

$$CSA^{le} = PCSA^{le} \times \frac{L_{fibre}^{le}}{L_{muscle}^{le}} \quad (E4.3)$$

Replacing E4.2 and E4.3 in E4.1:

$$\frac{\frac{P_{tet}^{ob}}{PCSA^{ob}} \times \frac{L_{muscle}^{ob}}{L_{fibre}^{ob}}}{\frac{P_{tet}^{le}}{PCSA^{le}} \times \frac{L_{muscle}^{le}}{L_{fibre}^{le}}} = 1.40 \quad (E4.4)$$

If $psP_o^{ob} \approx psP_o^{le}$ and $L_{muscle}^{ob} = L_{muscle}^{le}$, E4.4 becomes:

$$\text{For SM:} \quad \frac{L_{fibre}^{le}}{L_{fibre}^{ob}} = 1.40 \quad \text{or} \quad \frac{L_{fibre}^{ob}}{L_{fibre}^{le}} \approx 0.7 \quad \text{i.e.} \quad L_{fibre}(ob/ob) = 0.7 L_{fibre}(\text{lean})$$

$$\text{For SOL:} \quad L_{fibre}(ob/ob) = 0.8 L_{fibre}(\text{lean})$$

4.3.2 Parameters describing the contractile kinetics of EDL, SM and SOL muscles of ob/ob and lean mice

4.3.2.1 Kinetics of the twitch response

The values for the parameters describing the kinetics of the twitch response for EDL, SM and SOL muscles from *ob/ob* and lean mice are shown in Table 4.2, and representative twitch traces produced by the three muscles from *ob/ob* and lean mice, based on which the kinetic parameters were calculated, are displayed in Figure 4.4.

Table 4.2 Parameters describing the contractile kinetics of EDL, SM and SOL muscles of *ob/ob* and lean mice.

Mouse	EDL		SM		SOL	
	<i>ob/ob</i> (8)	lean (8)	<i>ob/ob</i> (6)	lean (6)	<i>ob/ob</i> (6)	lean (6)
<i>Twitch kinetics</i>						
TPT (ms)	21.9 ± 1.2	23.1 ± 1.2	17.3 ± 1.3	17.5 ± 1.8	50.8 ± 2.6*	40.8 ± 3.5 ^a
1/2RT (ms)	55.1 ± 5.3*	31.9 ± 3.0 ^a	24.8 ± 4.1	19.1 ± 2.1 ^a	89.9 ± 6.3	82.8 ± 4.0 ^a
W₅₀ (ms)	72.8 ± 6.2*	49.2 ± 3.4 ^a	38.2 ± 4.6	32.4 ± 3.0 ^a	130.3 ± 7.1*	111.6 ± 4.0 ^a
<i>Tetanus kinetics</i>						
+dP/dt.P_o⁻¹ (s⁻¹)	18.2 ± 0.9*	22.1 ± 1.0	23.1 ± 2.0	21.9 ± 2.0	10.6 ± 0.5	12.2 ± 0.5 ^a
1/2RT_{tet} (ms)	46.0 ± 2.3*	39.9 ± 1.3	45.9 ± 3.7	39.3 ± 2.6	101.1 ± 2.6*	86.5 ± 2.4 ^a
-dP/dt.P_o⁻¹ (s⁻¹)	45.7 ± 1.3	50.5 ± 2.6 ^a	32.3 ± 3.1	41.4 ± 2.7 ^a	16.4 ± 0.6*	22.2 ± 1.6 ^a
Linear phase of relaxation (s⁻¹)	2.0 ± 0.2	2.6 ± 0.3	3.8 ± 0.4	5.4 ± 0.6 ^a	1.4 ± 0.1*	2.0 ± 0.1
Linear phase duration (ms)	16.6 ± 1.3*	12.4 ± 1.1	11.7 ± 1.0	10.8 ± 0.5	24.0 ± 1.9	26.0 ± 2.8

Values are mean ± S.E. Significantly different from *lean counterpart and ^aother lean muscles (see text for specific significance levels). The number of muscles assessed is indicated in parentheses. EDL – extensor digitorum longus; SM – sternomastoid; SOL – soleus; TPT – time to peak twitch force; 1/2RT – twitch half-relaxation time; W₅₀ – duration of the twitch at half amplitude; +dP/dt.P_o⁻¹ – peak rate of force development; 1/2RT_{tet} – tetanic half-relaxation time; -dP/dt.P_o⁻¹ – peak rate of relaxation.

For the kinetics of the twitch response, the following significant differences were found among EDL, SM and SOL muscles of lean mice: (i) TPT values for EDL and SM were 57% ($p < 0.001$) and 43% ($p < 0.001$) of the SOL value, respectively; (ii) 1/2RT values for EDL and SM were 39% ($p < 0.001$) and 23% ($p < 0.001$) of the SOL value, respectively; (iii) the 1/2RT value for SM was 60% of that for EDL ($p < 0.05$); (iv) W_{50} values for EDL and SM were 44% ($p < 0.001$) and 29% ($p < 0.001$) of the SOL value, respectively; and (v) the W_{50} value for SM was 66% of that for EDL ($p < 0.01$).

The markedly greater proportion of type IIB fibres in EDL and SM muscles as compared to that in SOL (see Section 3.3.6) can easily explain the slower twitch kinetics displayed by SOL muscle. Fibre type composition differences cannot, however, explain the faster kinetics of the twitch response produced by SM as compared with EDL. This is because, as shown in Section 3.3.6, SM contained a 12.6% greater proportion of fibres expressing slower MHC isoforms (i.e. MHC IIa and IId). Previous work has indicated that, in SM from rat, these slower fibre types possess similar twitch kinetics to those of type IIB fibres (Dulhunty & Dlutowski, 1979; Luff, 1985). Therefore, it is speculated here that the faster twitch kinetics of SM as compared to EDL may be attributable to differences in the endogenous level of SR Ca^{2+} loading between fibres of the two muscles, because Posterino & Lamb (2003) showed that the twitch response is prolonged (i.e. greater W_{50}) with an increase in SR Ca^{2+} loading. Thus, a smaller endogenous SR Ca^{2+} content in SM fibres than in EDL fibres from lean mice may underlie the faster twitch response for SM.

As seen in Table 4.2, no differences were observed between *ob/ob* and lean mice with respect to the TPT values for EDL ($p = 0.500$) or SM (0.911), while SOL from *ob/ob* mice demonstrated a 25% greater value ($p = 0.045$) than muscles from lean mice. For 1/2RT, the

EDL value for *ob/ob* mice was 73% greater than that for lean mice ($p=0.002$), while no statistical differences were observed for SM ($p=0.246$) or SOL ($p=0.363$) values between the two mouse groups. As expected from TPT and 1/2RT data, both EDL ($p=0.005$) and SOL ($p=0.046$) from *ob/ob* mice demonstrated significantly larger values for W_{50} than those for their counterpart muscles from lean mice. Taken together, these results suggest that the contractile kinetics of the twitch response are affected in a muscle-specific manner, with only EDL and SOL of *ob/ob* mice showing different (viz. slower) kinetics from those of the control counterparts.

4.3.2.2 Kinetics of the tetanus response

The values for the parameters describing the kinetics of the tetanus for EDL, SM and SOL muscles from *ob/ob* and lean mice are shown in Table 4.2 and representative tetanus traces produced by the three muscles from *ob/ob* and lean mice, based on which these parameters were calculated, are displayed in Figure 4.4.

As seen in Table 4.2, there was a significant difference ($p<0.001$) among EDL, SM and SOL muscles from lean mice with respect to the peak rate of force development, normalised to peak tetanic force, with values for EDL and SM being 81% ($p<0.001$) and 80% ($p<0.001$) greater than SOL, respectively. For the parameters describing the relaxation kinetics of the tetanic response ($1/2RT_{tet}$, $-dP/dt.P_o^{-1}$ and the linear phase of the relaxation response), the following differences were found among the three muscles: (i) for $1/2RT_{tet}$, values for EDL and SM were 46% and 45% of the value for SOL ($p<0.001$), respectively; (ii) for the peak rate of force relaxation, normalised to peak tetanic force, the value for EDL was 22% greater than that for SM ($p<0.05$), while EDL and SM values were 2.3 and 2.0 times greater than the SOL value, respectively ($p<0.001$); and, (iii) for

the average slope of the linear phase of tetanic relaxation (when normalised to peak force), the EDL value was 51% smaller than that for SM ($p < 0.001$) but 33% greater than that for SOL ($p = 0.070$), while the SM value was 2.7 times greater than SOL ($p < 0.001$). Taken together, these data show EDL and SM from lean mice to have faster contractile kinetics of the tetanic response than those of SOL, as would be predicted given the fibre type composition of each muscle (see Section 3.3.6). Consistent with the difference found between the EDL and SM muscles with respect to $1/2RT$ of the twitch response, the SM value for the rate of tetanic relaxation in the linear phase was greater than that for EDL. Again, this difference in a kinetic parameter could not be explained by the differences in fibre type composition found for EDL and SM muscles.

When comparing the parameters describing the kinetic characteristics of the tetanic response between *ob/ob* and lean mice, it was found that the EDL value for the peak rate of force development, normalised to peak tetanic force, was 18% smaller for muscles from *ob/ob* mice ($p = 0.013$), while no differences were found for SM ($p = 0.661$) or SOL ($p = 0.057$). For parameters describing the relaxation kinetics, the values for $1/2RT_{\text{tet}}$ were greater for all three muscles of *ob/ob* mice compared to those of lean mice, with the 15% and 17% greater response for EDL ($p = 0.037$) and SOL ($p = 0.002$), respectively, reaching statistical significance. Similarly, the values for the peak rate of force relaxation, normalised to peak tetanic force, were smaller for all three muscles from *ob/ob* mice than those for muscles from lean mice, with responses being 10%, 22% and 26% smaller for EDL ($p = 0.127$), SM ($p = 0.052$) and SOL ($p = 0.006$), respectively. The values for the average slope of linear phase of tetanic relaxation, when normalised to peak tetanic force, were also smaller for the three muscles from *ob/ob* mice, with EDL, SM and SOL values being 22% ($p = 0.086$), 29% ($p = 0.051$) and 31% ($p = 0.002$) smaller, respectively, than

those for control muscles. The duration of the linear phase was 34% longer in EDL muscles from *ob/ob* mice compared to lean mice ($p=0.031$), while no statistical differences were observed between values for SM ($p=0.424$) or SOL ($p=0.564$) from the two mouse groups. Taken together, these data show that: (i) the contractile kinetics of the tetanic response are altered (being slower) in EDL, SM and SOL from *ob/ob* mice, with EDL being most affected, and (ii) across all three muscles, parameters describing the relaxation kinetics appear to be most affected in *ob/ob* mice.

4.3.3 Force-frequency relationship

The force-frequency relationships generated by EDL, SM and SOL muscles from lean mice over the range of stimulation frequencies 5-110 Hz, where force is expressed as a percentage of the peak tetanic force (%P_o), are compared in Figure 4.5. As expected based on the fibre type composition of EDL and SOL muscles (see Section 3.3.6), the force-frequency curve generated by SOL muscles was shifted to the left relative to that generated by EDL muscles. Interestingly, the force-frequency curve generated by SM, whose fibre type composition is not markedly different from that of EDL, overlapped with that produced by the EDL only at low frequencies of stimulation (≤ 30 Hz). Furthermore, the force-frequency curve generated by SM overlapped with that produced by SOL muscles at higher stimulation frequencies (70-90 Hz), even though the fibre type composition of the two muscles is markedly different. These data question the generally assumed tightness (Roy *et al.*, 1982; Jones, 1996; Asmussen *et al.*, 2003; Brooks *et al.*, 2004) of the relationship between the fibre type composition of a muscle and its force-frequency relationship.

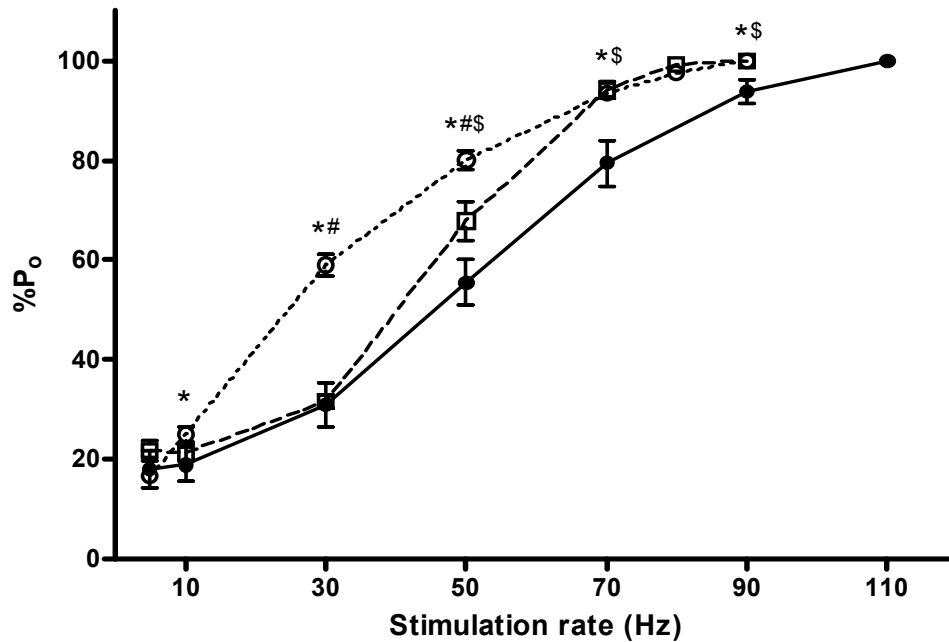


Figure 4.5 Force-frequency relationships for EDL, SM and SOL muscles from adult lean mice. Muscles are EDL (●— n=8), SM (□--- n=6) and SOL (⊙···· n=6). Ordinate axis (%P₀) represents force responses expressed as a percentage of peak tetanic force for each respective stimulation frequency (500 ms trains). Significant difference between *SOL and EDL, #SOL and SM, and \$EDL and SM, with *p=0.021 at 10 Hz, #p=0.010 at 50 Hz, \$p=0.006 at 50 Hz, and p<0.001 for all other differences. S.E. bars are shown.

Figure 4.6 shows comparisons of the force-frequency relationship for EDL, SM and SOL from *ob/ob* and lean mice. The force-frequency curves of all three muscles from *ob/ob* mice displayed a leftward shift compared with those of their respective controls, with significantly greater %P_o values being produced by the EDL and SOL muscles from *ob/ob* mice at 30 Hz and 50 Hz (for EDL) and at 10 Hz and 30 Hz (for SOL). No statistically significant differences were found between %P_o values for SM from *ob/ob* and lean mice over the entire range of stimulation frequencies used. These data suggest that the force-generating capacity of EDL and SOL muscles from *ob/ob* mice is enhanced at lower stimulation frequencies.

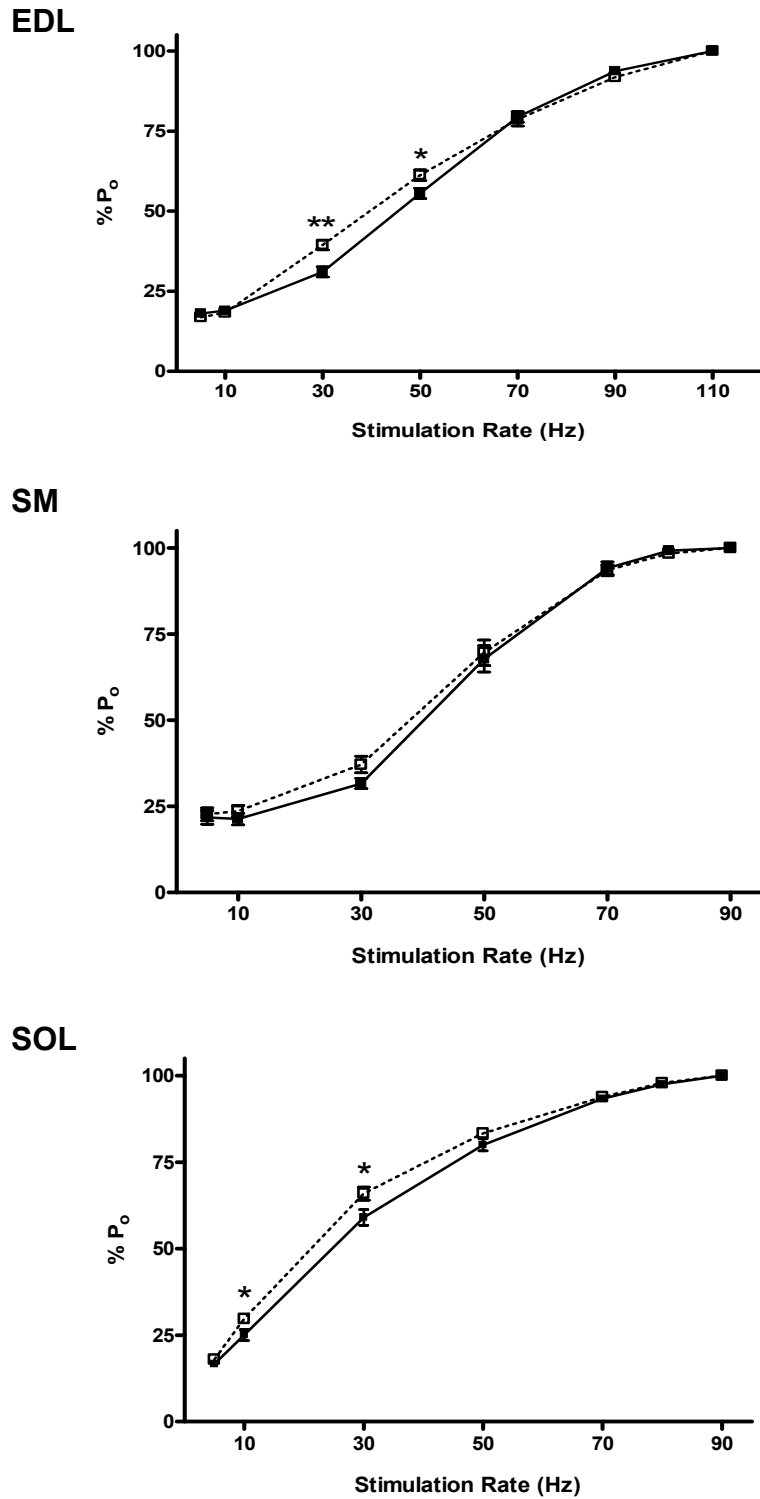


Figure 4.6 Force-frequency relationships for whole muscles from adult *ob/ob* (□) and lean (■) mice. Muscles are EDL (□ n=8; ■ n=8), SM (□ n=6; ■ n=6), and SOL (□ n=6; ■ n=6). Ordinate axis (%P₀) represents force responses normalised as a percentage of peak tetanic force. Significantly different from lean counterpart at *p<0.05 and **p<0.005. S.E. bars are shown.

Section 4.4 DISCUSSION

This is the first systematic investigation of both twitch and tetanic characteristics of skeletal muscles from *ob/ob* mouse. The data indicate that differences exist between skeletal muscles (EDL, SM and SOL) of *ob/ob* mice and those of lean mice, but the type and the extent of these differences are muscle-specific.

Force-generating capacity

The results of the present study indicate that SM and SOL muscles from *ob/ob* mice generate similar absolute peak tetanic forces as their control muscles. The P_0 value for EDL muscle from *ob/ob* mouse was 16% lower than that for the control. This difference, which did not reach statistical significance in the present study, is comparable with the (statistically significant) difference (-31%) reported by Bruton *et al.* (2002) for EDL muscles from *ob/ob* mice. The above data would suggest that the SM and SOL muscles from *ob/ob* mice retain their capacity to generate the necessary forces for normal physiological function *in vivo*. However, when P_0 was normalised to body mass, the values for all three muscles from *ob/ob* mice were 40-55% lower than those for the respective controls, with the largest difference (-54%) being recorded for the EDL muscle.

Physiologically, most murine postural and locomotor activity occurs at motor neuron firing frequencies below 60 Hz, with the majority falling in the 20-30 Hz range (Hennig & Lomo, 1985, 1987). The force-frequency data show that at a stimulation frequency of 30 Hz, EDL, SM and SOL muscles of *ob/ob* mice generated a greater relative force

(EDL: +8.4%; SM: +5.5%; SOL: +7.0%) than their respective control muscles, with the difference for EDL and SOL reaching statistical significance. However, when the absolute forces generated by the three muscles from the two mouse groups at 30 Hz were normalised to body mass (BM), the values for the muscles from obese mice, expressed as $\text{mN}\cdot\text{g}^{-1}$ BM (EDL: 1.6 ± 0.1 ; SM: 1.3 ± 0.1 ; SOL: 2.3 ± 0.1) were still significantly lower (34-42%) than those for controls (EDL: 2.7 ± 0.2 ; SM: 2.1 ± 0.2 ; SOL: 3.4 ± 0.2). Taken together these data indicate that skeletal muscles of *ob/ob* mice have a reduced force-generating capacity relative to body mass, regardless of their location and function or the motor neuron firing frequency at which they are stimulated.

Contractile kinetics

The results of this study indicate that EDL, SM and SOL muscles of *ob/ob* mice exhibit a general slowing of relaxation and, to a smaller extent, of force generation. These data are in agreement with the only two previous investigations of contractile function in skeletal muscles of *ob/ob* mice (Warmington *et al.*, 2000; Bruton *et al.*, 2002). Importantly, the data from the present work reveal that the type and the extent of the slowing process are muscle-specific.

The most conspicuous obesity-related alteration in contractile kinetics across all three muscles examined was a slowing of relaxation. EDL muscles from *ob/ob* mice were most affected, displaying a significantly longer $1/2\text{RT}$, W_{50} and $1/2\text{RT}_{\text{tet}}$ and a prolonged linear phase of relaxation of the tetanus. SOL muscles from *ob/ob* mice demonstrated a prolonged W_{50} , $1/2\text{RT}_{\text{tet}}$ and lower values for the normalised peak rate of relaxation and the slope of the linear phase of relaxation. In contrast, there were no statistical differences observed between SM muscles of *ob/ob* and lean mice for any parameter, though values

for the normalised peak rate of relaxation ($p=0.052$) and the slope of the linear phase of relaxation ($p=0.051$) suggest that a slowing of tetanic relaxation was also present in SM muscles of *ob/ob* mice.

Warmington *et al.* (2000) and Bruton *et al.* (2002) also provided evidence of slower relaxation in skeletal muscles of *ob/ob* mice, reporting a prolonged $1/2RT$ for EDL and SOL muscles and a prolonged $1/2RT_{tet}$ for EDL muscles, respectively. With the excitation-contraction-relaxation (E-C-R) cycle culminating in Ca^{2+} re-uptake by the SR, alterations in skeletal muscles of *ob/ob* mice at specific sites involved in cycle events may contribute to the observed slowing of muscle relaxation (Close, 1972; Fitts & Holloszy, 1977). With respect to SR Ca^{2+} re-sequestration, a number of SR features (e.g. SR volume; SERCA isoform expression; SERCA density) (Rüegg, 1992; Loukianov *et al.*, 1998; Johansson *et al.*, 2003) can influence this process. Also, alterations in the speed of cross-bridge detachment may influence the rate of muscle relaxation (Westerblad & Allen, 1993; Westerblad *et al.*, 1997b; Gordon *et al.*, 2000) and, in the present study, the lower values for the normalised rate of linear phase relaxation suggests that a slowing of this process may be involved.

Less pronounced in the present study is the evidence of obesity-related alterations in the rates of force development. EDL muscles from *ob/ob* mice exhibited a lower normalised peak rate of tetanic force development and SOL muscles from *ob/ob* mice displayed a prolonged TPT as compared to control muscles. Changes in these kinetic parameters have been proposed to reflect differences in Ca^{2+} release from the SR and/or the rate of Ca^{2+} binding to troponin-C (Fitts & Holloszy, 1978; Gordon *et al.*, 2000). No differences with

respect to kinetics of force development were observed between SM muscles of *ob/ob* and lean mice.

The altered contractile kinetics of muscles from *ob/ob* mice are likely to have influenced the changes observed in their force-frequency relationships. Prolongation of TPT, 1/2RT and W_{50} act to increase the tetanic force developed at submaximal frequencies of stimulation, as indicated by a leftward shift in the force-frequency curve (Metzger & Fitts, 1987b; Brooks & Faulkner, 1988; Thompson *et al.*, 1992). In the present study, EDL muscles from *ob/ob* mice displayed a significant increase in 1/2RT and W_{50} , while SOL muscles demonstrated a significantly longer TPT and W_{50} . These changes are consistent with both muscles displaying a significant leftward shift in the force-frequency relationship. This leftward shift is in agreement with previous work on EDL and SOL muscles from *ob/ob* mice (Warmington *et al.*, 2000; Bruton *et al.*, 2002). In contrast, SM muscles from *ob/ob* mice displayed no significant alterations in twitch kinetics when compared to control muscles and, subsequently, no significant differences at any stimulation rate in the force-frequency curve.

In conclusion, EDL, SM and SOL muscles of *ob/ob* mice exhibited alterations in parameters describing skeletal muscle contractile performance, when compared to the respective muscles from lean mice. Of these changes, a reduced force-generating capacity normalised to body mass was observed for all three muscles. These muscles also exhibited a shift in their contractile kinetics towards a slower phenotype, with EDL being most affected. A slowing of muscle relaxation in *ob/ob* mouse has been reported previously (Warmington *et al.*, 2000; Bruton *et al.*, 2002), but the mechanism/s responsible have not been elucidated. As muscle relaxation is brought about by the

removal of Ca^{2+} from the contractile apparatus and its re-uptake by the SR, it is proposed that alteration/s in these E-C-R cycle events may contribute to the slower relaxation observed for skeletal muscles of *ob/ob* mice.